BUREAU OF RECLAMATION

Technical Memorandum No. ENV-2020-064

Eloy-Maricopa Stanfield Basin Study: Development of Future Climate and Recharge Scenarios

U.S. Department of the Interior **January 2021**

Mission Statements

The Department of the Interior (DOI) conserves and manages the Nation's natural resources and cultural heritage for the benefit and enjoyment of the American people, provides scientific and other information about natural resources and natural hazards to address societal challenges and create opportunities for the American people, and honors the Nation's trust responsibilities or special commitments to American Indians, Alaska Natives, and affiliated island communities to help them prosper.

The mission of the Bureau of Reclamation is to manage, develop, and protect water and related resources in an environmentally and economically sound manner in the interest of the American public.

Cover Photo: The Rillito, a tributary of the Santa Cruz River in Southern Arizona, during monsoon season. Typically, this channel is dry. Photo Credit: (Brittney Bates, Montgomery & Associates).

Technical Memorandum No. ENV-2020-064

Eloy-Maricopa Stanfield Basin Study: Development of Future Climate and Recharge Scenarios

KRISTIN MIKKELSON

Digitally signed by KRISTIN MIKKELSON
Date: 2021.01.07 16:12:55 -07'00'

prepared by
Kristin Mikkelson, PhD,
Hydrologic Civil Engineer
Water Resources Engineering and Management (86-68210)

IAN FERGUSON

Digitally signed by IAN FERGUSON
Date: 2021.01.07 17:35:57 -07'00'

peer reviewed by
Ian Ferguson, PE, PhD,
Hydrologic Civil Engineer
Water Resources Engineering and Management (86-68210)

Executive Summary

The Eloy-Maricopa Stanfield (EMS) Basin Study is a collaborative study between Federal and non-Federal entities and stakeholders. The main goal of the study is to use the best available science and engineering to help water managers plan for the uncertain future in water resources. The EMS Basin Study area is in central Arizona, south of Phoenix and north of Tucson. It is an arid area dominated by groundwater supported agricultural activities. Future scenarios were developed to represent projected changes in climate conditions and water demands in the Basin Study area. An existing regional groundwater model was subsequently used to evaluate the impacts of future scenarios on groundwater resources in the area.

This report describes the development of a suite of future climate and groundwater recharge scenarios for the EMS basin study. Future climate scenarios were developed using the ensemble-informed hybrid-delta (HDe) method for two future time periods centered around 2060 and 2080. The HDe method identifies projected changes in climate between a historical baseline period and a future period, then maps those changes onto a dataset of observed historical climate conditions. The HDe climate scenarios developed for the EMS Basin Study span the range of uncertainty in projected future climate conditions from an ensemble of 64 downscaled climate projections, including a warm-Wet (WW), Warm-Dry (WD), Hot-Wet (HW), Hot-Dry (HD), and Central Tendency (CT) future.

All future climate scenarios suggest an increase in temperatures across the EMS Basin Study area over the next century. This projected increase ranges from 3 degrees Fahrenheit (°F) (WW) to 6.1 °F (HW) under the near future period 2060. Unlike projected changes in temperature, projected changes in precipitation are less certain. The dry scenarios (HD and WD) suggest a decrease in basin-averaged annual precipitation of 2.2 inches (-24%) whereas the wet scenarios (HW and WW) suggest an increase of almost one inch (+9%).

Despite this uncertainty in future precipitation trends, all scenarios suggest an increase in the frequency of extreme precipitation. Precipitation extremes are defined as basin-averaged annual precipitation less than the 5^{th} percentile of historic annual precipitation (extremely dry years) or greater than the 95^{th} percentile of historic annual precipitation (extremely wet years). For example, the historic baseline period (1981-2010) includes two extremely dry years over the 30 years. By contrast, eight out of 30 years are extremely dry under the HD scenario for the 2080 future time period (2065-2094).

Future groundwater recharge scenarios were developed for each of the five climate scenarios and two future time periods. Recharge scenarios represent projected changes to future groundwater recharge in response to future climate scenarios and will be incorporated in the regional groundwater model for the area.

Distributed recharge across the EMS Basin Study area from precipitation is generally negligible as the majority of precipitation contributes to evaporation or surface runoff. Natural groundwater recharge in the EMS Basin Study area is therefore limited to streambed infiltration. Two rivers are within the Basin Study area: the Gila River enters the study area from the east, and the Santa Cruz River enters the study area from the south. The Gila River receives the surface water spilled at Ashurst-Hayden Dam and, therefore, the streamflow entering the model domain from the Gila is the result of a managed system. Recharge from streambed infiltration on the Gila River is estimated as the difference between gaged annual inflows and outflow in the model area. Estimated recharge is then distributed across river cells in the groundwater model on a weighted basis. The Santa Cruz River, on the other hand, is ephemeral and natural flows are limited to high precipitation years, as the majority of flow is effluent-dominated. All natural streamflow (not effluent) from the Santa Cruz River entering the model domain is assumed to recharge the groundwater system as streambed infiltration. Recharge from the Santa Cruz river is then distributed non-linearly along the entire reach of the Santa Cruz River within the model domain.

Given the setup of the groundwater model, it was necessary to develop a historic relationship between precipitation and annual recharge for both rivers independently. Because recharge is estimated from streamflow entering the model domain, relationships were developed between historical precipitation and historical streamflow entering (and for the Gila exiting) the model domain. These relationships were used to estimate annual streamflow into the model domain from each river. Annual streamflow into the model domain was then used to estimate spatially-distributed recharge by streambed infiltration using a methodology previously developed for the regional groundwater model. While many different empirical and conceptual rainfall-runoff models were considered, it was found that an empirical power-law relationship between annual precipitation and streamflow represented the historical observed data the best for both rivers. In addition to annual streamflow being a significant predictor variable for the Gila River, the maximum annual rainfall multi-day event total was also a significant predictor variable, although it had a linear relationship to recharge as opposed to a power law relationship.

Empirical relationships between annual precipitation and annual streamflow were used to develop recharge scenarios for the Gila and Santa Cruz Rivers under each of the future scenarios and time periods considered in the EMS Basin Study. Similar to the future precipitation scenarios, future recharge scenarios are highly uncertain, with dry scenarios suggesting a decrease in average annual recharge and wet scenarios suggest an increase in average annual recharge. For the Gila River, the CT scenario for the near-future period (2045-2074) suggests that average annual recharge is projected to decrease by 23% compared to the historical conditions. For the Santa Cruz River, the CT scenario for the near-future period suggests that average annual recharge will decrease by 32% compared to historical conditions.

All scenarios also suggest that the number of extremely wet and dry recharge years are projected to increase by 2060. Extremely wet recharge years are anticipated to increase from 2 years out of a 30-year period to 3 years out of a 30-year period for the WW scenario for both rivers. In contrast, extremely dry recharge years on the Santa Cruz River are projected to increase from 10 years out of a 30-year period to 20 years out of a 30-year period for both the HD and WD scenarios. The extremely dry years for the Gila River are projected to increase from 3 years out of a 30-year period to 4 years out of a 30-year future period for the HD scenario.

Overall, while uncertainty in projected future precipitation trends propagates to projected future recharge trends, it is likely that there will be longer periods of time between large recharge events where groundwater stores are replenished.

Contents

Appendix

Tables

Figures

Acronyms

°F	degrees Fahrenheit
%	percent
ADWR	Arizona Department of Water Resources
AMA	Active Management Area
armax	autoregressive moving average linear transfer function
CDF	cumulative distribution function
cfs	cubic feet per second
cmd	catchment moisture deficit model
CMIP	Coupled Model Intercomparison Project (CMIP1, CMIP2, CMIP3, and CMIP5 refer to CMIP Phases 1, 2, 3, and 5, respectively)
CPC	Climate Prediction Center
cwi	catchment wetness index
DTR	diurnal temperature range
EMS	Eloy-Maricopa Stanfield
GCM	Global Climate Model
GHCN-Daily	Global Historical Climate Network—Daily
HDe	Ensemble-informed hybrid-delta method of developing climate scenarios
IHACRES	Identification of Hydrographs and Components from Rainfall, Evaporation, and Streamflow data model
IPCC	Intergovernmental Panel on Climate Change
km	kilometer
lambda	a transfer function with two exponential components and variable partitioning
LOCA	Localized Constructed Analogs (a method of downscaling climate projections)
NCEI	National Center for Environmental Information
NOAA	National Oceanic and Atmospheric Administration
NSE	Nash-Shutcliffe efficiency coefficient
NWS	National Weather Service
PCMDI	Program for Climate Model Diagnostics and Intercomparison
powuh	power law transfer function model
RCH	MODFLOW Recharge Package
RCP	Representative Concentration Pathway
Reclamation	Bureau of Reclamation
SCE	Shuffled Complex Evolution
SCIP	San Carlos Irrigation Project
SWB	USGS Soil Water Balance model
TAF	thousand acre-feet
USGS	U.S. Geological Survey
VIC	Variable Infiltration Capacity model

1. Introduction

Numerous studies have shown that global and regional climate conditions are changing, that climate change will continue and likely accelerate over the 21st century, and that climate change will significantly affect local and regional water supplies, demands, and management (IPCC, 2014a and 2014b). To facilitate analysis of future water supplies and demands in the Eloy-Maricopa Stanfield (EMS) Basin, a suite of future climate and recharge scenarios was developed to represent the projected range of future climate conditions over the study area. Climate scenarios were developed from an ensemble of bias-corrected and downscaled climate projections using the ensemble-informed hybrid-delta (HDe) scenario methodology. Recharge scenarios were developed from the application of these future climate scenarios in an empirical relationship between observed precipitation and groundwater recharge. These climate and recharge scenarios were subsequently used as the basis for evaluating future water supplies and demands in the Basin Study area using the Pinal Area regional groundwater model (Liu et al., 2014). This technical memorandum describes the climate and recharge scenarios developed for the EMS Basin Study. Sections 2 and 3 describe observed historical climate conditions and projected future climate conditions over the study region, respectively. Section 4 describes the suite of climate scenarios developed for the EMS Basin Study, and Section 5 describes the corresponding future recharge scenarios.

2. Observed Historical Climate

The term *weather* is generally used to describe the state of the atmosphere at a specific place and time, including characteristics such as temperature, precipitation, wind speed, and humidity. *Weather* thus refers to the day-to-day conditions directly experienced by people and the environment, including rainstorms and heat waves. The term *climate*, on the other hand, is generally used to describe the long-term average weather conditions over a given region. *Climate* thus describes "normal" or "average" conditions for a given place averaged over a given period.

Most of Arizona is characterized as arid or semi-arid with the exception of the mountainous areas which can receive upwards of 40 inches annual. Pinal County, where the EMS study area lies, is south of Phoenix in the south-central part of Arizona and has an average annual precipitation of around 9 inches. In general, Pinal County experiences hot, dry summers with a monsoon season in late summer. Winters are mild with occasional precipitation.

This section describes historical observed climate conditions in the EMS study area (Figure 1). Observational datasets used to characterize historical climate conditions are described in Section 2.1. Observed historical climate variability and climate trends are described in Section 2.2.

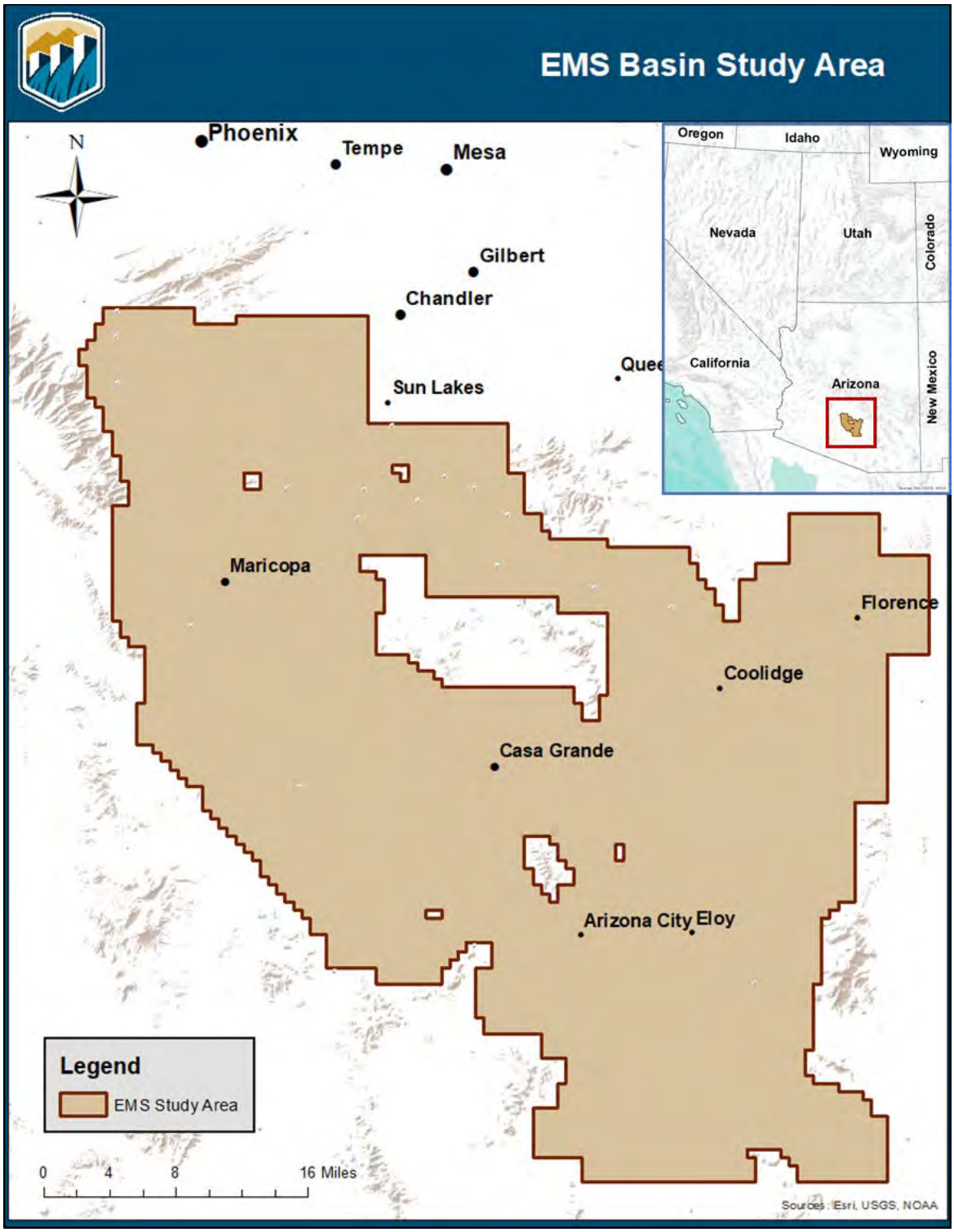

Figure 1. Map of the EMS Basin Study domain in relation to the Western United States.

2.1. Observational Datasets

A combination of weather station records and gridded observational datasets were used to characterize historical climate variability over the EMS Basin Study area.

Weather station records generally constitute the best-available information on weather and climate conditions at the station location and its immediate vicinity. However, weather station records often have missing values due to instrument malfunction, delays, or gaps in manual readings, as well as other operations and maintenance challenges. In addition, weather stations typically provide relatively sparse spatial coverage: many watersheds may contain just a few weather stations, and weather conditions at those station locations may not represent the entire watershed due to the effects of topography, land cover, and other factors on local-scale weather conditions. Using weather station records to characterize climate variability and trends over a region of interest is often challenging due to limited data coverage in both time and space (Livneh et al., 2015).

Gridded observational datasets, by contrast, provide a temporally and spatially complete record of climate conditions over a given area. Gridded observational datasets are typically developed from weather station records. Station data are interpolated onto a rectilinear grid using sophisticated interpolation procedures combined with scaling or adjustment to account for the influence of topography on local-scale weather conditions. Gridded observational datasets also use statistical techniques to minimize inconsistencies in weather station records over time, including impacts from weather stations coming online or going offline, being relocated, or being affected by changes in site conditions or surrounding landscape. Gridded observational datasets allow for analysis of spatio-temporal characteristics of weather and climate variability; provide a consistent input dataset for use with spatially-distributed hydrologic models; and provide a basis for evaluating, downscaling, and bias-correcting climate projections from global climate models (GCM).[1]

Analysis of historical climate conditions for the EMS Basin Study is based primarily on the gridded observational dataset developed by Dr. Ben Livneh (Livneh, 2016). Three versions of the Livneh dataset were merged to develop a spatially and temporally complete record covering the EMS Basin Study area for 1915-2015:

- *Livneh et al. 2013 (L2013)*
  Period of Record: 1915-2011
  Spatial Extent: Continental US, Mexico, and Southern Canada

- *Livneh et al. 2015 (L2015)*
  Period of Record: 1950-2013
  Spatial Extent: Continental US, Mexico, and Southern Canada

[1] Throughout this technical memorandum, the term *global climate model* and acronym *GCM* are used generally to refer to numerical models of the global climate system, including general circulation models, global climate models, earth system models, and related classes of models.

- *Livneh 2016 (L2016)*
  Period of Record: 1915-2015
  Spatial Extent: Continental US, Mexico, and Southern Canada

All three versions of the Livneh observational dataset were developed from ground-based weather station records. Station data were interpolated to a 1/16° rectilinear grid using the Synteny Mapping and Analysis Program (SYMAP) algorithm (Shepard, 1984) followed by orographic scaling to account for the effects of topography (Livneh et al., 2013 and 2015). All three datasets share the same 1/16° grid. The three datasets were compared over their overlapping period of record (1950-2011). Differences were found to be generally minor. The merged dataset used in this study was developed by using:

- the L2015 dataset as the primary dataset for the period 1950-2013. The L2015 dataset served as the observational basis for downscaling and bias correction in developing the LOCA downscaled climate projections (see Section 3; Pierce et al., 2014).

- The L2016 dataset to extend the period of record to include 1915-1949 and 2014-2015. The L2016 dataset represents the most recent version of the Livneh dataset and includes recent years that are not included in other versions (2014-2015) (Livneh, 2016).

- The L2013 dataset to fill a small number of missing values from the L2015 and L2016 datasets.

- Spatial interpolation between neighboring grid cells to fill remaining values that were missing from all three datasets.

The resulting merged dataset was compared to available weather station records from the Global Historical Climatology Network–Daily (GHCN-Daily) dataset to ensure that the gridded dataset was consistent with available station records. GHCN-Daily is an integrated database of daily climate summaries from more than 80,000 ground-based weather stations around the globe (Menne et al., 2012). Data are compiled by the National Oceanic and Atmospheric Administration (NOAA) National Centers for Environmental Information (NCEI; formerly the National Climatic Data Center) from numerous sources, including more than a dozen separate weather station networks and databases within the United States as well as international datasets shared by national meteorological and hydrological services and by personal communication between NOAA NCEI and international agencies. All station records are subjected to routine quality assurance checks prior to being integrated into the GHCN-Daily database.

GHCN-Daily stations from within the EMS Basin Study area (Figure 2) were identified and station records were compiled for precipitation, daily maximum air temperature, daily minimum air temperature, and daily mean air temperature. Station records were reviewed and screened based on the available period of record (start and end dates of station record)

and completeness of record (frequency of missing values). Stations with fewer than 20 years of data values (7,300 daily values) or with more than 50 percent missing values over their period of record were excluded from analysis. The merged Livneh dataset developed for the EMS Basin Study was ultimately compared to records from 9 GHCND stations for precipitation, 8 stations for daily maximum air temperature, and 8 stations for daily minimum air temperature. None of the local stations record daily mean air temperature.

In general, the merged gridded Livneh dataset has good general agreement with GHCND station data. All stations except the USC00020404 GHCND station at Arizona City have excellent agreement with the gridded Livneh data (e.g., Figure 3, Figure 4, Figure A1 and Figure A2) for recorded monthly precipitation, and monthly mean maximum and minimum temperatures from 1950 to 2015. Although the Livneh data captures the range of precipitation and temperature values recorded at the Arizona City station (Figure 5), values from the Livneh dataset are not well correlated with values from the station record for some months (Figure 6 and Figure 7).

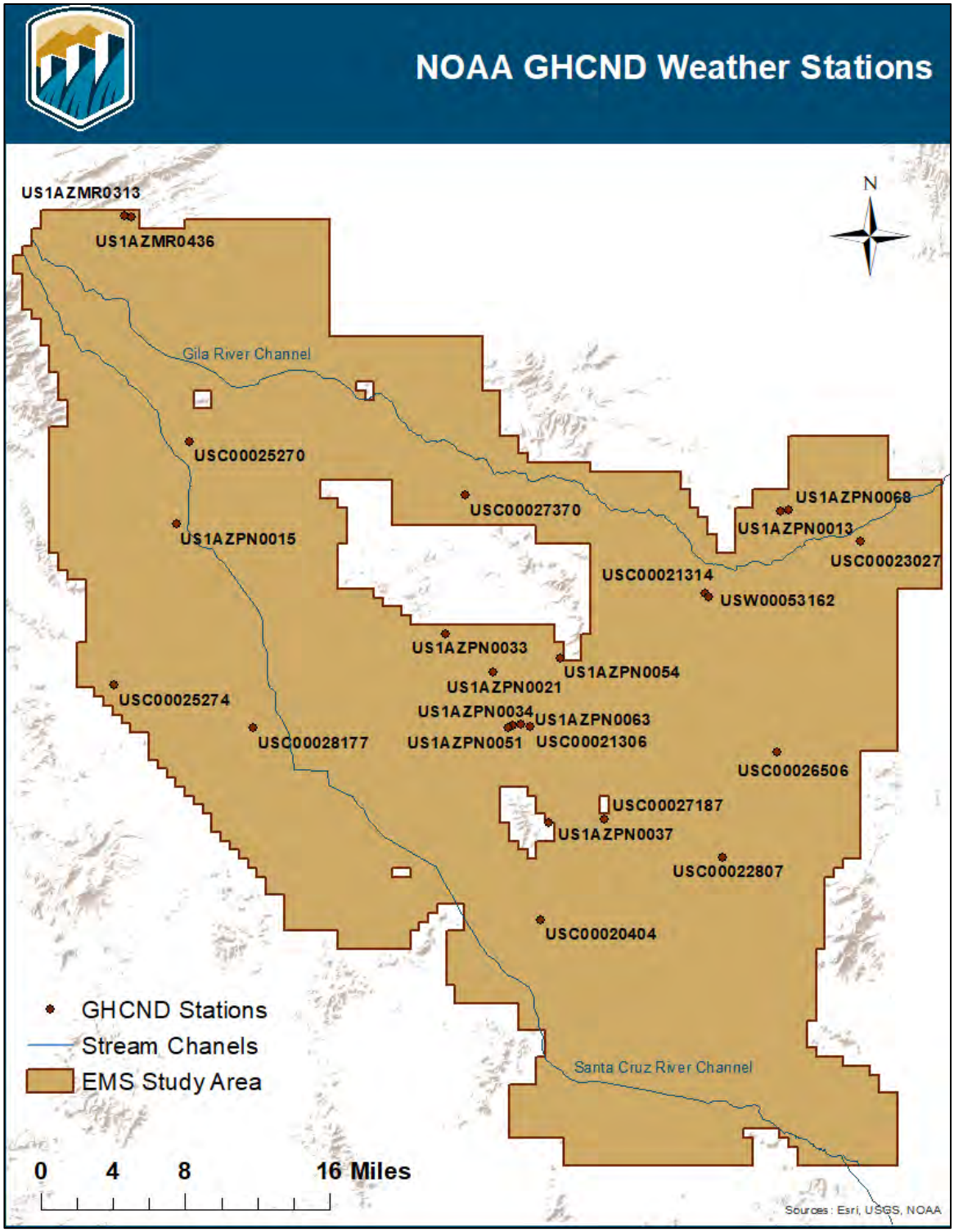

Figure 2. Map of the EMS Basin Study domain. The NOAA GHCND weather stations found within the study area are depicted by the dark red circles.

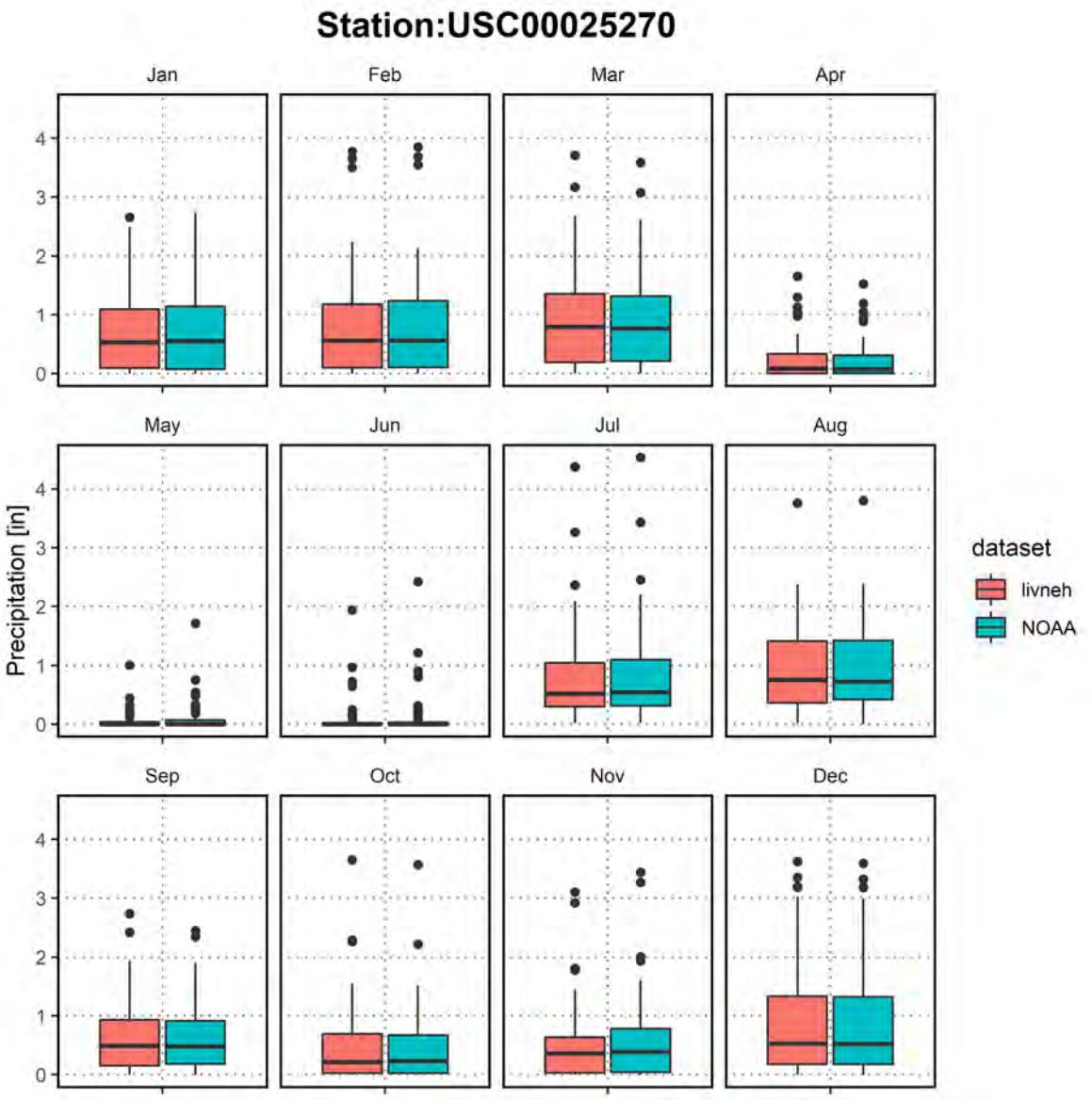

Figure 3. Boxplot of monthly precipitation from 1950- 2015 at the USC00025270 Maricopa GHCND station, compared to the corresponding L2015 data from the respective grid cell.

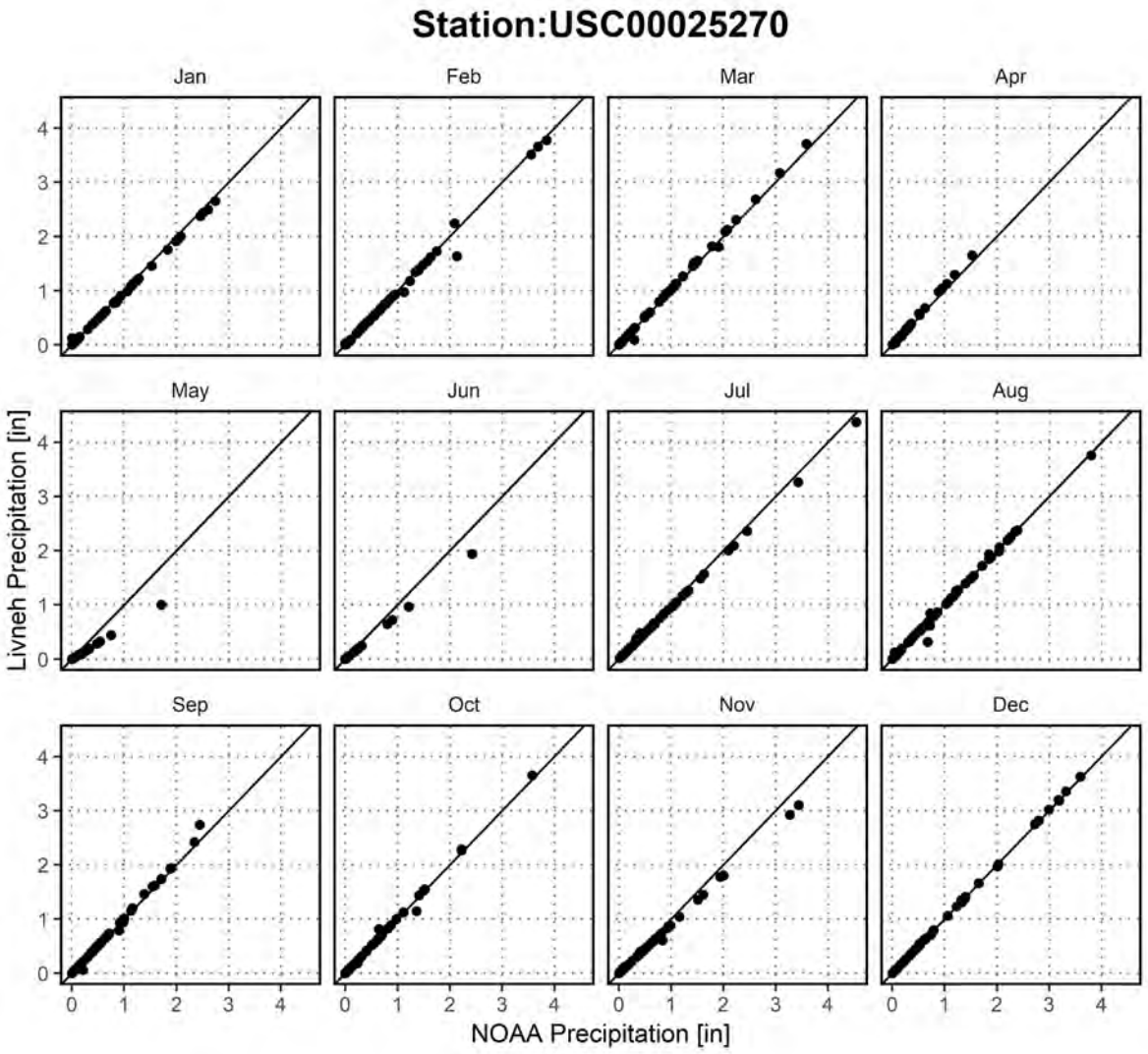

Figure 4. Scatterplot of monthly precipitation from 1950-2015 at the USC00025270 Maricopa GHCND station compared to the corresponding L2015 data from the respective grid cell.

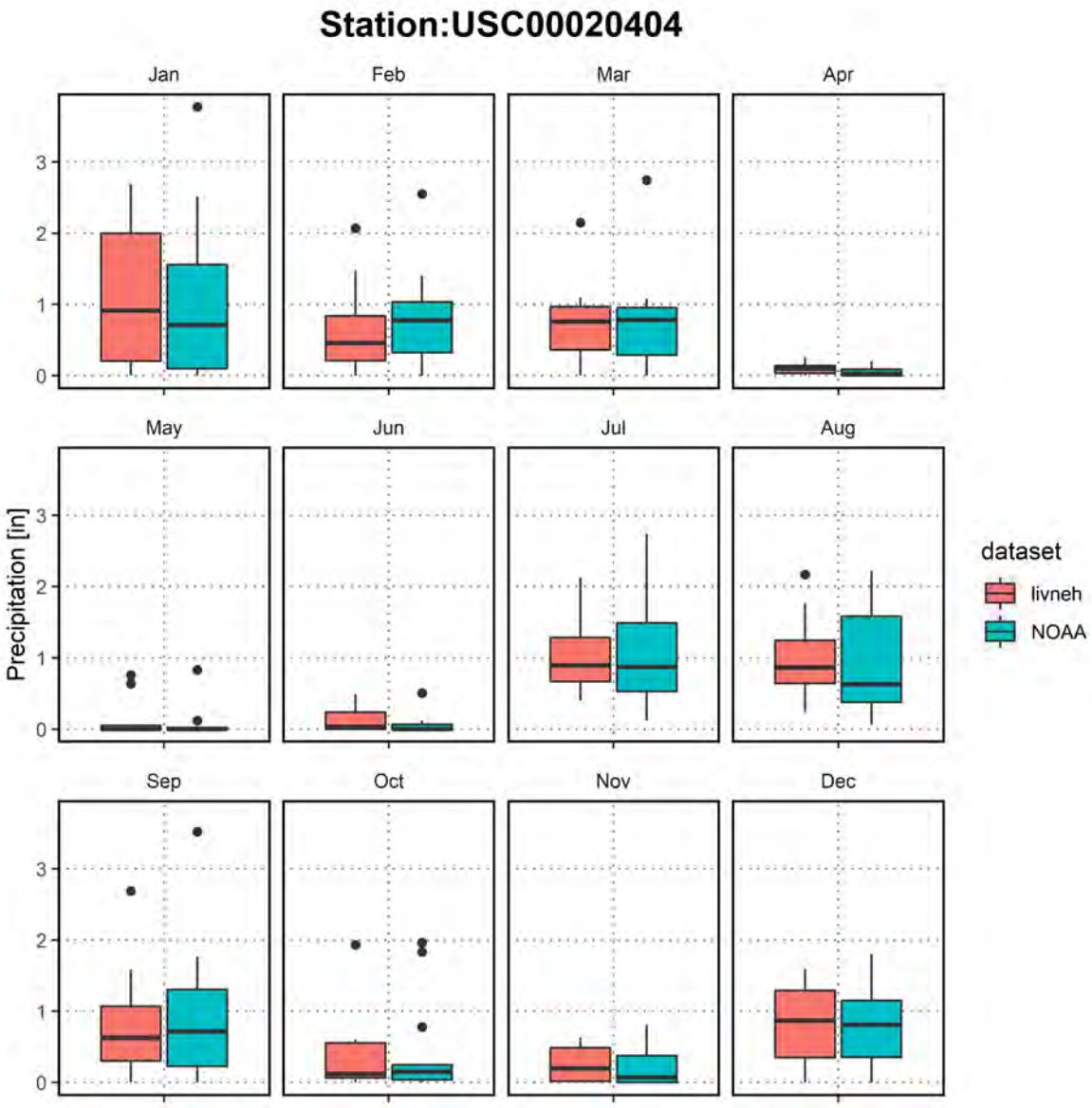

Figure 5. Boxplot of monthly precipitation from 1950 - 2015 at the USC00020204 Arizona City GHCND station, compared to the corresponding L2015 data from the respective grid cell.

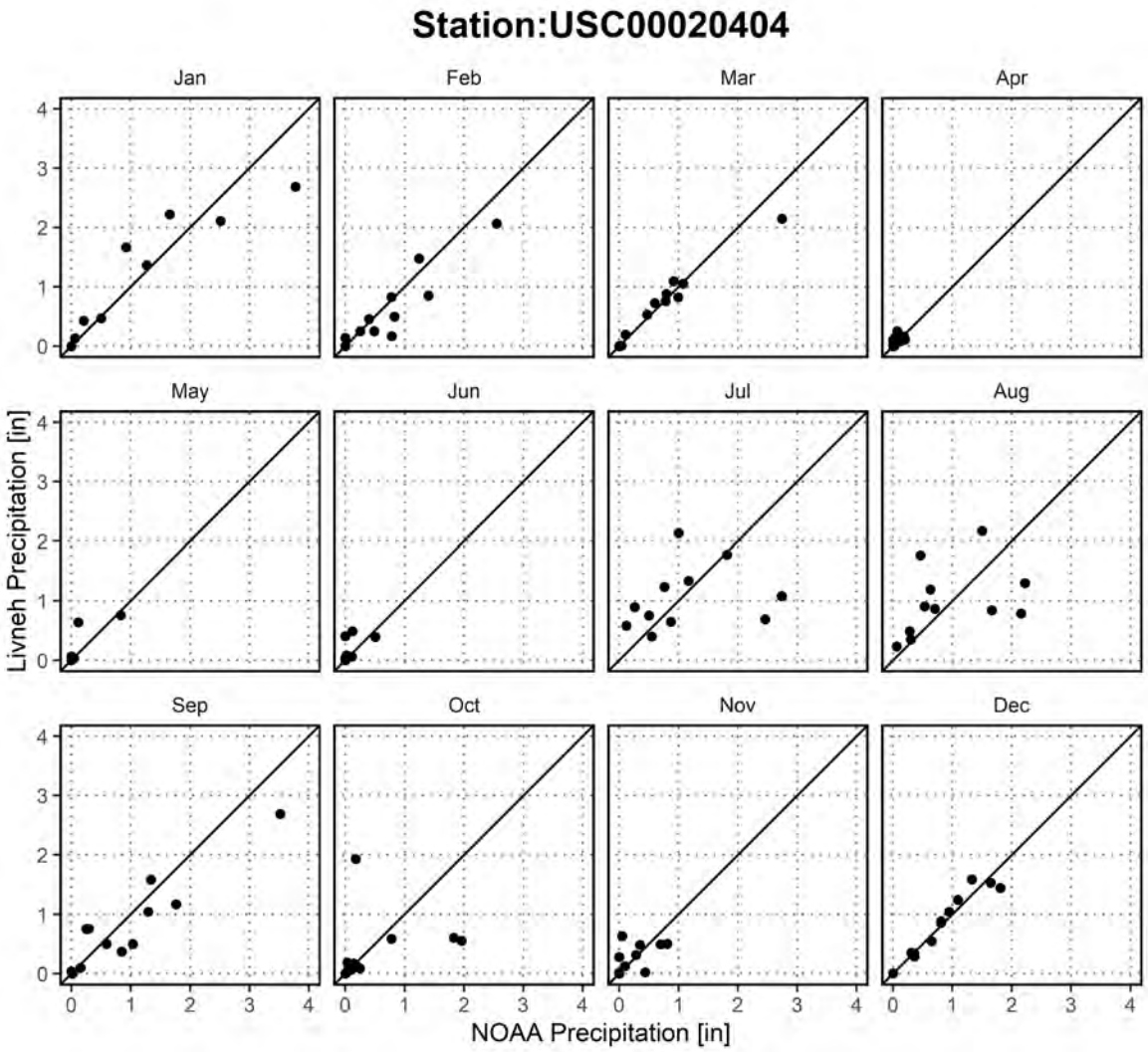

Figure 6. Scatterplot of monthly precipitation from 1950-2015 at the USC00020204 Arizona City GHCND station compared to the corresponding L2015 data from the respective grid cell.

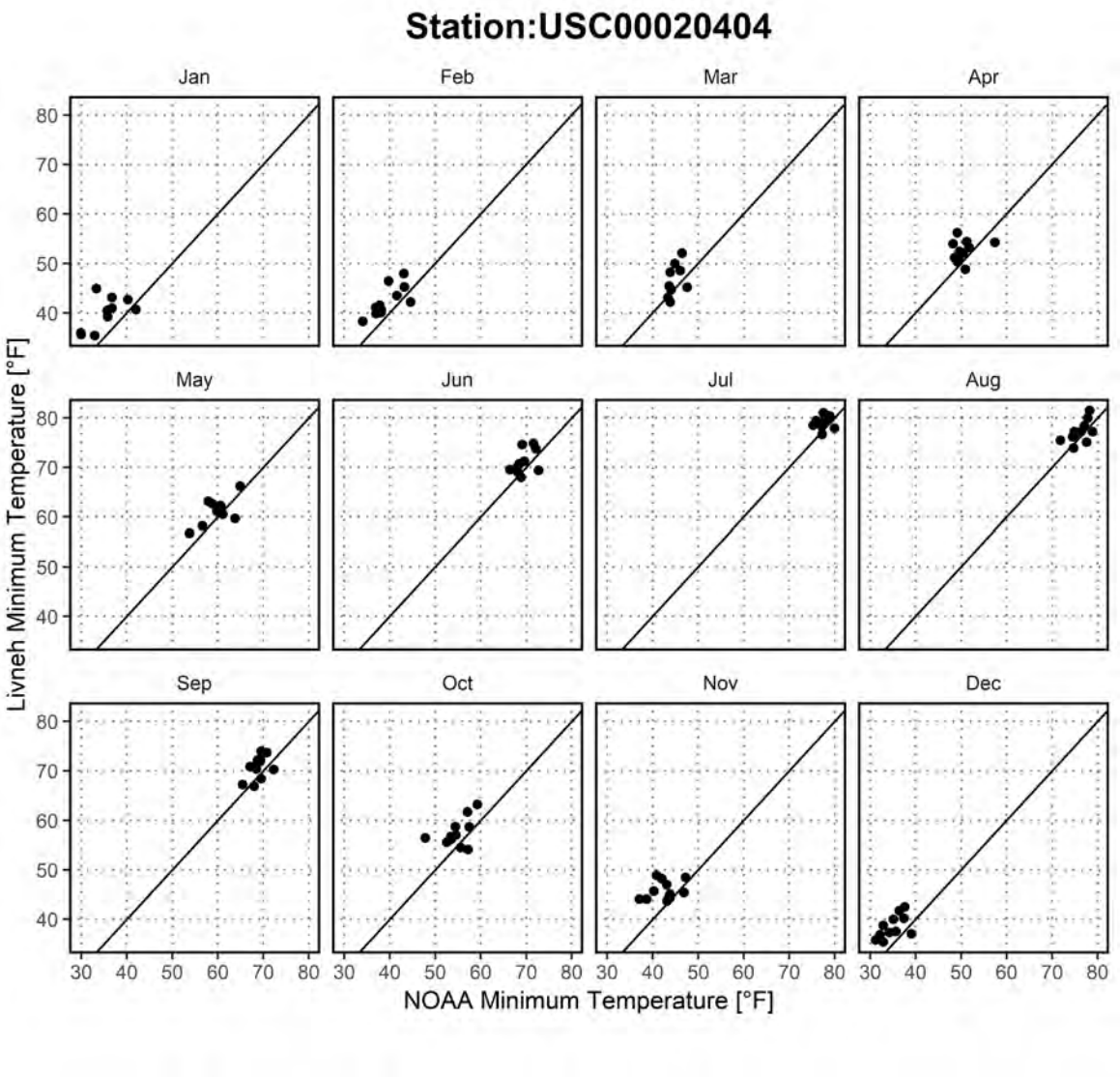

Figure 7. Scatterplot of monthly average minimum temperatures from 1950-2015 at the USC00020204 Arizona City GHCND station compared to the corresponding L2015 data from the respective grid cell.

2.2. Observed Historical Climate Conditions

Observed historical climate conditions were evaluated and characterized from 1915 to 2015 based on the gridded dataset described in Section 2.1. Climate conditions were evaluated on a $1/16^{th}$ degree grid and averaged over the EMS study area.

2.2.1. Observed Temperature

Historical temperatures in the EMS basin study area exhibit little spatial variability—but do show large temporal variability. Spatial variability in annual average temperature over the period 1981-2010 is shown in Figure 8. Annual average temperatures were computed by averaging the daily mean temperature at each grid cell over each water year.[2] The median (50th percentile) annual average temperature ranges from around 73 °F in the northern part of the study area to approximately 70 °F in the central and southern portions of the study area. The 5th percentile annual average temperature (i.e., the coolest 5% of years from 1981-2010) is up to 3 °F cooler than the median annual average temperature, while the 95th percentile (i.e., hottest 5% of years) is up to 3 °F warmer than the median.

Temperatures across the region exhibit strong seasonality. Spatial variability in seasonal average temperatures over the period 1981-2010 is shown in Figure 9; seasonal temperatures were computed by averaging daily mean temperatures over each season. As expected, the coldest temperatures occur during winter (January, February, and March) with the warmest temperatures occurring during summer (July, August, and September). Winters are typically mild with average temperatures around 55 °F and summers are typically hot with average temperatures close to 90 °F.

Monthly variability in temperatures across the EMS study area is illustrated in Figure 10. December and January are normally the coldest months while July and August are typically the warmest months. Monthly mean minimum temperatures range from approximately 37 °F in December to approximately 76 °F in July, while monthly mean maximum temperatures range from approximately 66 °F in December to 105 °F in July.

While there is little spatial variability in annual mean temperature across the EMS study area, there is considerable interannual variability. Timeseries of domain-averaged annual minimum, average and maximum temperatures are shown in Figure 11. Long-term trends in domain-averaged annual temperatures are listed in Table 1. Trends were evaluated over the period 1915-2015 using the Mann-Kendall Test with a significance threshold of 0.05 (95% confidence). The analysis reveals with 99.9% confidence (p-value < 0.001) that maximum, minimum, and average temperatures have all increased over the time period analyzed. Maximum temperatures have increased the least at 2.3 °F per century while minimum temperatures have increased the most at 5.3 °F per century. This may be due to the irrigation practices in the vicinity; as large-scale irrigation has been shown to enhance nighttime warming (i.e., when minimum temperatures are recorded) and cool daytime temperatures (i.e., when maximum temperatures are recorded) (Chen and Jeong, 2018).

[2] For the EMS basin study, a water year is defined as the period from October 1 to September 30. For example, water year 2000 is from October 1, 1999 to September 30, 2000.

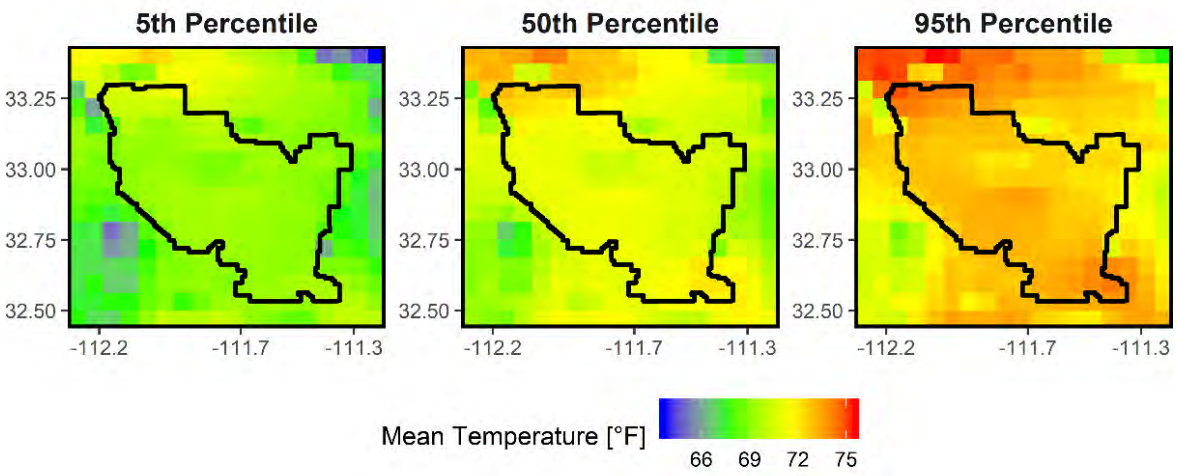

Figure 8. Spatial distribution of the 5th, 50th, and 95th percentiles of annual average temperature from 1981-2010. The outline of the EMS basin study area is delineated by the solid black line with the x and y axes representing latitude and longitude coordinates respectively.

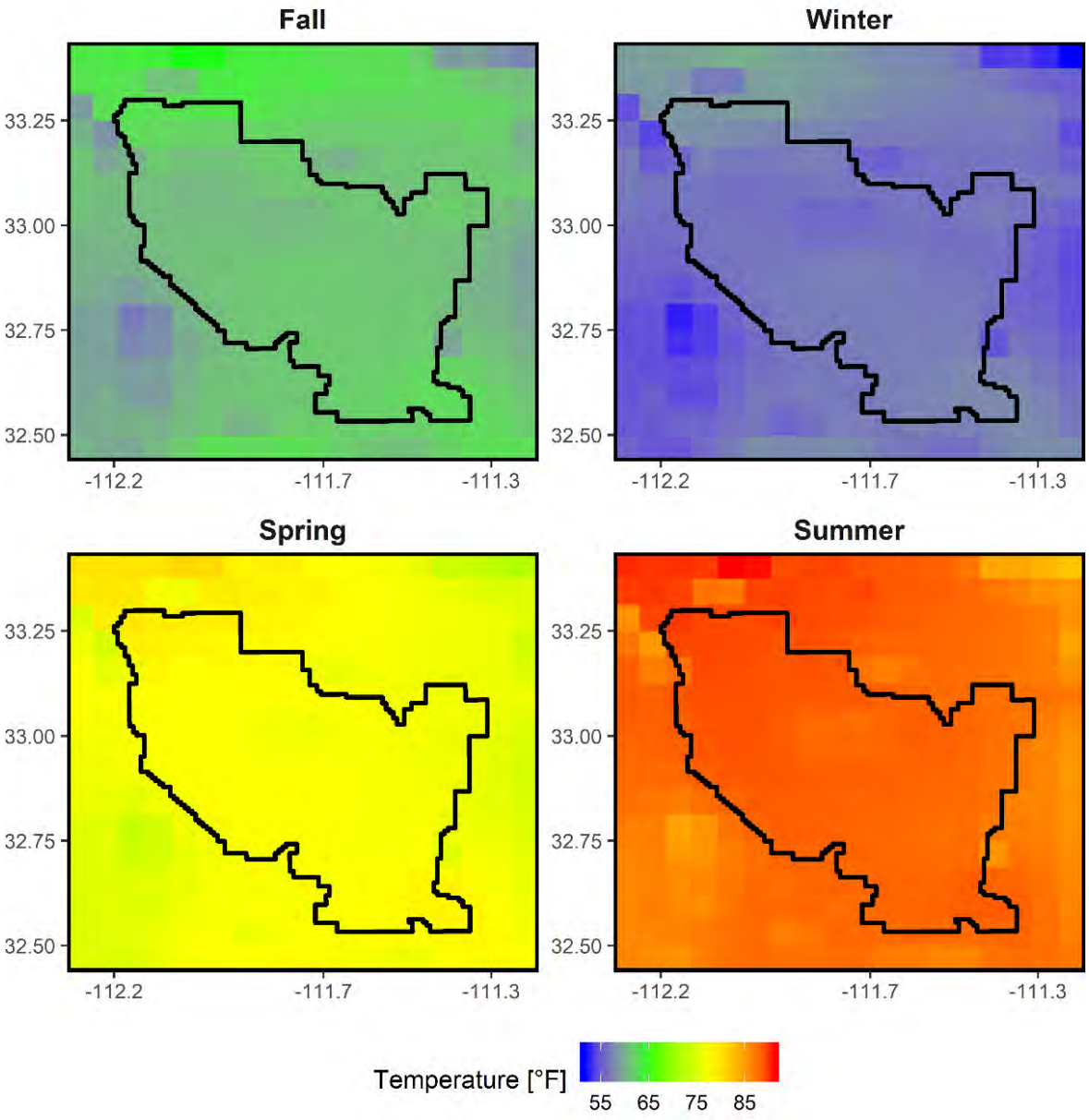

Figure 9. Spatial patterns of seasonal average temperature across the EMS basin study area. Seasonal means are computed for fall (October, November, and December), winter (January, February, and March), spring (April, May, and June), and summer (July, August, and September) for the period 1981-2010. The color scale indicates the magnitude of temperature, with red representing hotter temperatures and blue representing cooler temperatures. The outline of the EMS basin study area is delineated by the solid black line with the x and y axes representing latitude and longitude coordinates respectively.

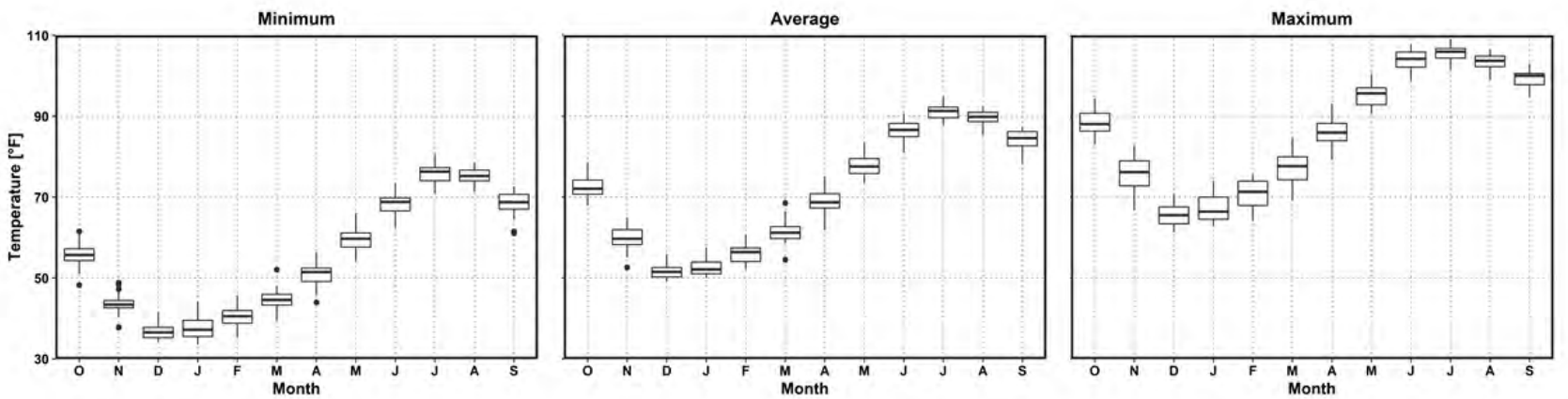

Figure 10. Boxplots of monthly minimum, average and maximum temperatures averaged over the EMS basin study area from the period 1981-2010. Box limits represent the 25th and 75th quartiles; solid lines within each box represent the median; whiskers represent values extending from the 25th and 75th quartiles to values within ± 1.5*(Interquartile Range); and outliers are represented by solid black circles. X-axis labels represent: O = October, N = November, D = December, J = January, F = February, M = March, A = April, M = May, J = June, J = July, A = August and S = September.

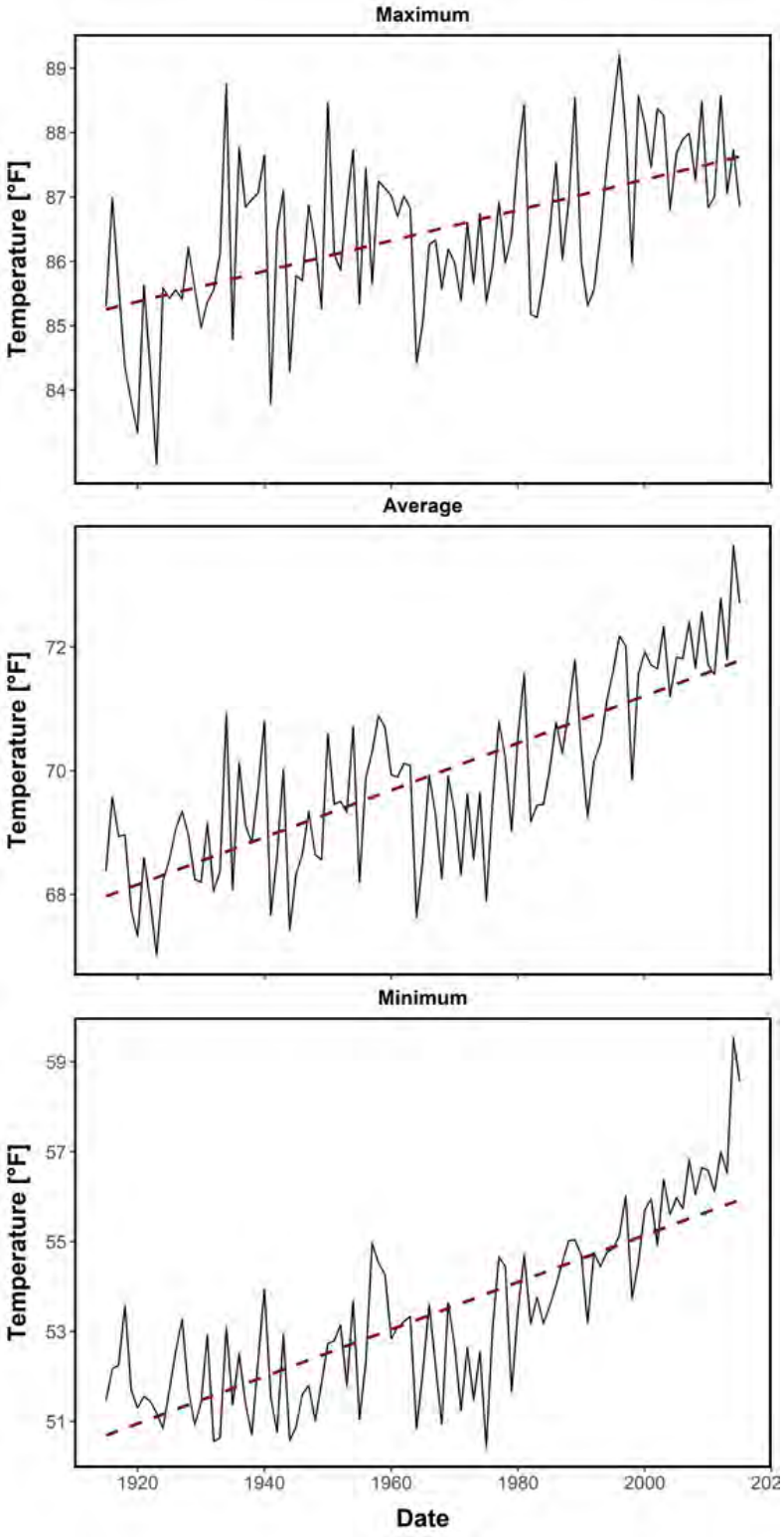

Figure 11. Timeseries of annual minimum, average and maximum temperatures averaged over the EMS basin study area. The solid black line indicates annual averages; the dashed red line indicates the significant trendline ($p < 0.001$) from 1915-2015. Note the different y-axes magnitudes.

Table 1. Observed trends in EMS study area-averaged historical precipitation and temperature over the period of 1915-2015

Historic Change per Century				
	Precip (in)	**Tavg (°F)**	**Tmax (°F)**	**Tmin (°F)**
EMS study area	-0.5	3.9	2.3	5.3

Notes:

- Change per century was calculated using Sen's slope (Hirsch et al., 1991).
- Bold and shaded values indicate a statistically significant increase or decrease over the period 1915-2015, where statistical significance was determined using the Mann-Kendall Test (p -value< 0.05).
- in = inches, Precip = annual precipitation, Tavg = annual mean of daily average temperature, Tmin = annual mean of daily minimum temperature, Tmax = annual mean of daily maximum temperature.

2.2.2. Observed Precipitation

Similar to observed historical temperatures, there is little spatial variability in seasonal and annual mean precipitation across the EMS basin study domain. Spatial variability in annual precipitation over the period of 1981-2010 is shown in Figure 12; annual precipitation was computed by summing the daily precipitation at each grid cell over each water year. The EMS study area lies in an arid part of Arizona, where the 50th percentile (median) annual precipitation is around 10 inches. Extremely wet years can see upwards of 15 inches, while very dry years only receive a couple of inches of precipitation.

Seasonal mean precipitation over the period 1981-2010 is shown in Figure 13; seasonal precipitation was computed by summing daily precipitation over each season. Precipitation in this arid region primarily occurs during two seasons. Winter and the monsoon season (which spans summer and fall) receive the largest amount of precipitation, which averages around 3 inches per season. On average, spring (April, May and June) is the driest season and typically receives an inch or less of precipitation.

Monthly precipitation trends mirror seasonal trends. Boxplots of domain-averaged monthly mean precipitation over the period of 1981-2010 are shown in Figure 14. Most months' median precipitation lies around 1inch, and the three spring months' (April, May, and June) median precipitation are less than half an inch. June is the driest month, and August and December are the wettest months. There is significant interannual variability in monthly precipitation totals, indicated by the presence of many outliers. As the region is arid, all outliers indicate 'wet' years in comparison to average years, although even wet years do not see any months receiving more than 4 inches of precipitation.

Interannual variability in precipitation is shown in Figure 15, where time series for annual precipitation totals across the EMS basin study area are plotted. Annual precipitation totals across the region range from approximately 4 inches in dry years to almost 16 inches in wet years. Wet years are typically followed by dry years and vice versa; consecutive wet years or dry years are rare. Unlike historic temperature trends, there is no significant trend upwards or downwards in precipitation from 1915 to 2015 (Table 1).

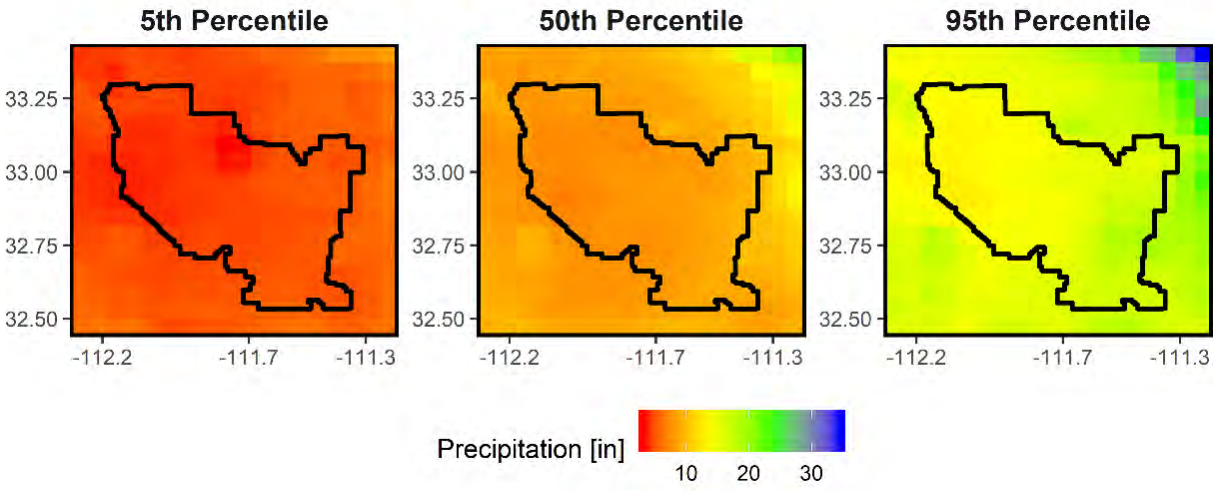

Figure 12. Spatial distribution of the 5th, 50th, and 95th percentiles of annual average precipitation from 1981-2010. The outline of the EMS basin study area is delineated by the solid black line with the x and y axes representing latitude and longitude coordinates respectively.

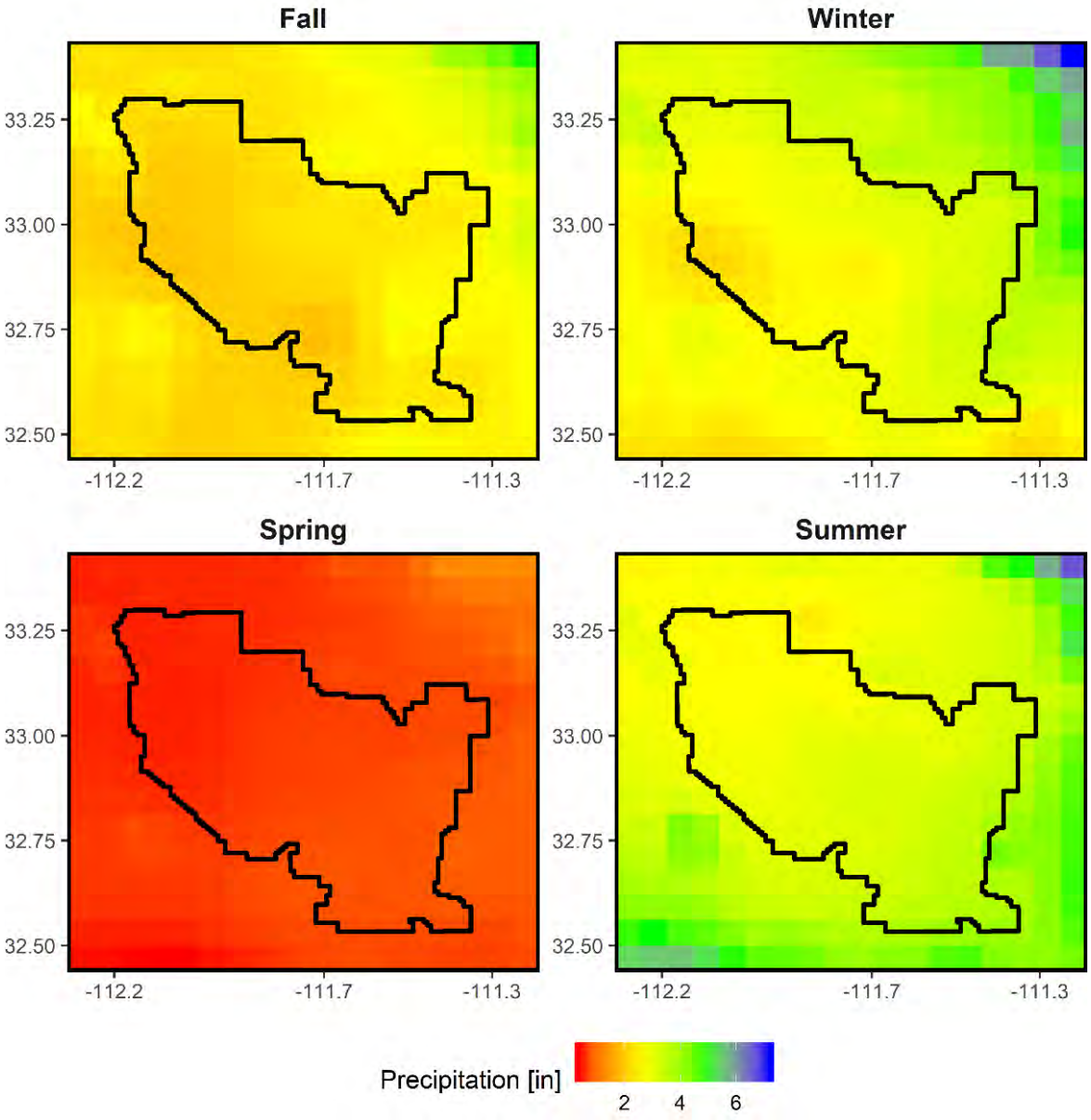

Figure 13. Spatial patterns of seasonal average precipitation across the EMS basin study area. Seasonal means are computed for fall (October, November, and December), winter (January, February, and March), spring (April, May, and June), and summer (July, August, and September) from 1981-2010. The color scale indicates the magnitude of the cumulative precipitation, with red representing less precipitation and blue representing more precipitation. The outline of the EMS basin study area is delineated by the solid black line with the x and y axes representing latitude and longitude coordinates respectively.

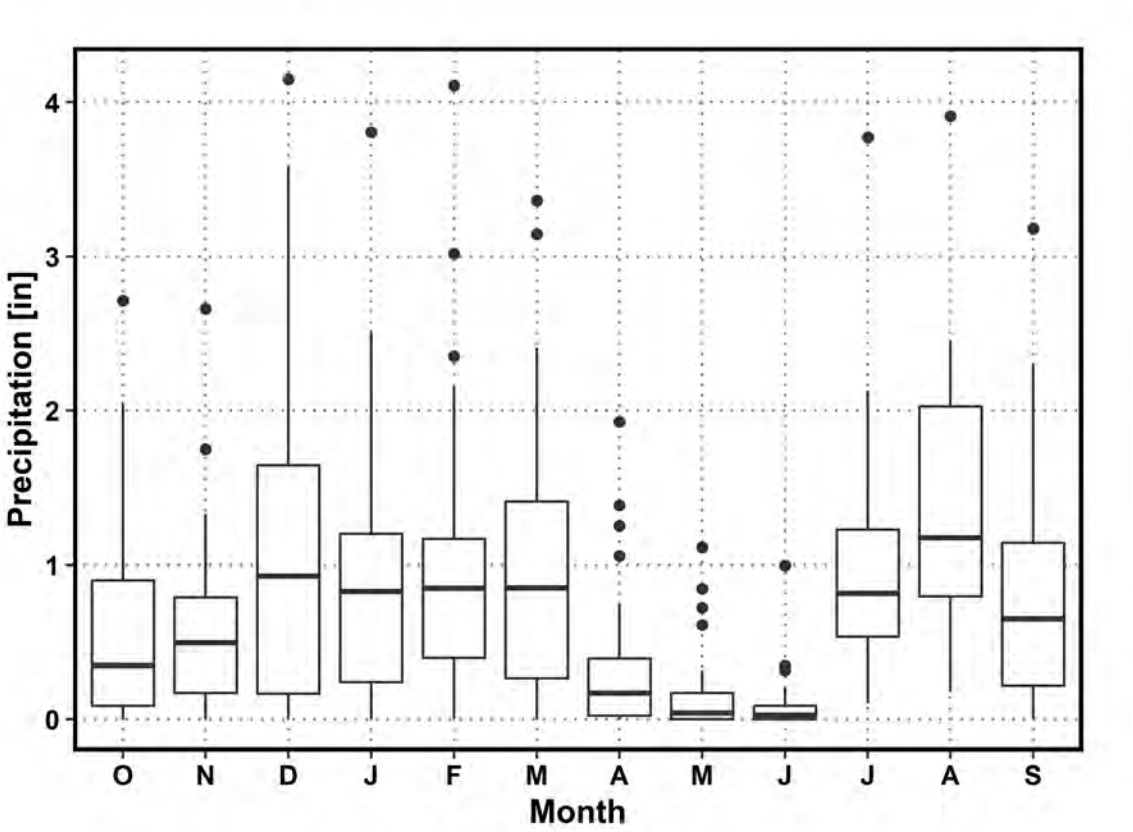

Figure 14. Boxplots of monthly precipitation averaged over the EMS basin study area from 1981-2010. Box limits represent the 25th and 75th quartiles; solid lines within each box represent the median; whiskers represent values extending from the 25th and 75th quartiles to values within ± 1.5*(Interquartile Range); and outliers are represented by solid black circles. X-axis labels represent: O = October, N = November, D = December, J = January, F = February, M = March, A = April, M = May, J = June, J = July, A = August and S = September.

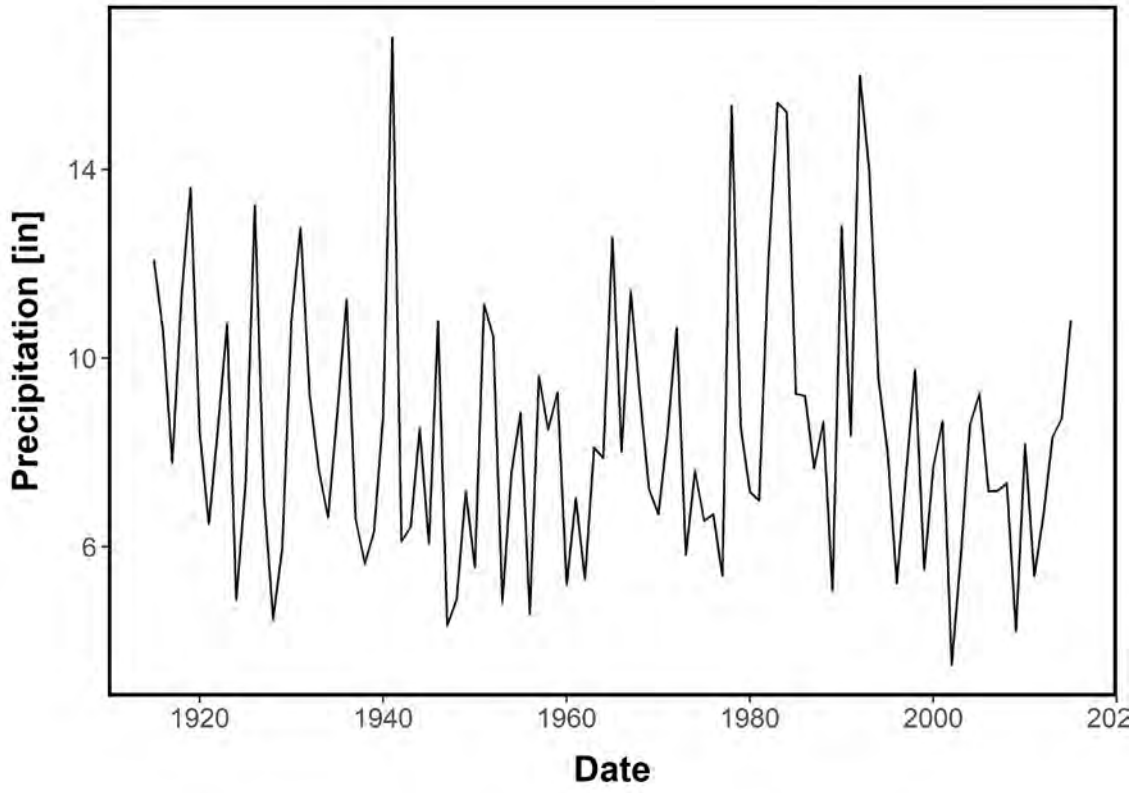

Figure 15. Timeseries of annual precipitation in the EMS basin study area from 1915 to 2015. There is no significant annual trend in precipitation over the time period.

3. Future Climate Projections

Climate change is driven by changes in atmospheric composition, namely increasing concentrations of greenhouse gasses and aerosols. Changes in atmospheric composition affect the earths energy balance—e.g., the reflection or absorption of energy from the sun, re-radiation of energy from the earth surface to the atmosphere, and movement of energy within the earth system—which in turn affect weather and climate at global, regional, and local scales (IPCC, 2013). Because weather and climate conditions directly affect water supplies and demands, climate change directly affects the assumptions underlying water resources planning and decision making.

This section describes projections of future climate conditions in the EMS study area (Figure 1). The climate projection dataset evaluated in this study is described in Section 3.1 and projected future climate conditions are described in Section 3.2.

3.1. Climate Projection Dataset

Analysis of projected future climate conditions in the EMS study area and development of climate scenarios for the EMS Basin Study are based on an ensemble of bias-corrected and spatially-downscaled climate projections. Global climate projections from the Coupled Model Intercomparison Project Phase 5 (CMIP5; Taylor et al., 2012) were bias corrected and downscaled over the continental United States, southern Canada, and northern Mexico using the Localized Constructed Analogs (LOCA) method (Pierce et al., 2014). Bias-corrected and downscaled projections over the study region were obtained from the Downscaled CMIP3 and CMIP5 Climate and Hydrology Projections archive hosted on the Lawrence Livermore National Laboratory Green Data Oasis (Lawrence Livermore National Laboratory [LLNL], 2019). A total of 64 bias-corrected and downscaled climate projections were used in the EMS Basin Study, including projections from 32 different GCMs under two future atmospheric scenarios.

Climate projections are typically developed by using GCMs to simulate changes in the earth's energy balance, and corresponding changes in weather and climate conditions, in response to projected changes in atmospheric composition. The NOAA National Weather Service (NWS) defines climate models as "mathematical model[s] for quantitatively describing, simulating, and analyzing the interactions between the atmosphere and underlying surface (e.g., ocean, land, and ice)" (NWS, 2015). The NOAA Climate Prediction Center (CPC) further describes GCMs as computer models capable of reproducing the earth's weather patterns and that can be used to predict and analyze changes in global weather and climate (CPC, 2015).

The World Climate Research Programme (WCRP) initiated CMIP in 1995 to coordinate international climate modeling efforts focused on better understanding the global climate system, including projected climate changes resulting from changes in atmospheric composition. Facilitating the development, analysis, and application of global climate projections is a key focus of CMIP. To this end, CMIP has developed standards and guidelines to facilitate comparison of GCM results from scientists and research groups around the world. The U.S. Department of Energy's Program for Climate Model Diagnostics and Intercomparison (PCMDI) works closely with CMIP to compile GCM datasets from modeling centers around the globe and make them freely available to the scientific community. The multi-model datasets developed by each phase of CMIP constitute the primary source of climate projections used by the international climate science community to evaluate climate change and its potential impacts (IPCC, 2013).

At the time of this report, the CMIP5 Multi-Model Dataset is the best-available source of global climate projections for the 21st century, as CMIP6 projections are still being developed and archived. The multi-model dataset includes climate projections from a total of 61 GCMs from 27 modeling centers representing 15 countries around the world. CMIP5 projections of

21st century climate are based on two primary scenarios of future greenhouse gas and aerosol emissions, referred to as Representative Concentration Pathways (RCP) 4.5 and 8.5. RCP 8.5 represents a "higher emissions" future emissions trajectory where greenhouse gas concentrations continue to rise unchecked. RCP 4.5 represents a medium-level future emissions trajectory where greenhouse gas emissions peak around 2040 and decline thereafter. RCPs 4.5 and 8.5 have been widely used to evaluate climate change and its impacts around the globe. RCPs do not represent forecasts or projections of future atmospheric composition; rather, RCPs represent plausible future trajectories of atmospheric composition under various assumption of population growth, economic growth, technology development, and governmental policies regarding greenhouse gas emissions.

The spatial (grid) resolutions of GCM-based climate projections from the CMIP5 multi-model dataset is typically on the order of one to two degrees latitude by one to two degrees longitude, or roughly 110-220 kilometers (km) by 110-220 km over mid-latitudes. Local weather and climate conditions, by contrast, vary significantly across a degree of latitude or longitude due to variations in topography, land cover, and many other factors that affect local climate. In addition, GCM-based projections generally exhibit biases in simulated climate conditions that stem largely from the coarse spatial resolution of GCMs and the use of simplified parameterizations to represent physical processes that cannot be explicitly represented at the GCM grid scale. Coarse spatial resolution and biases limit the direct application of GCM-based climate projections to local and basin-scale analyses.

A broad range of methods have thus been developed to bias-correct and downscale GCM-based climate projections to support local and basin-scale analyses, planning, and decision making. Climate projections selected for the EMS Basin Study were downscaled using the Localized Constructed Analogs (LOCA) downscaling procedure. The LOCA procedure uses the L2015 grid observational dataset (see Section 2.1) to develop relationships between large-scale and local-scale weather and climate conditions. These relationships are then used "downscale" coarse-resolution GCM projections onto a finer resolution grid—i.e., observed relationships between large-scale and local-scale weather and climate are used to estimate projected climate conditions on a finer-resolution grid from coarser-resolution GCM projections (Pierce et al., 2014).

The LOCA procedure was used to downscale GCM projections to a finer resolution of 1/16° latitude by 1/16° longitude (approximately six kilometers by six kilometers). The LOCA procedure was applied at a daily timestep. Compared to other downscaling methods, the LOCA procedure has been shown to preserve regional patterns of projected changes in precipitation and temperature. In addition, the LOCA procedure better preserves extreme hot days and heavy precipitation events, which are often damped by other downscaling methods. An ensemble of LOCA projections is available from Dr. David Pierce at the Scripps Institution of Oceanography. The LOCA ensemble includes bias-corrected and downscaled projections of daily precipitation, daily minimum temperature, and daily maximum temperature for the period 1950-2099. Projections are provided at a spatial resolution of 1/16° latitude by 1/16° longitude and cover the continental United States and portions of Mexico and Canada. The LOCA ensemble includes climate projections from 32 GCMs under the RCP 4.5 and RCP 8.5 emissions scenarios for a total of 64 climate projections.

3.2. Projected Future Climate Conditions

Projected future climate conditions were evaluated and characterized based on the LOCA ensemble of downscaled climate projections described above in Section 3.1. Projected climate was compared between the 30-year historic period (1981-2010) and two future periods centered around 2060 (2045-2074) and 2080 (2065-2094). Similar to observed historical climate conditions, projected future climate conditions were evaluated on a 1/16° grid and averaged over the EMS study area.

3.2.1. Future Temperature

All LOCA projections indicate a significant increase in annual and seasonal average temperatures over the EMS basin study area by the end of the 21st century. The range of projected basin-averaged seasonal and annual average temperatures are shown in Figure 16. The ensemble median of 64 LOCA projections suggests that increases in temperature over the EMS study area will be greater during the spring, summer and fall months, with temperatures increasing by approximately 6.3 - 6.4 °F by 2080 (Table 2). Projected warming is least during the winter months, with a median projected increase of 5.5 °F by 2080. Projections of daily maximum and minimum temperatures suggest different seasonal trends, with significantly more warming occurring during the summer months as compared to the spring and fall months (Table 2). Maximum temperatures are projected to increase more than minimum temperatures would during the summer months, with up to a 6.6 °F increase by 2080. However, minimum temperatures are projected to increase more than maximum temperatures would during the spring, fall, and winter months.

All LOCA projections indicate that warming will be largely consistent throughout the EMS study area. The spatial distribution of projected change in annual average temperature by 2080 from each of the 64 LOCA projections is shown in Figure 17. While all projections suggest uniform warming across the study area, there is considerable variability in the magnitude of projected warming between individual projections. Projected warming by 2080 ranges from about 2 °F to 11 °F. The range of projected warming reflects uncertainties in future atmospheric composition (i.e., differences between RCP 4.5 and RCP 8.5) as well as uncertainties in how global, regional, and local climate will respond to future changes in atmospheric composition.

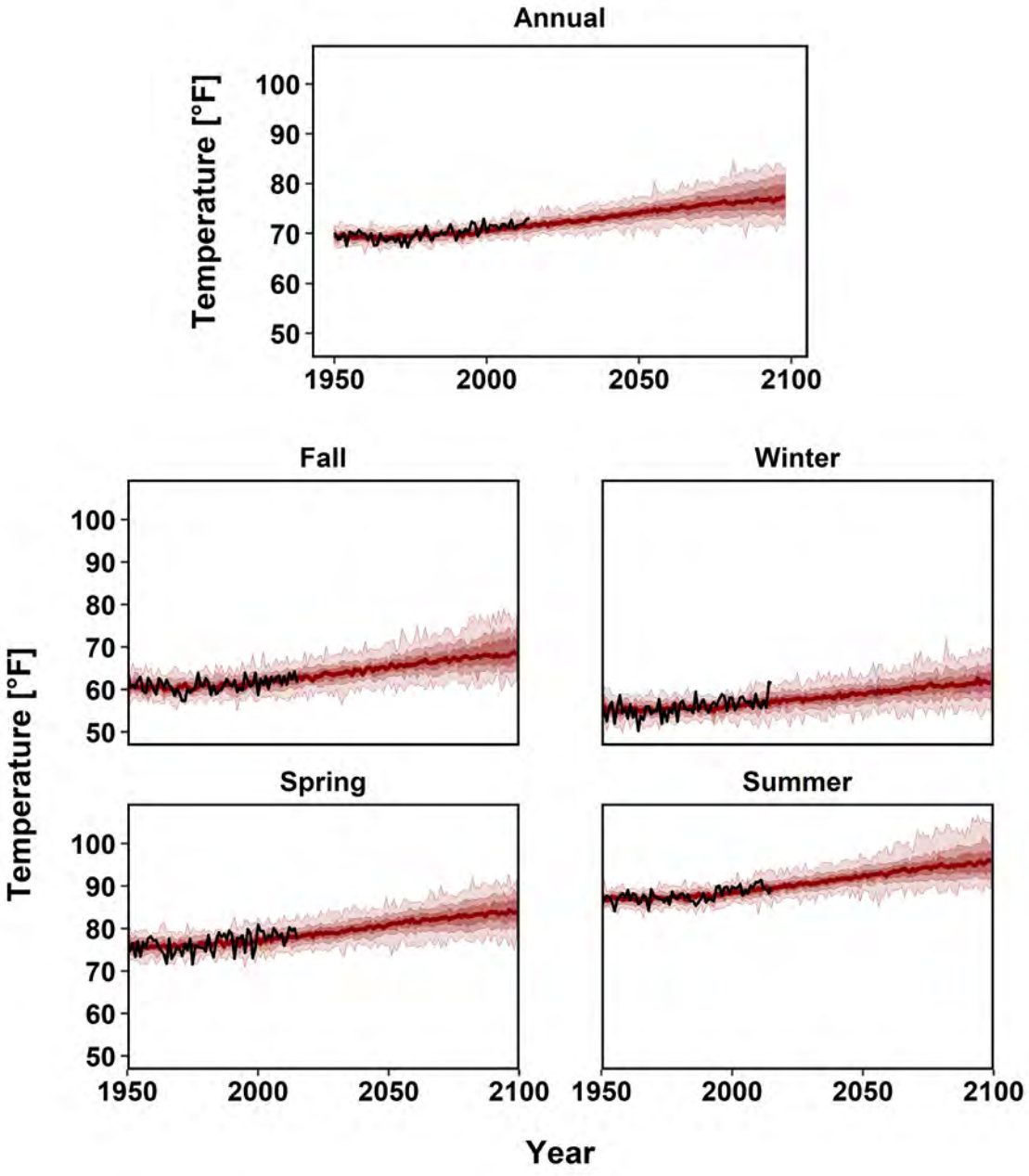

Figure 16. Timeseries of area-weighted, domain-averaged seasonal and annual projections of average air temperature over the EMS basin study area for 1950-2099. The dark red line shows the ensemble median; dark red shading indicates the range between ensemble 25th and 75th percentile values; medium red shading indicates the range between ensemble 10th and 90th percentile values; light red shading indicates the maximum and minimum ensemble values; black line shows observed Livneh dataset historical values.

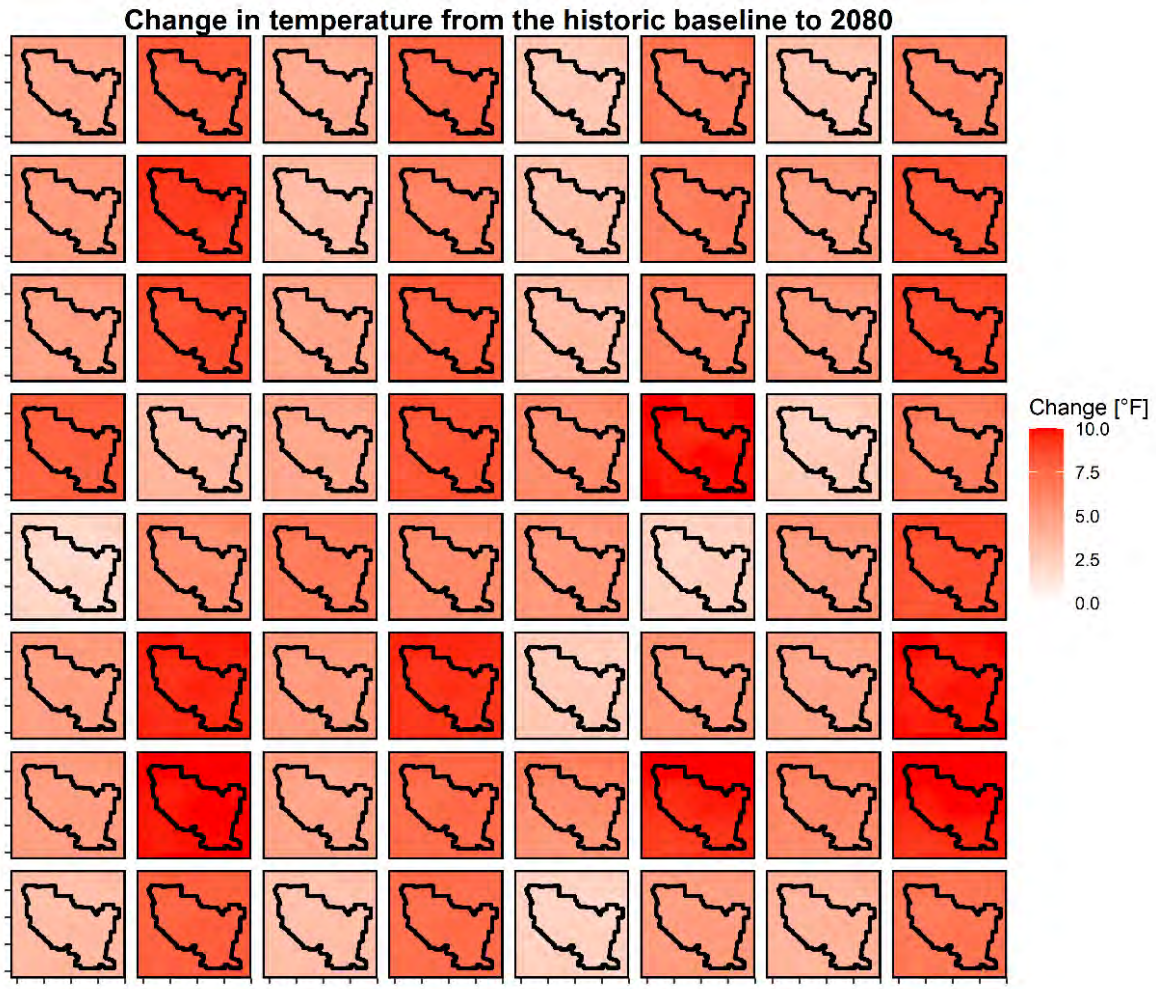

Figure 17. Spatial distribution over the EMS study area of the average change in annual mean temperature between historical (1981-2010) and future (2065 -2094) periods for each of the 64 LOCA projections. Axes are longitudinal and latitudinal coordinates. The outline of the EMS basin study area is delineated by the black solid line.

Table 2. Ensemble median projected change in basin-averaged precipitation and temperature over the EMS study area from 1981-2010 to 2065-2094

Projected Future Change in Climate Variables				
	Precip (in)	**Tavg (°F)**	**Tmax (°F)**	**Tmin (°F)**
Fall	-6.4	6.3	5.9	6.0
Winter	-10.5	5.5	4.3	4.9
Spring	-35.9	6.4	5.6	6.0
Summer	-3.9	6.3	6.6	6.5

Notes:

- Projected change was calculated by comparing the basin-averaged ensemble-median projection for the EMS study area between the historical period 1981-2010 and future period 2065-2094.
- % Δ = percent change, Precip = percent change in basin-averaged seasonal mean precipitation, Tavg = change in basin-averaged seasonal mean daily surface air temperature, Tmax = change in seasonal mean of daily maximum surface air temperature and Tmin = change in seasonal mean of daily minimum surface air temperature.

3.2.2. Future Precipitation

In contrast to temperature projections, there is no clear trend in projected future precipitation over the EMS study area. The range of projected domain-averaged annual and seasonal precipitation over the EMS study area is shown in Figure 18. More than half of the 64 projections indicate an overall decrease in annual precipitation with a median projected decrease of 5.3% by 2080. However, as the EMS basin study area is an arid environment, the median projected decrease in annual precipitation only equates to 0.4 inches. The average annual precipitation during the baseline period (1981-2010) was 8.4 inches while the projected average annual precipitation during 2080 (2065-2094) is 8.0 inches.

Projected seasonal trends in precipitation are similar to annual trends, with a median projected decrease during all seasons. Spring is projected to have the largest decrease in precipitation of up to 36%, while summer is projected to have the smallest decrease in precipitation with a 3.9% decrease (Table 2). This suggests that the driest season will become even drier with little to no precipitation occurring during the months of April, May, and June.

The large uncertainty in projected annual precipitation is further illustrated in Figure 19, which shows the spatial distribution over the EMS study area of the projected change in annual precipitation by 2080. Several projections suggest a decrease in annual precipitation of up to 40%, while others suggest an increase in annual precipitation of around 20%. In addition, some projections indicate a projected increase over some parts of the study area, while others indicate a projected decrease. The large uncertainty in projected precipitation changes suggests that multiple climate projections or scenarios need to be used to represent the potential impacts of climate change on water supplies within the study area

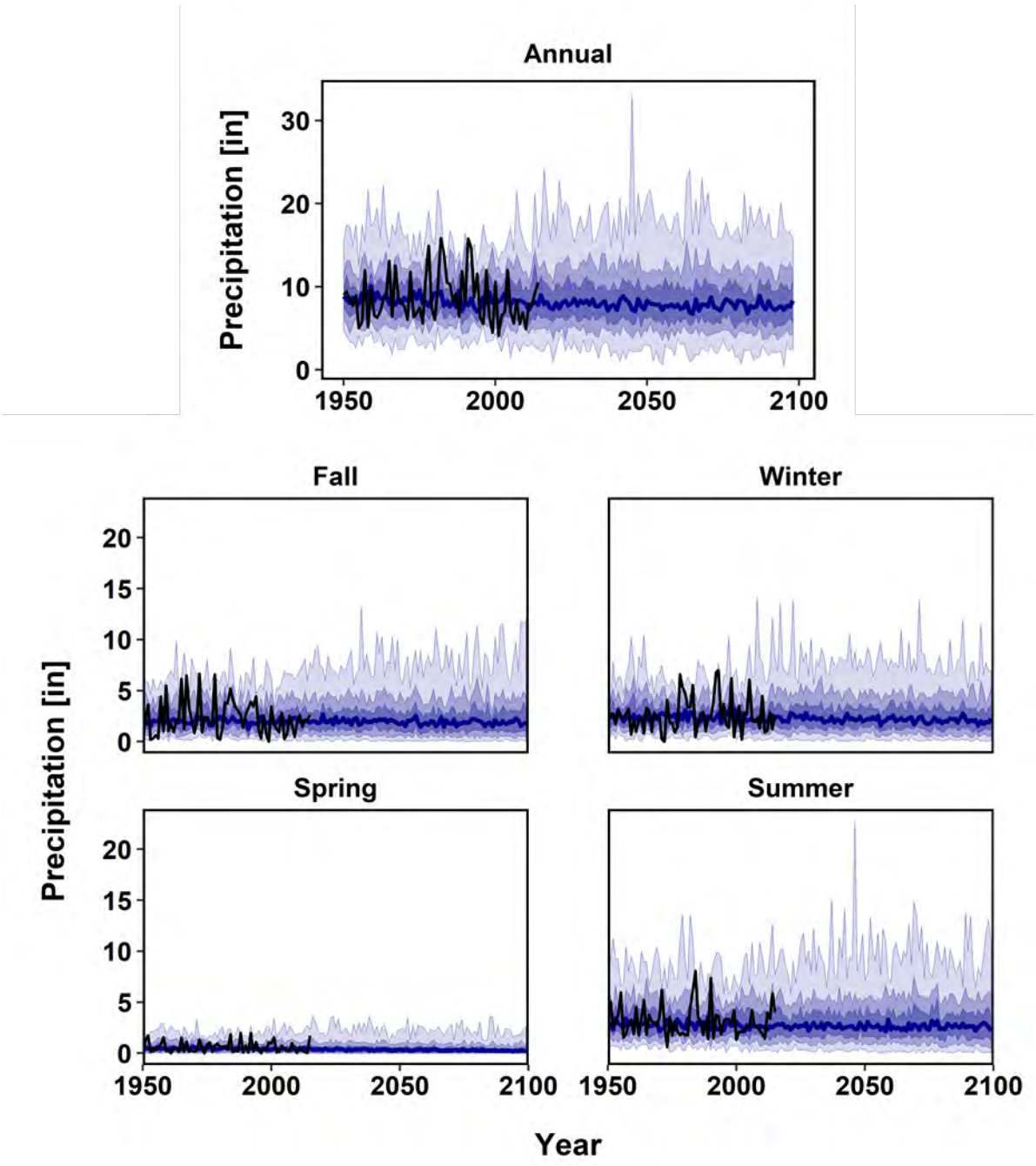

Figure 18. Timeseries of area-weighted, domain-averaged seasonal and annual precipitation over the EMS basin study area for 1950-2099. The dark blue line shows the ensemble median; dark blue shading indicates the range between ensemble 25th and 75th percentile values; medium blue shading indicates the range between ensemble 10th and 90th percentile values; light blue shading indicates the maximum and minimum ensemble values; black line shows observed Livneh dataset historical values.

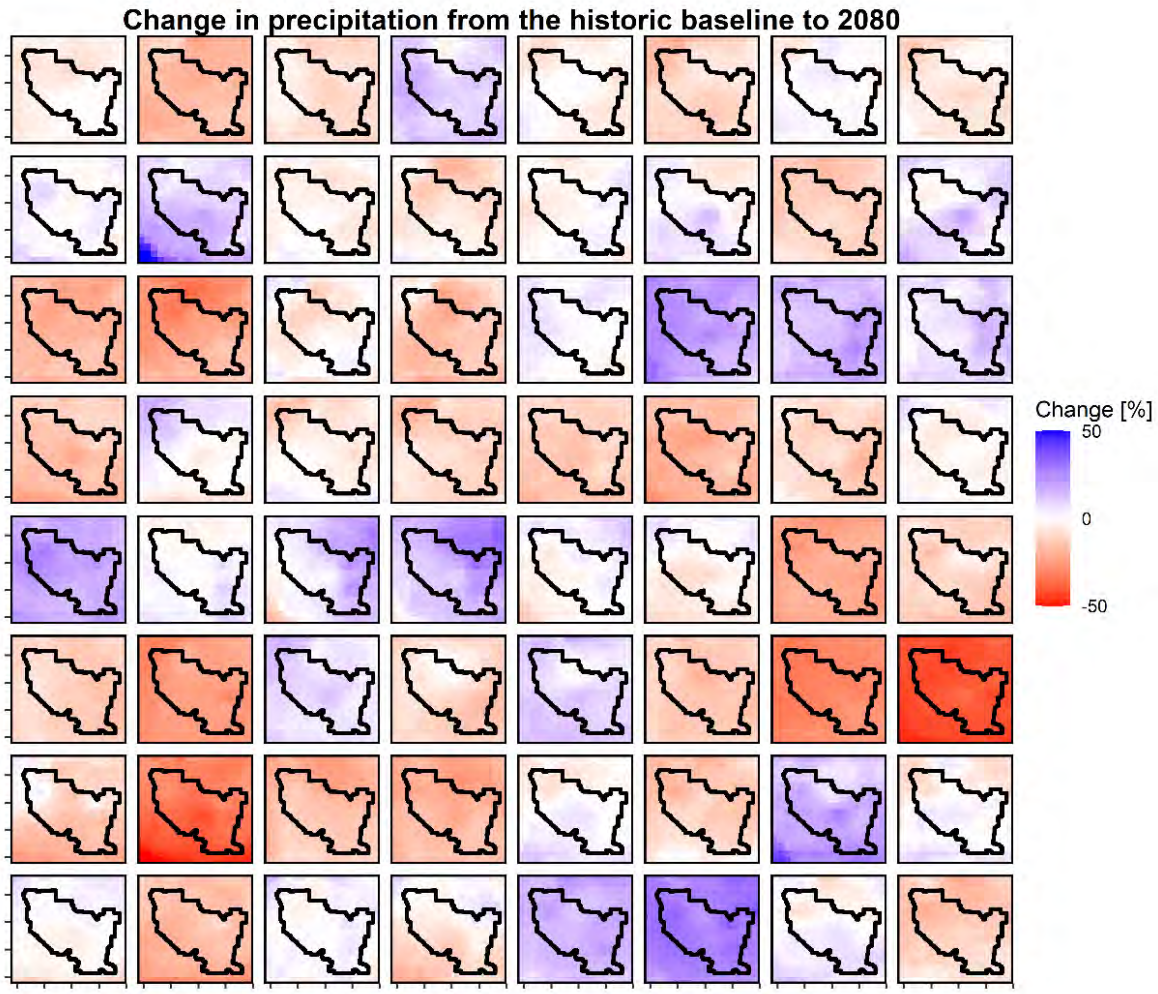

Figure 19. Spatial distribution over the EMS study area of the average change in annual precipitation between historical (1981-2010) and future (2065-2094) time periods for each of the 64 LOCA projections. Axes are longitudinal and latitudinal coordinates. The outline of the EMS basin study area is delineated by the black solid line.

4. Future Climate Scenarios

A suite of future climate scenarios was developed as the basis for analyzing future water supplies and demands in the EMS study area. Climate scenarios were developed using the ensemble-informed hybrid-delta method (HDe; Bureau of Reclamation [Reclamation], 2010).

In the context of water resources planning, climate scenarios provide several advantages compared to direct use of downscaled climate projections. Climate scenarios distill the range of uncertainty across a large ensemble of GCM-based climate projections into a relatively small number of scenarios for detailed analysis. Climate scenarios thus allow for consideration of uncertainty in future climate conditions while significantly reducing the number of future conditions that must be modeled and analyzed. Climate scenarios can also be developed to align with specific planning horizons of interest, such as defined levels of development or build-out conditions. Lastly, the HDe methodology retains the sequencing of observed historical climate variability—e.g., droughts and pluvials—but with climate conditions adjusted to reflect projected climate change. Retaining historical climate variability facilitates comparison of drought and surplus conditions between historical climate and future climate scenarios. In addition, retaining historical climate variability reduces potential biases in GCM-simulated interannual and decadal variability, which is not explicitly addressed in most downscaling and bias correction procedures.

EMS climate scenarios were developed based on projected changes in precipitation and temperature between a historical baseline period (1981-2010) and two future periods: 2045-2074 (centered around 2060) and 2065-2094 (centered around 2080). These two future periods were chosen as the study partners were interested in future conditions centered around 2060 along with a later time horizon for comparison. For each future period, a suite of five climate scenarios was developed to reflect the uncertainty in projected climate change across the ensemble of 64 LOCA projections analyzed in the EMS Basin Study (see Section 3). The five climate scenarios for each future time period include Warm-Wet (WW), Warm-Dry (WD), Hot-Wet (HW), Hot-Dry (HD), and Central Tendency (CT) scenarios.

A baseline scenario was developed by de-trending observed data such that the data are representative of mean climate conditions and interannual climate variability over the historical base period (1981-2010). The baseline scenario therefore represents a 101-year record of observed historical climate variability that is consistent with monthly and annual mean climate conditions over the historical reference period (1981-2010). Similarly, each future climate scenario represents a 101-year record of climate variability that reflects projected changes in monthly and annual mean climate conditions between the historical reference period and a given future period.

This section describes the climate scenarios developed to represent projected future climate conditions over the EMS study area. Climate scenarios are used as the basis for developing recharge scenarios, which in turn are used to analyze future water supplies, demands, and

management in the EMS Basin Study. The HDe climate scenario methodology is described in Section 4.1 and the resulting climate scenarios are characterized in Section 4.2.

4.1. Climate Scenario Methodology

The HDe climate scenario methodology was developed by Reclamation as a basis for evaluating the impacts of projected climate change on water supplies, demands, and management. The HDe methodology has been applied in numerous studies, including several Impact Assessments and Basin Studies carried out under the WaterSMART Program (Reclamation, 2016b, 2016a, and 2020).

The HDe methodology involves adjusting a dataset of observed historical precipitation and temperature to remove historical trends, then adjusting this de-trended dataset to reflect projected changes in climate conditions between a historical reference period and a selected future period. The de-trended observed historical dataset is referred to as the baseline scenario. The baseline scenario reflects observed historical climate variability from 1915-2015, adjusted such that monthly and annual mean climate conditions over the full 101-year period are consistent with the historical reference period (1981-2010). Each future scenario was based on projected climate change derived from a subset (or sub-ensemble) of climate projections. Precipitation and temperature from the baseline scenario were adjusted by applying quantile-based climate change factors that represent projected changes in the probability distributions of precipitation and temperature between the historical and future time periods. Similar to the baseline scenario, future climate scenarios reflect historical climate variability over the period 1915-2015. However, future scenarios were adjusted so that monthly and annual mean climate conditions reflect projected changes in climate conditions between the historical reference period (1981-2010) and a selected future period (2045-2074 or 2065-2094).

The HDe methodology consists of three primary steps: selection of climate projections for each scenario; development of quantile-based climate change factors; and application of quantile-based climate change factors to a de-trended observed historical climate dataset. Each of these steps is summarized below.

4.1.1. Selection of Climate Projection Subsets

Each HDe climate scenario was developed based on a subset of projections from the LOCA ensemble (see Section 3.1. *Climate Projection Dataset*). The projections in each subset were determined based on the distribution of projected changes in basin-average annual mean precipitation and temperature over the EMS study area between a historical base period and a selected future period.

First, timeseries of basin-average annual precipitation and temperature over the EMS study area were computed for each of the 64 bias-corrected and downscaled projections from the LOCA ensemble. Timeseries of annual precipitation and temperature were then averaged over a specified historical base period and selected future periods. The EMS climate scenarios were developed using the historical base period 1981-2010 and two future periods: 2045-2064 and 2065-2094. This resulted in period-mean, basin-average precipitation and temperature for each projection over each time period.

Next, projected changes in period-mean, basin-average precipitation and temperature were computed for each projection for each future time period. Projected changes in temperature were computed as the simple difference between a given future period and the historical base period. Projected changes in precipitation were computed as the percent difference between a given future period and the historical base period. This resulted in differences in period-mean basin-average precipitation and temperature for each projection for each future time period.

Projected changes in precipitation and temperature between the historical base period 1981-2010 and the future period centered around 2080 are illustrated by the points in Figure 20. Each point in Figure 20 represents the projected change in period-mean, basin-average temperature (x-axis) and precipitation (y-axis) for one projection from the LOCA ensemble.

The 10th, 50th, and 90th percentiles of projected changes were then computed for each time period. The 10th percentile change in precipitation represents the drier extent of projected precipitation changes, the 50th percentile represents the median or center of the range of projected precipitation change, and the 90th percentile represents the wetter extent. Similarly, the 10th percentile change in temperature represents the lower extent of projected temperature changes, the 50th percentile represents the median or center of the range of projected temperature changes, and the 90th percentile represents that higher extent.

The 10th, 50th, and 90th percentiles of projected changes in precipitation and temperature are illustrated by the dotted and dashed lines in Figure 20. The vertical dotted lines in Figure 20 represent the 10th and 90th percentiles of projected changes in temperature and the horizontal dotted lines represent the 10th and 90th percentiles of projected changes in precipitation. The vertical thick dashed line in Figure 20 represents the 50th percentile (median) projected change in temperature and the horizontal thick dashed line represents the 50th percentile (median) projected change in precipitation.

Lastly, the subset of projections used in a given scenario was selected based on the distance between points representing the projected changes in precipitation and temperature from individual projections and points representing the intersection of selected percentiles. For example, projections were selected for the Central Tendency (CT) scenario based on the distance between each individual point and the point representing the 50th percentile (median) projected change in temperature and the 50th percentile (median) projected change in precipitation. Projected changes in temperature (˚F) are plotted on the x-axis and projected changes in precipitation (%) are plotted on the y-axis. Due to the different units of the abscissa and ordinate, the distance between points is computed as the Mahalanobis distance rather than the Euclidian distance. The Mahalanobis distance is a unitless and scale-invariant measure of distance that takes into account covariance within a dataset.

A subset of six LOCA projections was selected for each of the five EMS scenarios. Subsets were selected based on the projections nearest to the intersection of selected

percentiles:

- Warm-Dry (WD): 10^{th} percentile precipitation
10^{th} percentile temperature
- Warm-Wet (WW): 90^{th} percentile precipitation
10^{th} percentile temperature
- Central Tendency (CT): 50^{th} percentile precipitation
50^{th} percentile temperature
- Hot-Dry (HD): 10^{th} percentile precipitation
90^{th} percentile temperature
- Hot-Wet (WW): 90^{th} percentile precipitation
90^{th} percentile temperature

The resulting subsets are illustrated by the color of the points Figure 20 and the corresponding polygons. Projections selected for the WD scenario are represented by yellow points and the yellow polygon. Projections selected for the WW scenario are in blue, projections selected for the CT scenario are in green, projections selected for the HD scenario are in red, and projections selected for the HW scenario are in purple. The subset selection process illustrated in Figure 20 was repeated two times to develop climate scenarios for the EMS, once for each of the selected future time periods: 2045-2064 and 2065-2094.

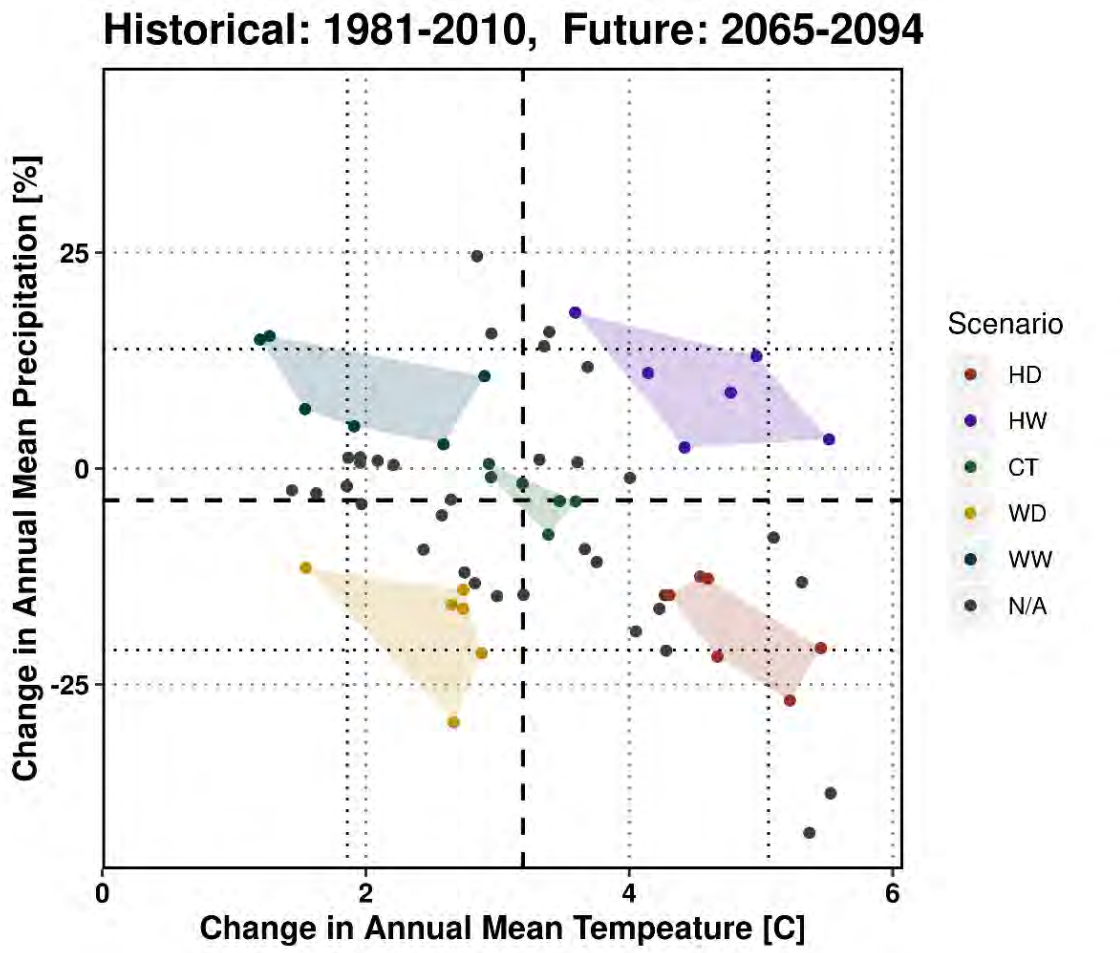

Figure 20. Scatterplot of projected changes in period-mean, basin-average temperature (x-axis) and precipitation (y-axis). Each point represents one projection from the LOCA ensemble; the color of each point represents the scenario to which that point is assigned (red = HD; brown = HW; green = CT; purple = WD; blue = WW; black = N/A). Vertical dotted lines represent the 10th and 90th percentiles of projected changes in temperature; horizontal dotted lines represent the 10th and 90th percentiles of projected changes in precipitation. Vertical thick dashed lines represent the 50th percentile (median) projected change in temperature; horizontal thick dashed line represents the 50th percentile (median) projected change in precipitation.

4.1.2. Development of Quantile-Based Climate Change Factors

HDe climate scenarios are developed by adjusting observed historical precipitation and temperature to reflect projected climate change between a historical base period and a selected future period. Projected climate change was represented through quantile-based change factors, which represent the projected change in probability distributions of precipitation and temperature between historical and future periods.

Quantile-based change factors were developed for each scenario from the corresponding subset of LOCA projections (see Section 4.1.1). Change factors were computed and applied on a monthly basis to capture differences in projected climate change during

different parts of the year. In addition, change factors were computed and applied on a grid-cell-by-grid-cell basis to capture spatial differences in projected climate change.

To develop quantile-based change factors, monthly precipitation and temperatures were computed from daily LOCA projections. Monthly precipitation and temperature were computed for each grid cell over the EMS basin study area. Monthly precipitation was computed as the total accumulated precipitation over each month. Monthly temperatures were computed as averages of daily maximum temperature and daily minimum temperature over each month. In addition, monthly mean diurnal temperature range (DTR) was computed as the average of the daily DTR over each month, where the daily DTR is the difference between the daily maximum and minimum temperatures on a given day.

Monthly precipitation and temperature were then pooled to develop cumulative distribution functions (CDF) of historical and projected precipitation and temperature for each HDe climate scenario. Monthly values were first pooled over the historical base period (1981-2010) and each of the future time periods selected for the EMS climate scenarios (2045-2064 and 2065-2094). Next, monthly values were pooled over the subset of LOCA projections selected for each HDe scenario. This created two sets of monthly precipitation and temperature values for each scenario: one for the historical base period and one for each future period. Monthly precipitation and temperature values were then segregated by month and sorted from least to greatest. This results in CDFs for monthly precipitation and temperature at each grid cell for each period.

Example CDFs for monthly precipitation and maximum temperature are illustrated in Figure 21 and Figure 22, respectively. CDFs in Figure 21 and Figure 22 are for the CT scenario and the future time period centered around 2080. CDFs correspond to the LOCA grid cell overlying the Northern Maricopa weather station (Figure 2). Colors in the CDF figures represent the six projections' 30-year historical (orange hues) or future (blue hues) time period selected for each future scenario. The y-axis represents the monthly precipitation or monthly average temperature over the respective time period, while the x-axis is the quantile[3] associated with each precipitation or temperature value. For example, in Figure 21 during July, precipitation for one of the projections is approximately 8 inches for the 1.0 quantile (the dark blue point in the upper right-hand corner). This means that all 30 of the monthly July precipitations from the future period centered around 2080 were 8 inches or below.

For a given scenario and future time period, climate change factors were computed from the corresponding CDFs of monthly precipitation and temperature at each grid cell. Precipitation change factors were computed as the ratio of future CDF to historical CDF. The change factor was assumed to be 1.0 when the historical CDF value is zero to avoid dividing by zero. Temperature change factors were computed as the difference between the future CDF and historical CDF.

[3] Quantiles are defined as the probability that a given value is less than or equal to the selected value (i.e., non-exceedance probability).

Just as CDFs represent the distribution of monthly precipitation and temperature values as a function of cumulative probability, also referred to here as quantile, climate change factors are also represented as a function of quantile. Climate change factors thus capture differences in projected climate change across the distribution of a given climate variable. For example, projected changes in extreme values may differ from projected change values near the middle of the distribution.

Examples of change factors for monthly precipitation and maximum temperature are illustrated in Figure 23 and Figure 24, respectively. Change factors in Figure 23 and Figure 24 are for the CT scenario for the future time period centered around 2080 at the LOCA grid cell overlying the Northern Maricopa weather station; change factors correspond to the CDFs illustrated in Figure 21 and Figure 22, respectively. Values above the horizontal line at 1.0 and 0.0 indicate an increase in precipitation or temperature respectively, while values below that line indicate a decrease in precipitation or temperature for the respective quantile.

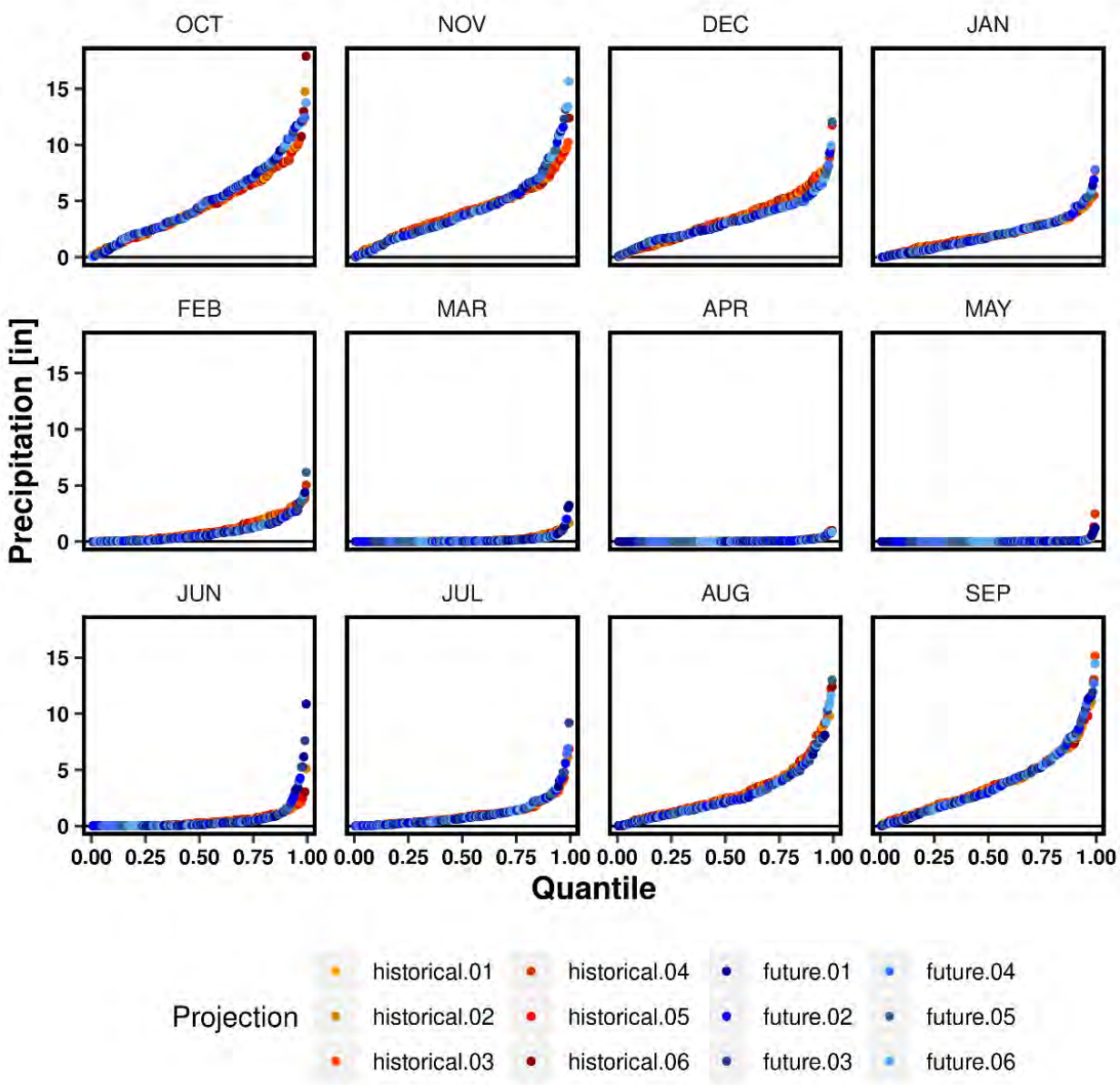

Figure 21. Cumulative distribution functions of monthly precipitation (inches) at the Northern Maricopa weather station. CDFs are from the historical reference period (1981-2010) and the future period centered around 2080 for the six projections from the CT future scenario. Blue colors represent CDFs from the projections' future period and the yellow-red colors represent the CDFs from the projections' historical period.

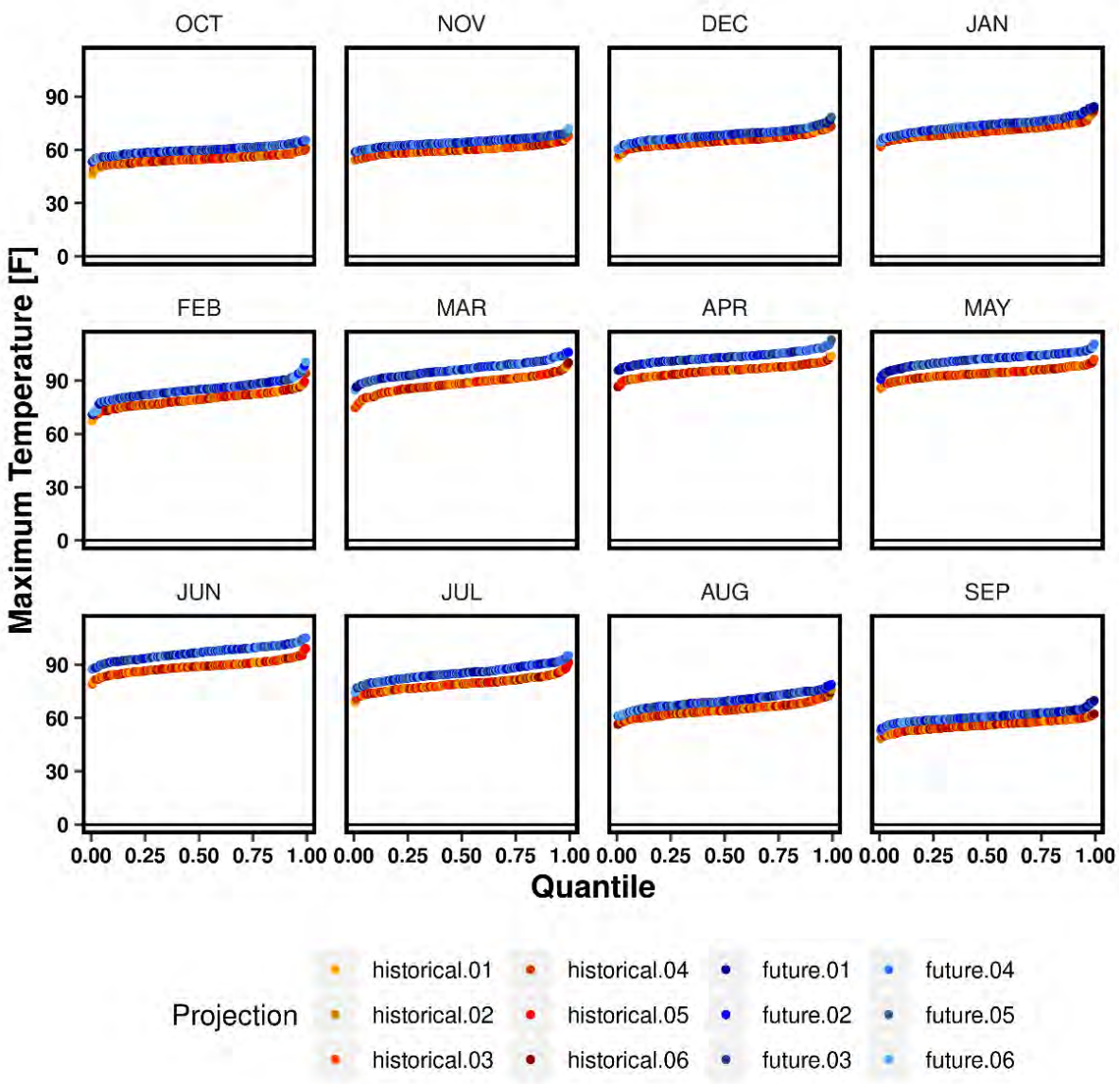

Figure 22. Cumulative distribution functions of average monthly maximum temperature (°F) at the Northern Maricopa weather station. CDFs are from the historical reference period (1981-2010) and the future period centered around 2080 for the six projections from the CT future scenario. Blue colors represent CDFs from the projections' future period and the yellow-red colors represent the CDFs from the projections' historical period.

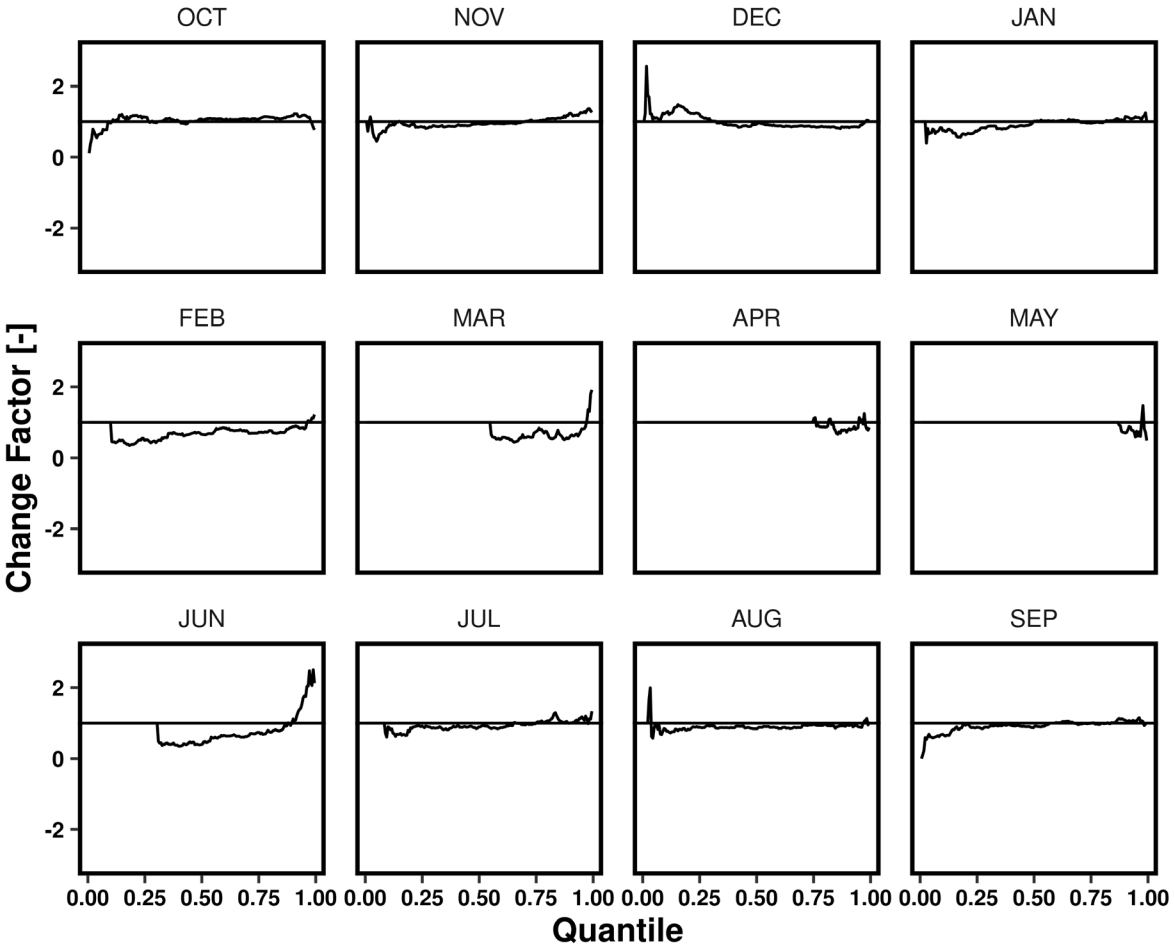

Figure 23. Precipitation change factors as a function of quantile from the grid cell overlying the Northern Maricopa weather station. Change factors were computed from the historical period (1981-2010) and the future period (2065-2094).

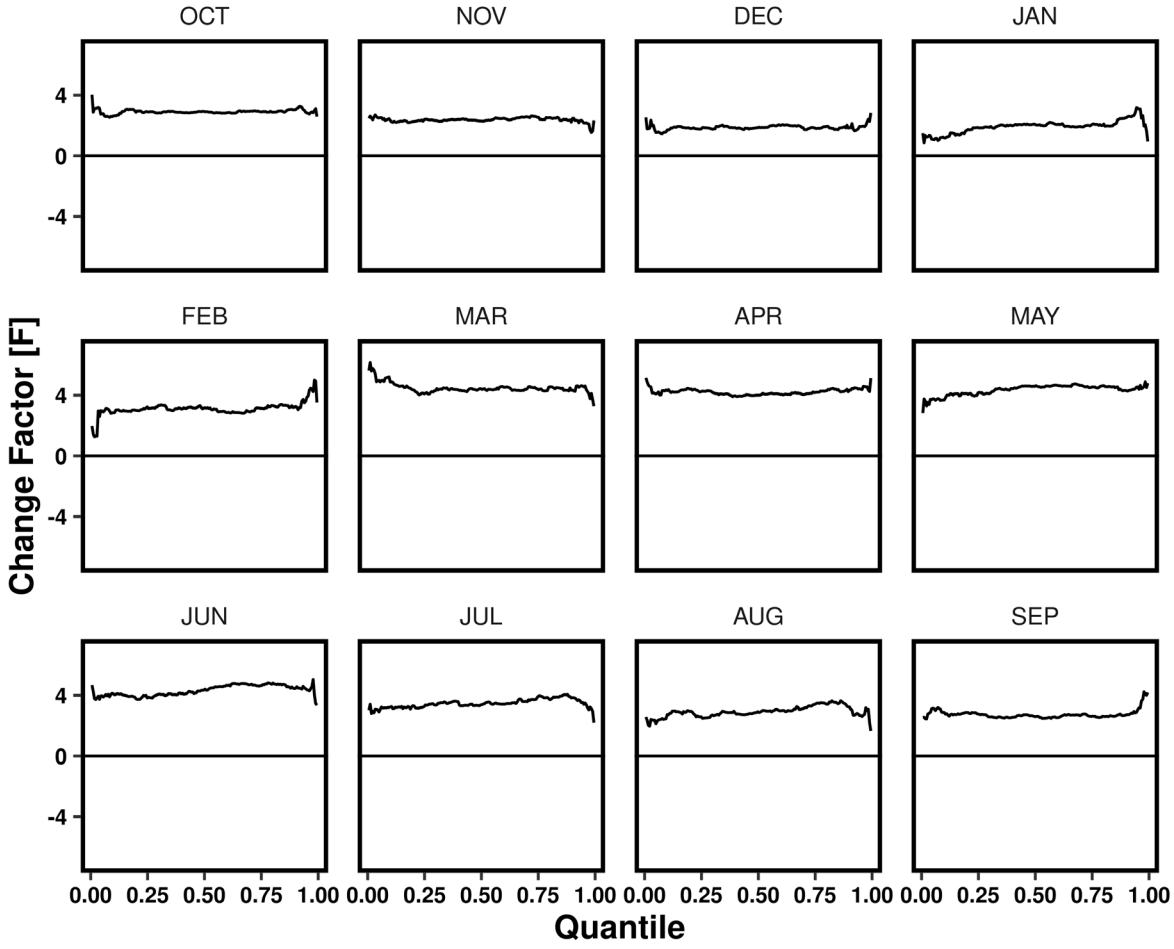

Figure 24. Maximum temperature change factors (°F) as a function of quantile from the grid cell overlying the Northern Maricopa weather station. Change factors were computed from the historical period (1981-2010) and the future period (2065-2094).

4.1.3. Application of Quantile-Based Change Factors

Monthly precipitation, monthly mean maximum temperature, and monthly mean diurnal temperature range (DTR) for each future climate scenario are computed by applying the respective quantile-based change factors to adjust the baseline climate scenario.

Precipitation change factors are applied according to Equation (1):

$$P^*_{ym} = P_{ym} \cdot \Delta^*_{Q[P_{ym}]} \quad (1)$$

Where:

P^*_{ym} is monthly precipitation in month *m* of year *y* under a given future scenario, P_{ym} is monthly precipitation in month *m* of year *y* under the baseline scenario (see Section 4.1), and

$\Delta^*_{Q[P_{ym}]}$ is the precipitation change factor for the given scenario for the quantile (Q) corresponding to the baseline monthly precipitation value (P_{ym}).

As described in Section 4.1.2, precipitation change factors are based on the ratio of the precipitation CDF for a selected future period to the precipitation CDF for the historical reference period (1981-2010). Precipitation under future scenarios is thus computed by multiplying the baseline precipitation value by the corresponding change factor.

Temperature change factors are applied according to Equation (2):

$$T^*_{ym} = T_{ym} + \Delta^*_{Q[T_{ym}]} \quad (2)$$

Where:

T^*_{ym} is monthly mean maximum temperature or monthly mean DTR for month *m* of year *y* under a given future scenario,

T_{ym} is monthly mean maximum temperature or monthly mean DTR for month *m* of year *y* under the baseline scenario (see Section 4.1),

and $\Delta^*_{Q[T_{ym}]}$ is the maximum temperature or DTR change factor for the given scenario for the quantile (Q) corresponding to the baseline monthly temperature value (T_{ym}).

Temperature change factors—including change factors for monthly mean maximum temperature and monthly mean DTR—are based on the difference between temperature CDFs for a selected future period the historical reference period (1981-2010). Temperature variables under future scenarios are thus computed by adding the change factor to the corresponding baseline temperature value.

The procedure used to compute monthly precipitation and monthly temperature variables under future climate scenarios from the baseline scenario and change factors is described below. The procedure is applied independently for each future time period. For each future time period, the procedure is applied independently at each 1/16° by 1/16° LOCA grid cell throughout the EMS Basin Study domain (see Figure 1).

- *Develop CDFs for Baseline Scenario*
  Change factors were applied to the baseline scenario on a quantile basis. To do this, CDFs were first developed for each climate variable under the baseline scenario. CDFs were then developed using the same procedure described above for developing CDFs of monthly climate conditions from the pooled LOCA projections selected for each future scenario (see Section 4.1.2). First, monthly precipitation, monthly mean maximum temperature, and monthly mean DTR from the baseline scenario were partitioned by month and by period. These were computed by converting monthly precipitation and temperature values from a timeseries (one-dimensional vector) into a two-dimensional matrix, with each row of the matrix containing monthly values over a single year and each column containing values for a single month over each year in the record (i.e., rows represent years, columns represent months). Only the historical reference period (1981-2010) was used in developing the baseline CDFs.

  Monthly values were then sorted along columns from least to greatest and the cumulative exceedance probability, also referred to as quantile, of each value is estimated based on its Weibull plotting position. This results in set of 12 CDFs of monthly climate conditions from the baseline scenario: one for each month of the year, at each grid cell in the EMS Basin Study domain.

- *Apply Change Factors to Baseline Scenario*
  Change factors were applied to monthly precipitation, monthly mean maximum temperature, and monthly mean DTR from the baseline climate scenario as follows. First, a set of look-up functions was developed to determine the quantile (cumulative probability) of a given value with respect to the baseline CDF. A second set of look-up functions was then developed to determine the change factor for given quantile. Each set included 12 look-up functions: one for each month of the year.

  Look-up functions were then used to apply a change factor to each monthly value from the baseline scenario to compute the corresponding monthly value for the future climate scenario. A compute script was used to loop over all months in the baseline scenario period of record (January 1915-December 2015). The first look-up function was used to determine the quantile of the baseline value for that month from the corresponding baseline CDF. The second look-up function was used to determine the change factor for that month and quantile. The future scenario value for that month was then computed according to Equation 1 for precipitation or Equation 2 for temperature variables.

4.1.4. Assumptions and Limitations

Several important assumptions are inherent in the HDe methodology. The HDe methodology is based on adjusting a baseline scenario to reflect projected changes in the probability distributions of precipitation and temperature between two period. As described in Section 4.1, the baseline scenario was developed by removing long-term trends from a dataset of observed historical climate conditions. As a result, the baseline scenario and all

future scenarios reflect observed historical interannual climate variability. The HDe methodology thus allows users to distinguish between natural climate variability and anthopogenic climate change, which in turn allows users to evaluate a broad range of climate variability under a given projection of future climate change. For example, the HDe method allows users to evaluate the extent to which dry conditions in a given climate scenario are driven by climate change (projected drying) compared to natural climate variability (drought conditions).

However, because future climate scenarios are based on a de-trended baseline scenario, the HDe methodology does not reflect the timing of projected changes in climate. HDe scenarios, therefore, cannot be used to assess when future climate conditions are likely to cross a given threshold that may be relevant to planners and resource managers. For example, HDe scenarios cannot be used to assess when annual mean snowpack is projected to decrease by a certain percentage or when annual mean temperatures are projected to exceed a given threshold. The HDe methodology is consistent with to planning approaches that rely on projected build-out conditions to evaluate future water supplies, without explicit consideration of when those build-out conditions will be reached. Moreover, limitations of the HDe method to assess trends or timing of certain thresholds are mitigated in this study by evaluating HDe scenarios for multiple future time periods.

In addition to limitations regarding analysis of trends and projected timing of threshold conditions, HDe scenarios do not reflect potential changes in climate variability, including the frequency, intensity, duration of weather extremes such as extreme heat events and extreme precipitation events as well as climate extremes such as drought events. Previous analyses of historical observations and GCM-based projections of future climate suggest that climate change may affect the frequency and duration of weather and climate extremes. However, the characteristics of such change remain uncertain due to limitations of GCMs in simulating these extremes. While the HDe method does not reflect projected changes in the frequency, intensity, and duration of weather and climate extremes, it ensures that characteristics of weather and climate variability on daily to inter-decadal timescales is realistic and is not affected by limitations of GCMs.

4.2. Future Climate Scenarios

Future climate scenarios were developed to represent a plausible range of future climate conditions over the EMS study area. The EMS climate scenarios were evaluated to characterize the range of future climate conditions represented in the EMS Basin Study. Similar to observed historical climate and LOCA projections, future climate scenarios were evaluated on a $1/16^{th}$ degree grid and averaged over the EMS study area.

4.2.1 Future Temperature Scenarios

Consistent with individual LOCA projections (see Section 3.2), all EMS climate scenarios indicate an increase in annual and seasonal average temperatures over the EMS study area. Table 3 shows the projected change in annual temperature for all future scenarios and time periods averaged across the EMS study area, while Figure 25 shows the spatial distribution

of this projected change for all future scenarios and time periods. The projected change in average temperature by 2060 ranges from 3.0 °F for the Warm-Wet (WW) scenario to 6.1 °F for the Hot-Wet (HW) scenario. This rise in average temperature is projected to be even larger by 2080, with the Warm-Wet (WW) scenario suggesting 3.4 °F and the Hot-Dry (HD) scenario suggesting an 8.6 °F increase. Most scenarios and future time periods see a larger increase in maximum temperatures than minimum temperatures.

Spatial and seasonal patterns of temperature variability in all scenarios are consistent with observed historical patterns across the EMS study area, as would be expected based on the scenario methodology (see Section 4.1). The spatial distribution of seasonal average temperature across the EMS study area for the Central Tendency (CT) scenario centered around 2080 is illustrated in Figure 26; all future scenarios show winter remaining the coolest season and summer remaining the warmest season, with very little spatial variability across the EMS study area in all seasons. While seasonality remains similar in the future, there are larger projected increases in temperature during the fall and summer than during the spring and winter (Figure 27).

Figure 28 shows a timeseries of basin-averaged temperatures for each scenario and future time period and Figure 29 shows boxplots of the range of annual average temperatures for each scenario and time period. All future scenarios show an increase in temperature relative to the baseline during all years, with larger increases under the 2080 climate. The hot-wet scenario shows the most warming in the near future (2045-2074 scenarios), while the Hot-Dry (HD) scenario shows the most warming in the far future (2065-2094 scenarios). The Warm-Wet (WW) scenario shows the least warming in both the near and far futures. The difference in warm compared to hot scenarios also becomes more apparent in the far future than the near future.

As discussed in Section 4.1, the HDe methodology preserves the pattern of climate variability, where the historic sequencing of wet and dry years or hot and cool years is preserved in the climate scenarios (Figure 28). However, the projected increase in temperature results in more extreme events; where extreme events are defined as temperatures that exceed the 95th percentile of observed annual temperatures during the historic baseline period (1981-2010). For the EMS Basin Study area, the threshold for extreme basin-averaged annual temperatures is 56.4 °F for annual minimum temperatures, 72.9 °F for annual average temperatures and 89.5 °F for annual maximum temperatures.

By definition, observed historical temperatures exhibit extreme annual temperatures in one or two years during the historical reference period (1981-2010). The number of occurrences of extreme annual temperatures during the corresponding 30-year period of each scenario are listed in Table 5. Only 2 years during the historic baseline time period surpassed the annual extreme temperature threshold; however, under far future scenarios (2065-2094), almost all the scenarios suggest that every year will surpass the 95th percentile. This indicates a significant increase in extremely high temperatures across the EMS basin study area under all scenarios for this time period.

Table 3. Changes in basin-averaged annual precipitation and temperature from the baseline scenario to future climate scenarios over the EMS basin study area

Projected Climate Change						
Time Period	**Scenario**	**Precip (in)**	**Precip (%)**	**Tavg (°F)**	**Tmax (°F)**	**Tmin (°F)**
1981 - 2010	Baseline	9.2	-	71	87.1	54.9
2045 - 2074	CT	-0.8	-9.2	4.6	5.2	4.0
	HD	-1.6	-17.6	5.8	6.3	5.3
	HW	0.3	3.7	6.1	6.2	6.1
	WD	-1.6	-17.2	3.3	3.8	2.7
	WW	0.4	4.5	3.0	3.0	3.0
2065 - 2094	CT	-0.3	-3.8	5.8	6.3	5.4
	HD	-2.2	-23.8	8.6	9.1	8.1
	HW	0.6	6.1	8.2	8.1	8.3
	WD	-1.8	-19.8	4.6	5.1	4.1
	WW	0.8	8.8	3.4	3.4	3.5

Notes:

- *Projected change was calculated by comparing annual mean basin-average precipitation and temperature over the EMS basin study area from 1915-2015 between baseline and future climate scenarios.*
- *Precip = change in basin-average annual mean precipitation over the ARBS climate scenario extent (in), Tavg = change in basin-average annual mean of daily average temperature (°F), Tmin = change in basin-average annual mean of daily minimum temperature (°F), Tmax = change in basin-average annual mean of daily maximum temperature (°F), CT = Central Tendency, HD = Hot-Dry, HW = Hot-Wet, WW = Warm-Wet, and WD = Warm-Dry.*
- *Annual mean basin-average values for the baseline scenario were calculated from 1915-2015 and are listed in the first row.*

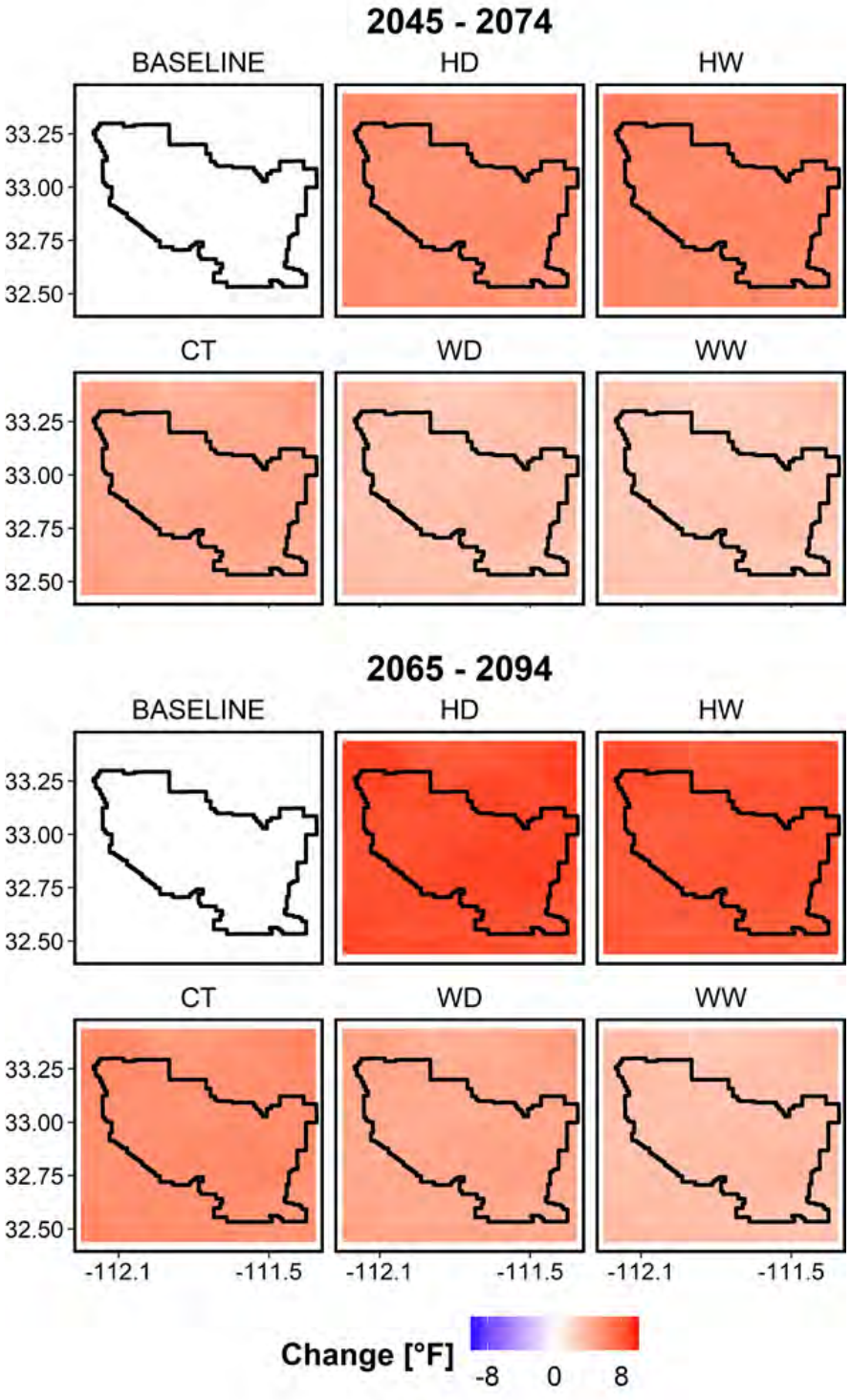

Figure 25. Spatial distribution of the change in annual average temperature compared to the baseline scenario under each climate scenario. CT = Central Tendency, HD = Hot-Dry, HW = Hot-Wet, WW = Warm-Wet, and WD = Warm-Dry. Axes are longitudinal and latitudinal coordinates. The outline of the EMS Basin Study area is delineated by the black solid line.

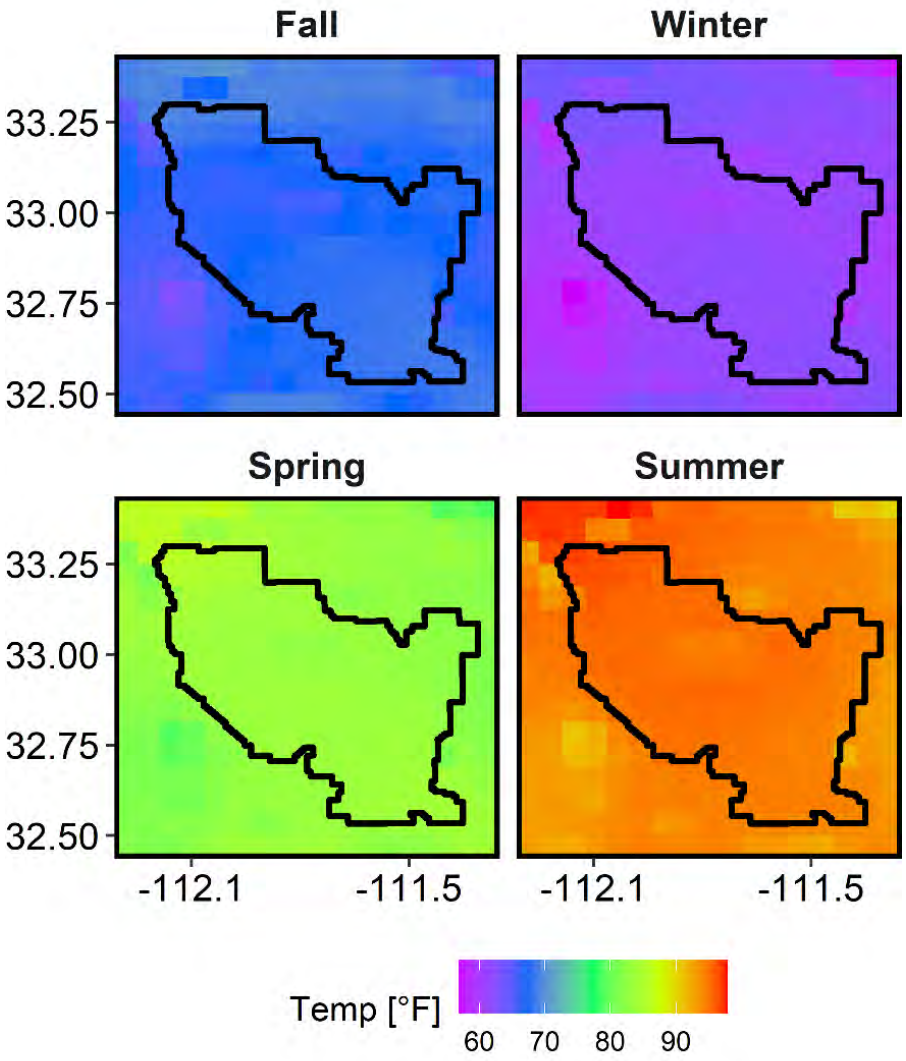

Figure 26. Spatial distribution of average seasonal temperature under the **Central Tendency (CT)** scenario for 2065-2094. Axes are longitudinal and latitudinal coordinates. The outline of the EMS Basin Study area is delineated by the black solid line.

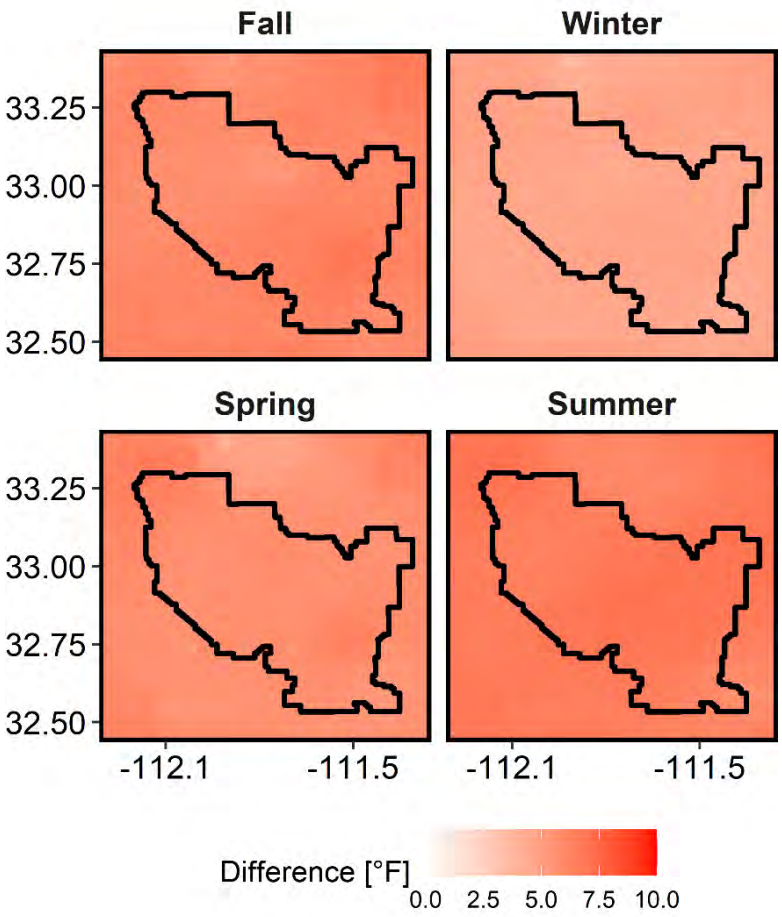

Figure 27. The difference (°F) in average seasonal temperature between the baseline and the **Central Tendency (CT)** scenarios for 2065-2094. Axes are longitudinal and latitudinal coordinates. The outline of the EMS Basin Study area is delineated by the black solid line.

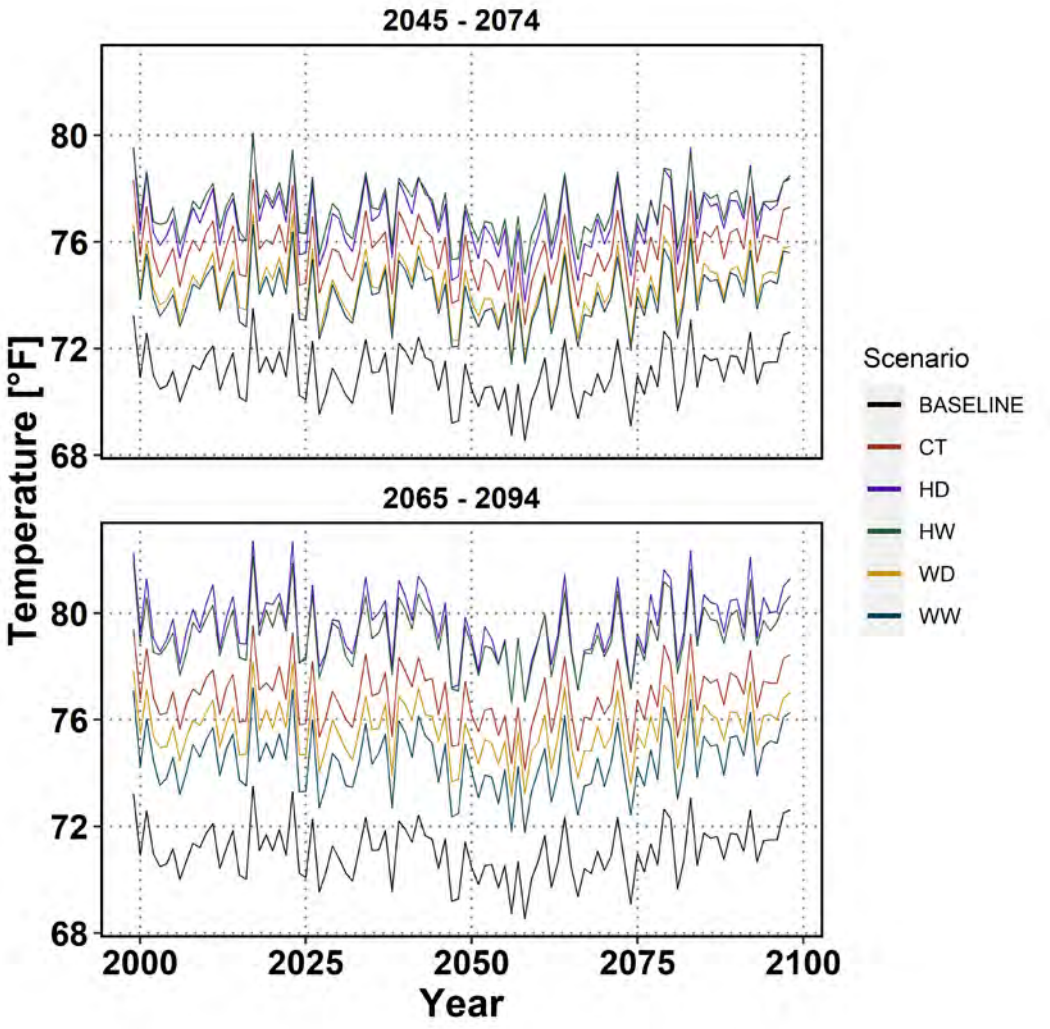

Figure 28. Timeseries of basin-averaged annual average temperature over the EMS study area for each scenario and future time period. CT-Central Tendency, HD = Hot- Dry, HW = Hot-Wet, WW = Warm-Wet, and WD = Warm-Dry.

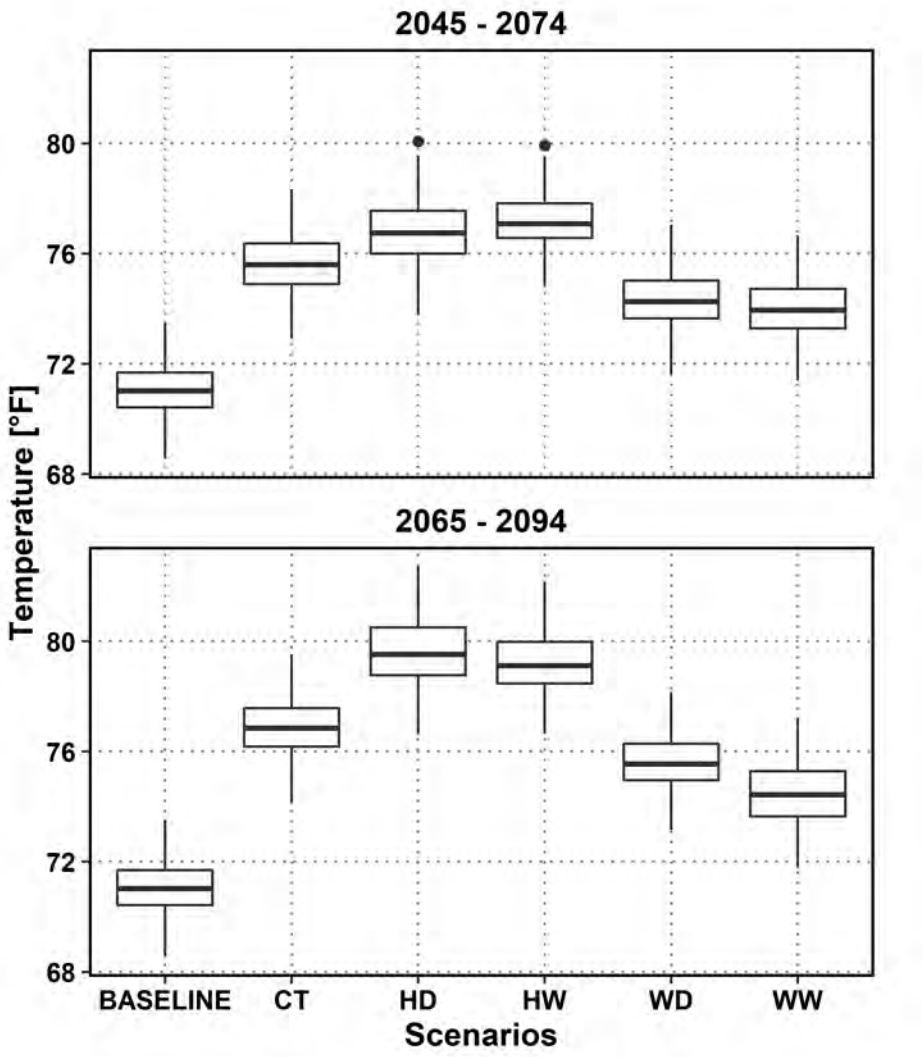

Figure 29. Boxplots of basin-averaged annual average temperature for the entire 101-year time period under the baseline and future scenarios. Box limits represent the 25th and 75th quartiles; solid lines within each box represent the median; whiskers represent values extending from the 25th and 75th quartiles to values within ± 1.5*(Interquartile Range); and outliers are represented by solid black circles. CT = Central Tendency, HD = Hot-Dry, HW = Hot-Wet, WW = Warm-Wet, and WD = Warm-Dry.

Table 4. The number of years during a 30-year historic or future period where the annual temperature exceeds the 95th percentile historic temperature

Time-period	Scenario	Frequency		
		Tavg	Tmax	Tmin
1981 - 2010	Historical	2	2	2
2045 - 2074	CT	30	30	30
	HD	30	30	30
	HW	30	30	30
	WD	27	27	28
	WW	27	18	28
2065 -2094	CT	30	30	30
	HD	30	30	30
	HW	30	30	30
	WD	30	30	30
	WW	28	22	29

**The historic 95th percentile average, maximum and minimum temperatures were 72.9 °F, 89.5 °F and 56.4 °F respectively. CT = Central Tendency, HD = Hot-Dry, HW = Hot-Wet, WW = Warm-Wet, and WD = Warm-Dry.*

4.2.2 Future Precipitation Scenarios

Similar to the LOCA projections (as described in Section 3), projected changes in precipitation are less certain than projected changes in temperature, with the drier scenarios (HD and WD) indicating a decrease in annual precipitation and wetter scenarios (HW and WW) indicating an increase (Table 3). Figure 30 shows the percent change in annual average precipitation for each future scenario and time period across the EMS study area relative to the baseline scenario. Despite projected changes in annual precipitation for both the Wet and Dry scenarios, the EMS study area will still remain a dry, arid environment. The drier scenarios indicate a decrease in annual precipitation of up to 20% (approximately two inches) across the study area, while the wetter scenarios indicate an increase of less than 10% (approximately one inch) across the EMS study area. The Central Tendency (CT) scenario indicates a slight increase in annual average precipitation over the northern part of the study area and a slight decrease over the remainder of the study area.

Figure 31 shows seasonal average precipitation under the Central Tendency (CT) scenario for the 2080 future period. As described in Section 4.1, the HDe methodology preserves the spatial and temporal variability of observed historical precipitation. Spring remains very dry, and the other seasons all receive similar amounts of precipitation. Figure 31 shows also shows little spatial variability in seasonal average precipitation over the EMS study area. However, while seasonality remains similar, all scenarios project different magnitudes of change in each season. In the Central Tendency (CT) scenario, spring is

projected to get even drier and summer is projected to get wetter (Figure 32). Fall and winter appear to have smaller changes in seasonal average precipitation than the other two seasons under the Central Tendency (CT) scenario. The drier scenarios (HD and WD) suggest all seasons will get drier with the most pronounced change in spring. The wetter scenarios (HW and WW) indicate more uncertainty in seasonal changes, although summer appears to get wetter and spring appears drier.

As in the temperature scenarios, all precipitation scenarios reflect the sequencing and magnitude of seasonal and interannual variability from the historical record (Figure 33). However, the far future (2080) scenarios show larger differences in annual precipitation from the baseline scenario than the near future (2060).

Figure 34 shows boxplots of the range of annual precipitation across scenarios. The median annual precipitation under the dry scenarios is approximately 2 inches less than the baseline median. While the median annual precipitation under the wet scenarios is similar to the baseline median, the wet scenarios exhibit a larger range as reflected by an increase in the 75th quartile values. This is important as most historic streamflow recharge occurs in response to large precipitation events.

Table 5 also reiterates the increase in frequency of wetter years under the wetter scenarios, including extremely wet years in which annual precipitation surpasses the historic 95th percentile of 14.9 inches. Interestingly, the dry scenarios (HD and WD) indicate an even larger increase in the frequency of extremely dry years in which annual precipitation is less than the historic 5th percentile of 4.6 inches. Both dry scenarios project that 5-8 years out of 30 years would have annual precipitation below 4.6 inches.

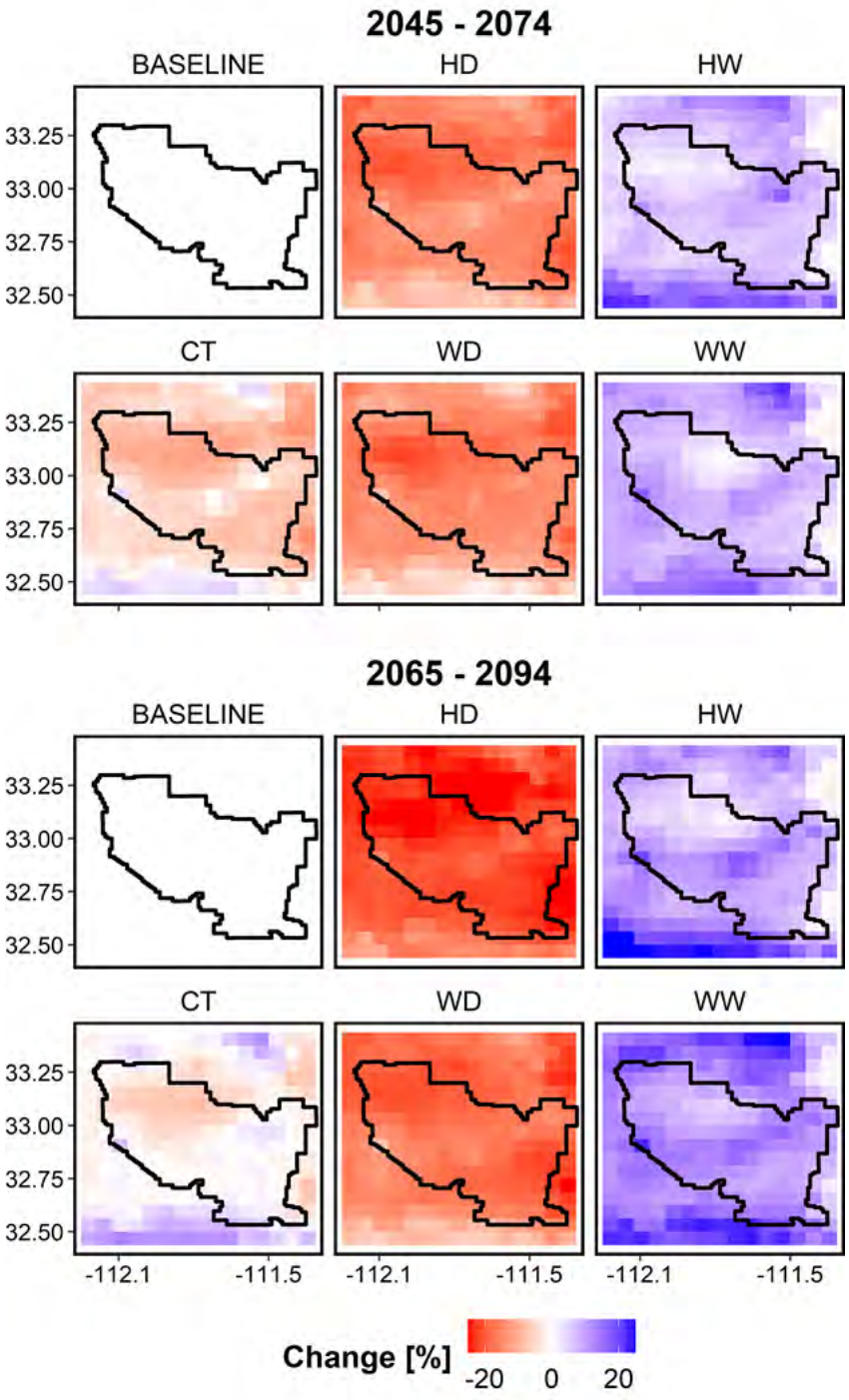

Figure 30. Spatial distribution of the change in annual precipitation compared to the baseline under each climate scenario. CT = Central Tendency, HD = Hot-Dry, HW = Hot-Wet, WW = Warm-Wet, and WD = Warm-Dry. Axes are longitudinal and latitudinal coordinates. The outline of the EMS Basin Study area is delineated by the black solid line.

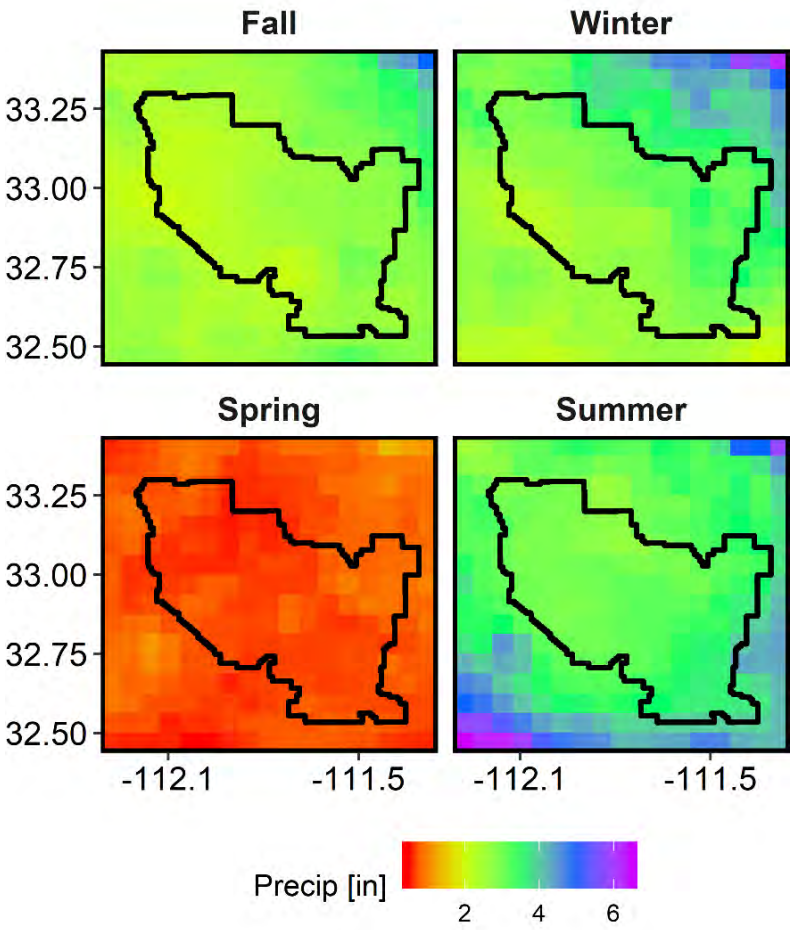

Figure 31. Spatial distribution of average seasonal precipitation under the **Central Tendency (CT)** scenario for 2065-2094. Axes are longitudinal and latitudinal coordinates. The outline of the EMS Basin Study area is delineated by the black solid line.

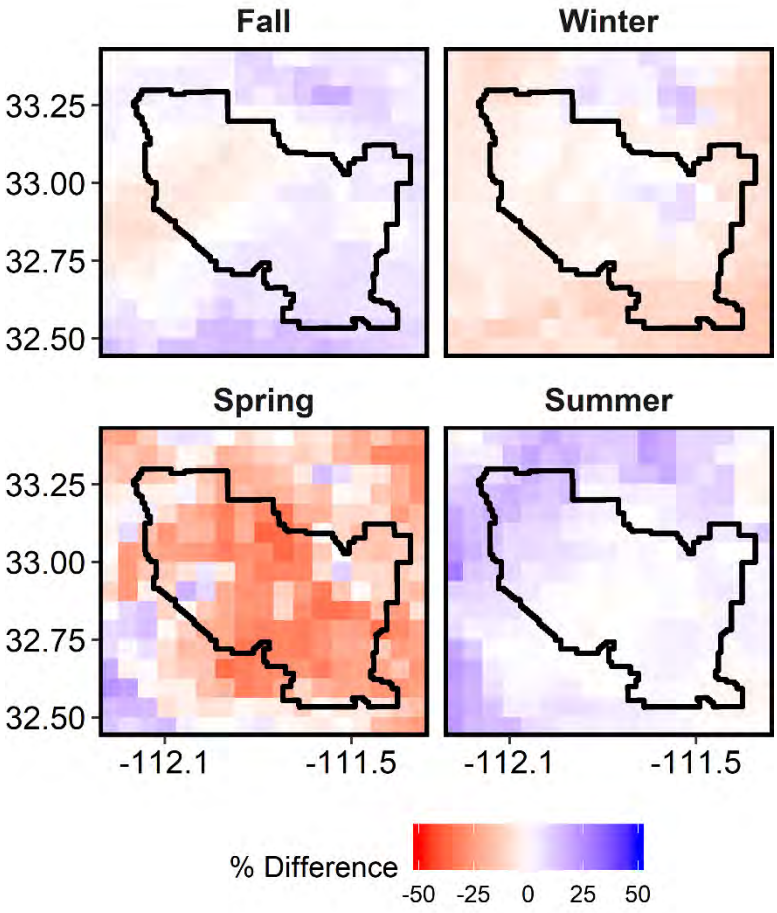

Figure 32. Spatial distribution of the percent difference in average seasonal precipitation between the baseline and the **Central Tendency (CT)** scenarios for 2065-2094. Axes are longitudinal and latitudinal coordinates. The outline of the EMS Basin Study area is delineated by the black solid line.

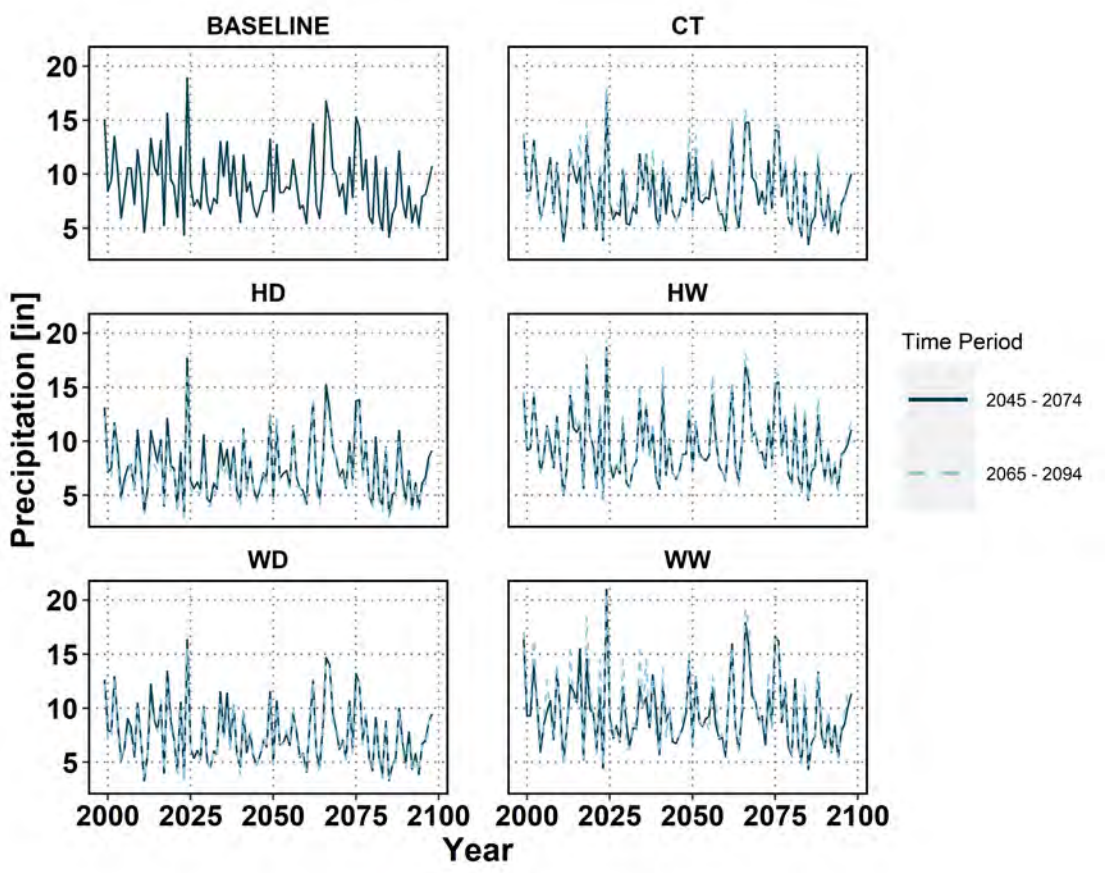

Figure 33. Timeseries of basin-averaged annual precipitation over the EMS study area for each scenario and future time period. Line color represents the scenario future time period except for the baseline scenario which represents the historic baseline period of 1981-2010. CT=Central Tendency, HD = Hot- Dry, HW = Hot-Wet, WW = Warm-Wet, and WD = Warm-Dry.

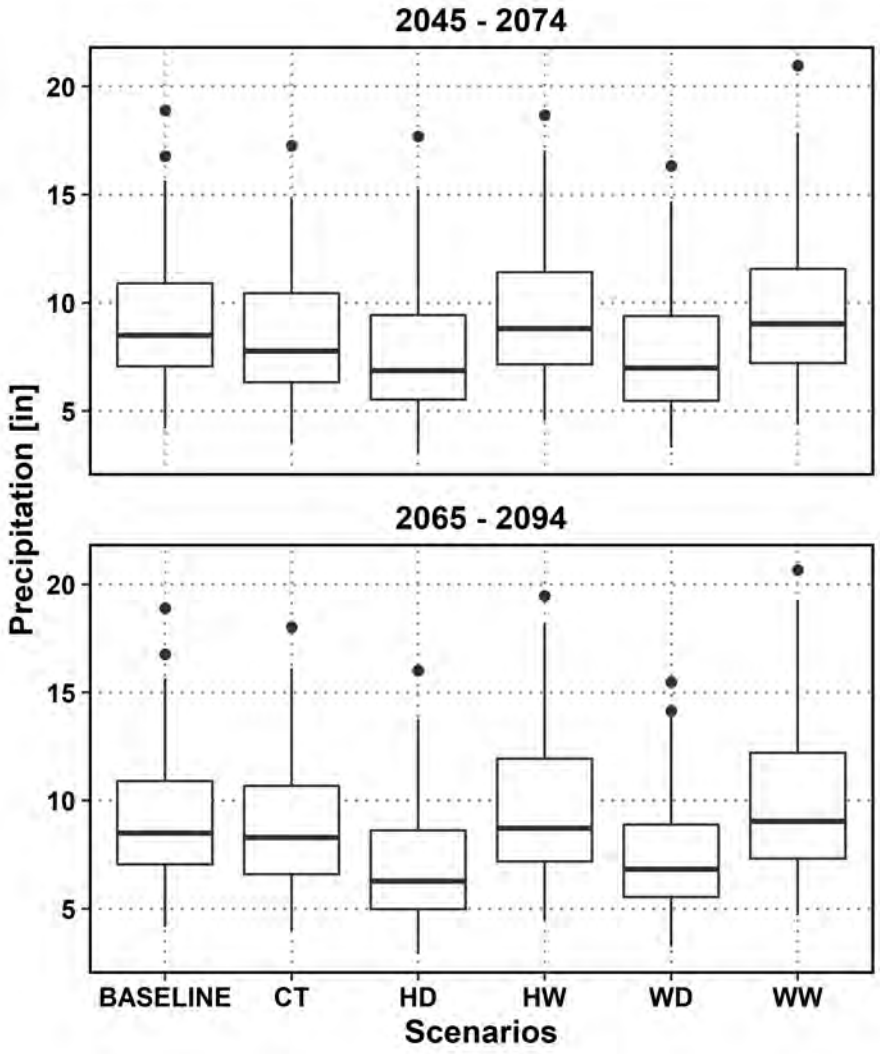

Figure 34. Boxplots of basin-averaged annual precipitation under the baseline and each future scenario and period. Box limits represent the 25th and 75th quartiles; solid lines within each box represent the median; whiskers represent values extending from the 25th and 75th quartiles to values within ± 1.5*(Interquartile Range); and outliers are represented by solid black circles. CT=Central Tendency, HD = Hot-Dry, HW = Hot-Wet, WW = Warm-Wet, and WD = Warm-Dry.

Table 5. The number of years during a 30-year period when annual precipitation is below the 5th percentile or above the 95th percentile of observed annual precipitation

Time-period	Scenario	Frequency	
		Extreme Wet Years	Extreme Dry Years
1981 - 2010	Historic	2	2
2045 - 2074	CT	3	0
	HD	6	1
	HW	1	4
	WD	5	0
	WW	1	4
2065 -2094	CT	2	1
	HD	8	0
	HW	1	4
	WD	6	0
	WW	0	4

Notes:

- The 95th percentile historic annual precipitation was 14.9 inches and the 5th percentile historic annual precipitation was 4.6 inches. CT = Central Tendency, HD = Hot-Dry, HW = Hot- Wet, WW = Warm-Wet, and WD = Warm-Dry.

5. Future Recharge Scenarios

To evaluate how projected changes in natural groundwater recharge (i.e., streambed infiltration) might impact the water balance in the EMS basin study area, future recharge scenarios were developed. These recharge scenarios helped to evaluate impacts of climate change on natural recharge and thus the water balance within the EMS Basin Study area. The projected recharge will be incorporated into predictive runs of the Pinal Active Management Area (AMA) Regional Groundwater model which covers the EMS Basin Study Area (Liu et al., 2014).

The development of these future recharge scenarios is described in Section 5.1., and the scenarios are described in Section 5.2.

5.1. Future Recharge Scenario Methodology

Natural recharge in the EMS basin study area consists mostly of streamflow infiltration.[4] Distributed recharge across the basin study area due to precipitation is negligible in most circumstances as the majority of precipitation either becomes surface runoff or evaporates. Mountain front recharge is not a significant source of groundwater recharge in the EMS Basin Study area and was held constant in historical groundwater simulations and will be held constant in the predictive simulations as well. Figure 35 shows the different sources of recharge that were applied historically in the EMS regional groundwater model (Liu et al., 2014), with the blue bars indicating streambed infiltration. Most of natural recharge across the basin study area occurs as streamflow infiltration. However, it is apparent from Figure 35 that recharge from canal seepage and agricultural return flows is significantly greater than natural recharge except during high precipitation years.

There are two surface water flows within the EMS Basin Study area: the Gila River which enters the study area from the northeast, and the Santa Cruz River which enters the study area from the south. Figure 36 shows the spatial distribution of natural recharge in the Pinal Regional Groundwater Model. Streambed infiltration from the Gila River was applied to the blue and orange cells and streambed infiltration from natural flows from the Santa Cruz River was applied to the green cells. The Gila River upstream of the model domain is a highly managed system. The Gila River streamflow entering the model domain consists entirely of surface water spilled below Ashurst-Hayden Dam. Water released from Coolidge Dam, located upstream of the study area, is diverted at Ashurst-Hayden Dam for delivery to the San Carlos Irrigation Project (SCIP) within the EMS basin study area. Excess streamflow at Ashurst-Hayden Dam is periodically spilled or sluiced from the Ashurst-Hayden Dam into the Gila River below the dam. Annual estimates of the volume of water spilled or sluiced below Ashurst-Hayden Dam can be found in the SCIP annual reports.

The Pinal groundwater model uses the MODFLOW Recharge Package (RCH) to simulate recharge from streambed infiltration on the Gila River. Runoff to the Gila River within the model domain is generally negligible, except in cases of extreme storm events. Recharge from the Gila River was therefore estimated as the difference between gaged annual inflows and outflows in the model area. Annual inflows to the model area are estimated as the annual amount of water spilled or sluiced to the Gila River below Ashurst-Hayden Dam. Annual outflows are estimated as measured flows at two U.S. Geological Survey (USGS) gages: the USGS 09479500 gage near Laveen (pre-1995) and the USGS 09479350 gage near Maricopa (post-1995) (Figure 37). The difference between the inflows (SCIP annual reports) and outflows (USGS gages) was then distributed as recharge across all blue river cells (Figure 36) on a weighted basis. During high flow years, additional flow was assumed to infiltrate in the orange cells as well. A pre-processing approach was developed by Liu et al. (2014) to spatially distribute estimated recharge over the blue and orange river cells illustrated in Figure 36.

[4] Therefore, in this TM, natural recharge and streambed infiltration are synonymous.

The Pinal groundwater model similarly uses the RCH package to simulate recharge from streambed infiltration on the Santa Cruz River. The Santa Cruz River is ephemeral, and streamflow is limited to occasional runoff events during high precipitation years. The Santa Cruz River also receives effluent flows upstream of the model domain, which are separated from the natural flows and the subsequent streambed infiltration is distributed differently spatially in the groundwater model. All streamflow into the domain from the Santa Cruz River is assumed to be recharge by streambed infiltration, as flow in the ephemeral channel does not reach the northern part of the domain. Similar to recharge from the Gila River, a pre-processing approach was used develop spatially-distributed annual recharge from the Santa Cruz River based on the annual volume of streamflow entering the domain. Recharge was distributed non-linearly along the entire reach of the Santa Cruz River within the model domain (Figure 36 green cells). The volume of natural annual flow into the domain was estimated from the Arizona Department of Water Resources (ADWR) Tucson Active Management Area groundwater flow model (Mason and Hipke, 2013).

Given the setup of the groundwater model, it was necessary to develop a historic relationship between precipitation and annual recharge for both rivers independently. A relationship between precipitation and recharge iwa needed to estimate recharge from streambed infiltration (i.e., natural recharge) under each of the future climate scenarios described in Section 4. Figure 38 shows a timeseries of the total annual streambed infiltration applied in the Pinal AMA Regional groundwater model before calibration for both the Gila and Santa Cruz Rivers. These annual values of streambed infiltration were then used in conjunction with the Livneh dataset domain-averaged precipitation (Section 2) to develop a statistical relationship between the annual precipitation and annual recharge.

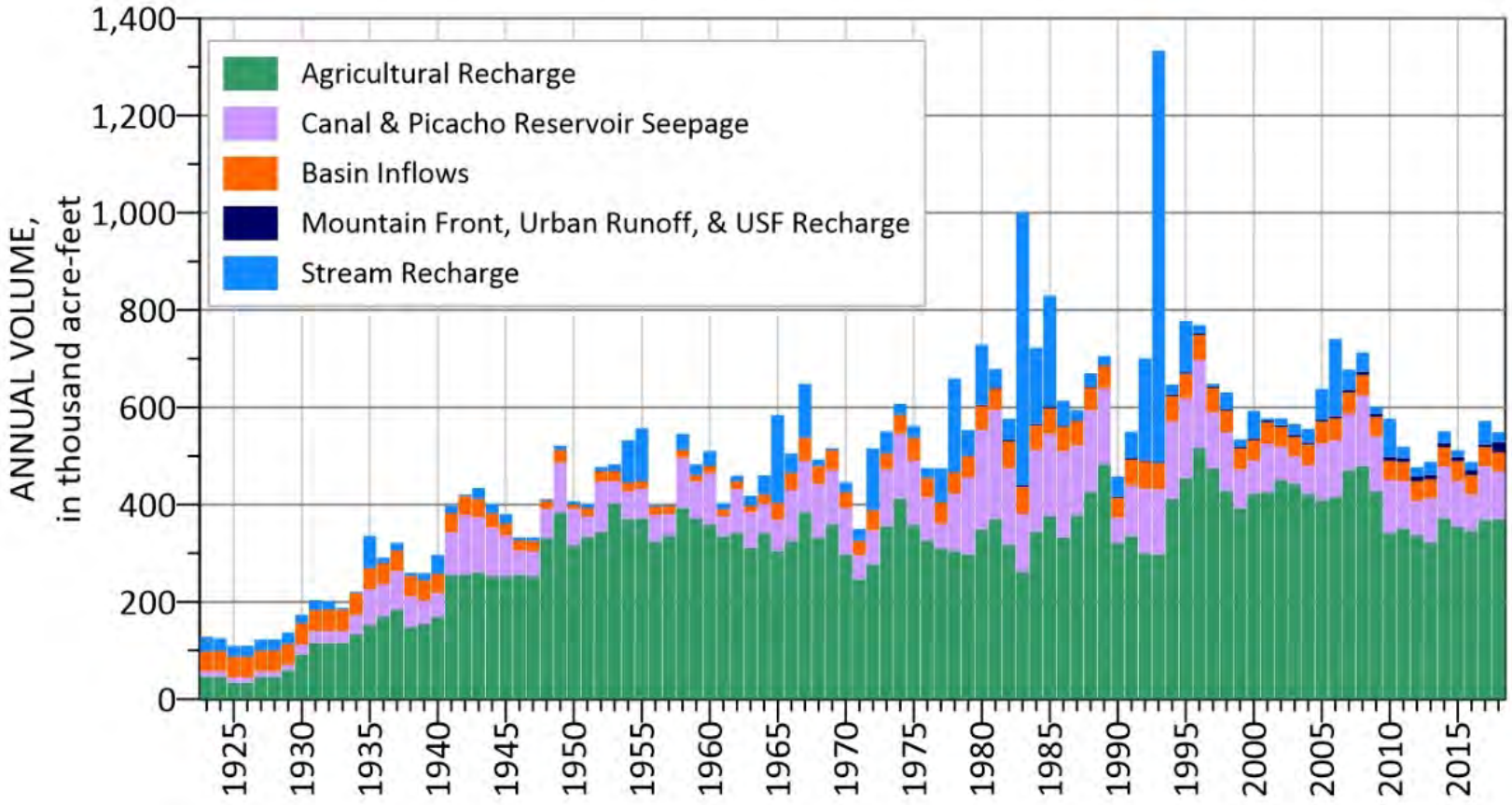

Figure 35. The different sources of historic recharge in the groundwater model for the EMS basin study area. (Bates, 2020).

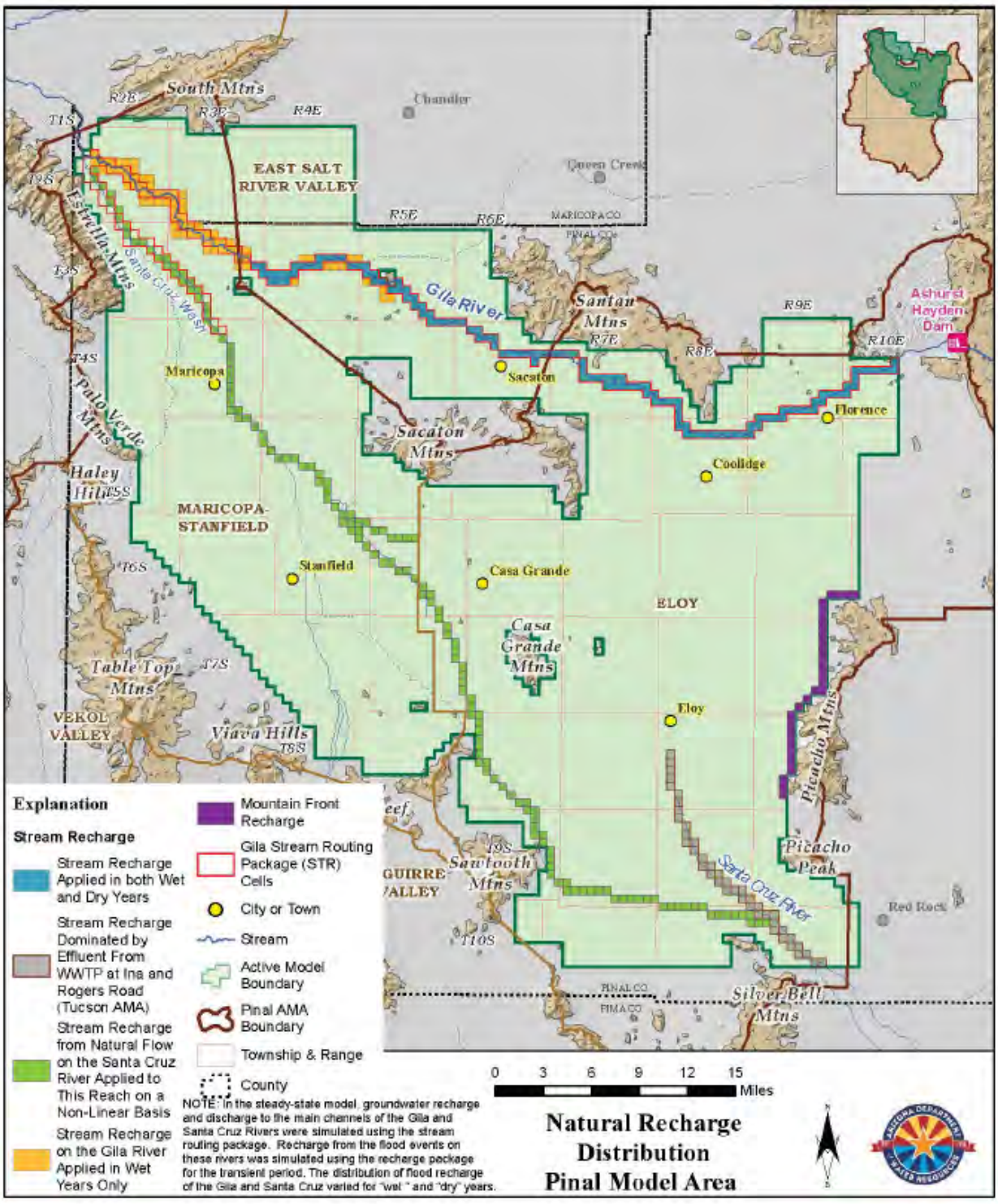

Figure 36. The spatial distribution of natural recharge in the groundwater model for the EMS basin study area. The blue and orange colors represent the cells the Gila future recharge will be applied to and the green color represents the cells the Santa Cruz future recharge will be applied to (figure from Liu et al., 2014).

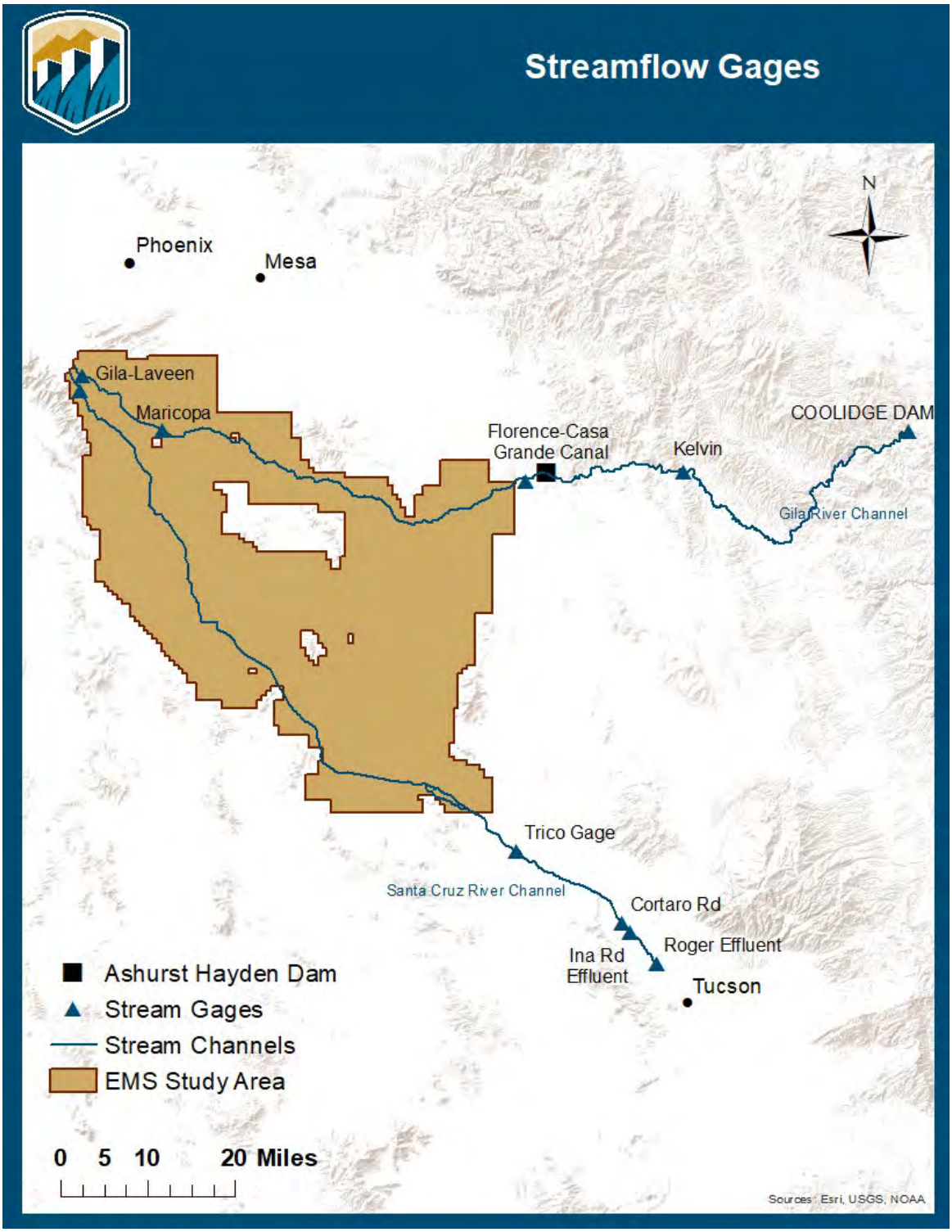

Figure 37. Stream gages near the EMS basin study area.

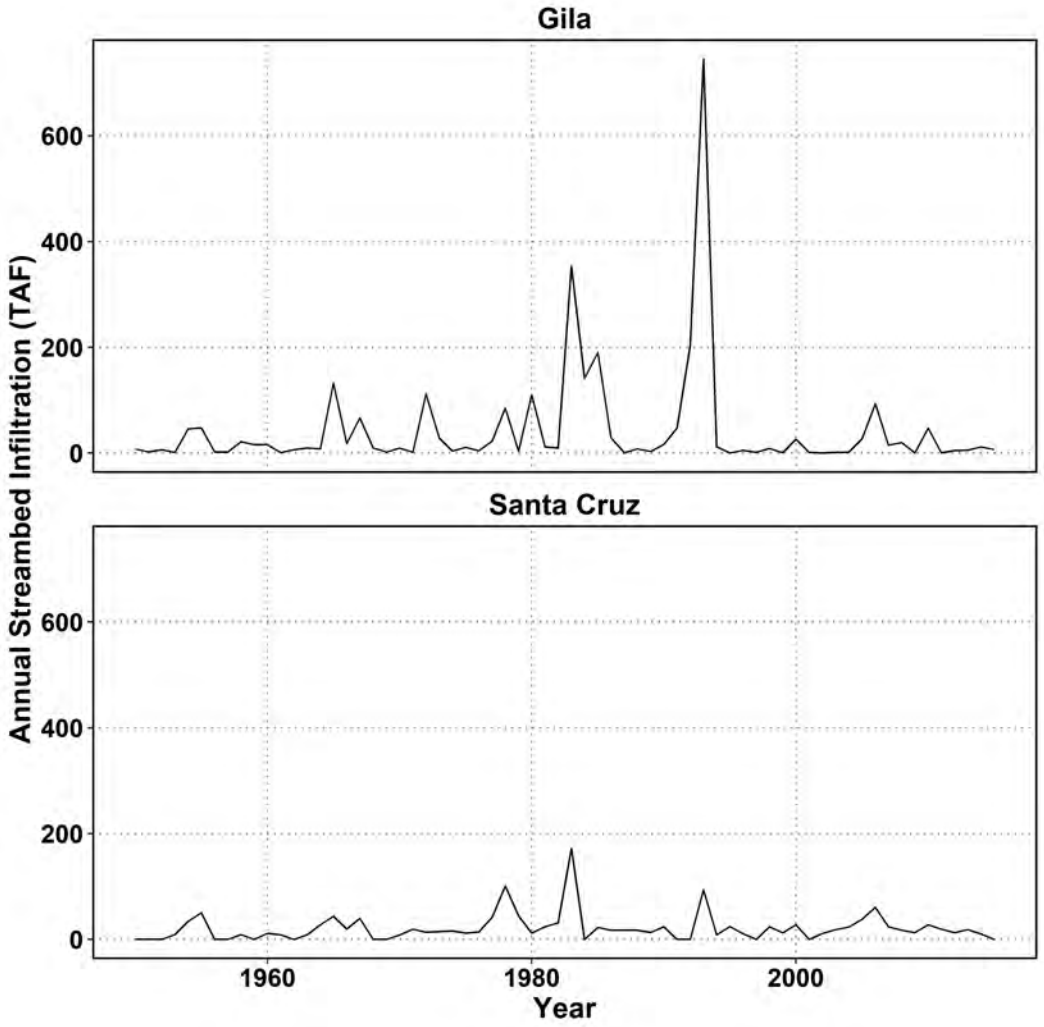

Figure 38. Annual streambed infiltration for the Gila and Santa Cruz Rivers applied in the Pinal AMA groundwater model before calibration.

5.1.1. Model Development

Several types of multivariate regressions were investigated to determine the best statistical fit between all domain-averaged climate variables (precipitation, average temperature, maximum temperature, and minimum temperature) and historic recharge for both rivers (see Section 5.1 above). Observed historical climate data included basin-averaged precipitation and temperature from the Livneh dataset described in Section 2. All climate variables were considered, and precipitation was found to be the only significant predictor variable in all regressions. Linear, power law, and autoregressive models were developed, calibrated and assessed based on their accuracy in simulating estimated historical recharge from streambed infiltration as a function of observed precipitation. Statistical models were developed for daily, monthly and annual timescales. As the observed recharge data for each river was only available on an annual scale, temporal disaggregation or estimation was performed prior to developing daily and monthly models. Further details on disaggregation methods can be found in the Appendix.

Two precipitation metrics were found to be significant predictors of recharge: spatially-averaged annual rainfall and the annual maximum precipitation event (Figure 39). The annual maximum precipitation event was calculated based on the sum of basin-averaged precipitation over each rain event, where rain events were defined as consecutive days with basin-averaged precipitation above 0.1 inches. This variable was identified as a potential predictor based on conceptual grounds. In arid environments characterized by ephemeral streams, a large, multi-day precipitation event can be a better indicator of streamflow volume than total annual runoff.

Regression models were evaluated based on model accuracy and evaluation of residuals (i.e., differences between observed and modeled values). The accuracy of each empirical model was assessed based on the Nash-Shutcliffe efficiency coefficient (NSE; Moriasi et al., 2007; Equation 3). NSE is a goodness-of-fit measure often used to assess hydrologic models (for example, Lin et al., 2017). Lin et al. (2017) reports that typically a NSE threshold of 0.65 indicates adequate performance of a given model for most applications.

$$NSE = 1 - \frac{\sum_{t=1}^{N}(obs(t) - mod(t))^2}{\sigma^2} \qquad \text{(Equation 3)}$$

In Equation 3, NSE is calculated as the sum of the squared difference between each observational value (obs) and model (mod) value at each time step divided by the variance of the observed data (σ^2).

In addition to NSE, autocorrelation of model residuals was evaluated using the Box-Ljung test. Autocorrelation of residuals implies that model errors are not independent and that the previous error or residual can be used to predict the following residual. Autocorrelation often suggests that there is a slowly varying process that is not adequately represented by the model.

Coefficients in all models were fitted using the Shuffled Complex Evolution (SCE) algorithm (Duan et al., 1992 and 1994), which is a global optimization method that provides effective and efficient calibration of rainfall-runoff models (Thyer et al., 1999).

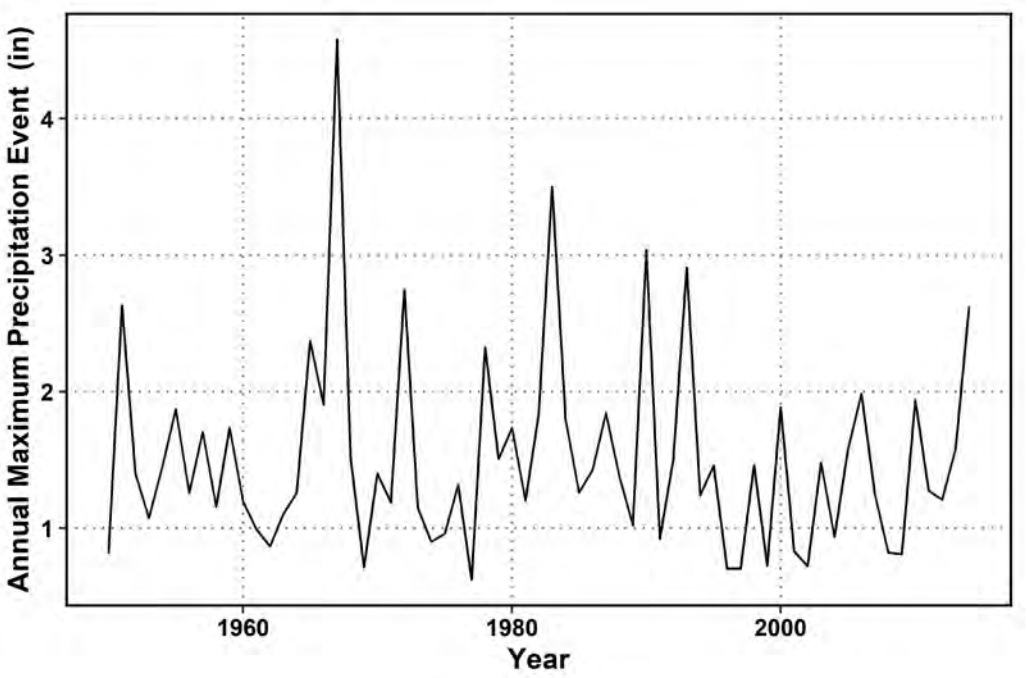

Figure 39. The total precipitation delivered during the largest annual rain event in the EMS basin study area.

5.1.2. Model Results

After running all regression models at daily, monthly, and annual timescales; it was determined that streambed infiltration from the Gila River was best represented by an annual multivariate threshold model with power-law and linear relationships. Power-law relationships between precipitation and streamflow have been observed many studies across a wide variety of catchments, including arid and semi-arid catchments (for example Cheng, 2008 and Crosbie et al., 2013). In the final model, when annual precipitation in the EMS basin study area was below 5.1 inches, streambed infiltration or recharge was set equal to a baseflow of 250 acre-feet/year. When annual precipitation was above 5.1 inches, recharge was a function of a power-law relationship with annual precipitation and a linear relationship with the annual maximum precipitation event (Equation 4; Figure 40).

The Gila streamflow model was calibrated using all available annual recharge data except the data for the large flood event in 1993. This produced the best model and can be justified by the fact that the Gila is a managed system and the amount of water released from the Ashurst-Hayden Dam during 1993 was an outlier compared to all other years (Appendix Figure A4). Figure 41 shows the observed (blue) and modeled (red) recharge results for the Gila River from 1950 to 2015. The NSE for the Gila model is 0.57, which is very reasonable given the managed nature of this system and the residuals were not autocorrelated (Appendix Figure A5). In addition, the total recharge observed from 1950 to 2015 (omitting 1993) was 2.11 million acre-feet, and the total modeled recharge over this same period was 2.10 million acre-feet. This equates to a 0.4% difference in total natural recharge over the 65-year period.

Gila recharge regression model

$$\textbf{If Precip} < \textbf{5.1 inches}$$
$$Recharge(t) = 250 \text{ acre-feet}$$
$$\textbf{If Precip } \geq \textbf{5.1 inches}$$
$$Recharge(t) = 0.0001 * Precip(t)^{7.7} + 15{,}000 * Max.Rain.Event(t)$$

(Equation 4)

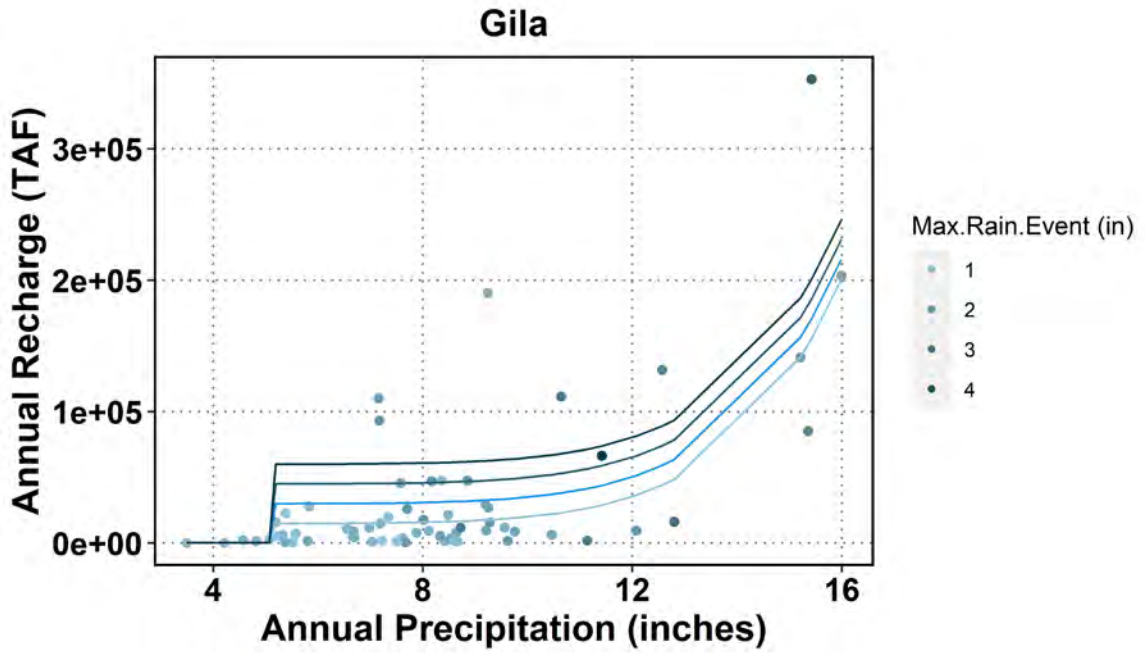

Figure 40. Scatter plot of annual precipitation compared to observed recharge (in thousand acre-feet, TAF) for the Gila River. Color indicates the maximum annual rain event total for the corresponding year. Lines show the power law relationship with annual precipitation and the linear relationship for different maximum annual rainfall events.

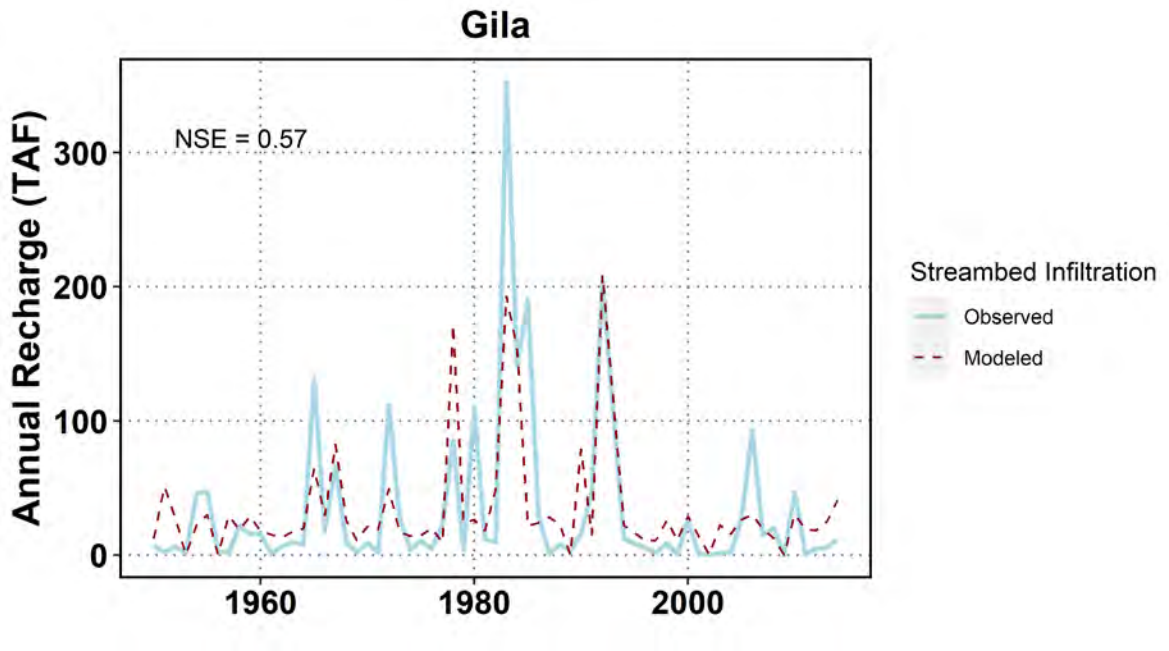

Figure 41. Observed (solid light blue line) and modeled (dashed red line) recharge (i.e., streambed infiltration) in thousand acre-feet (TAF) for the Gila River from 1950 to 2015. Data for 1993 was an outlier and omitted. NSE = Nash-Shutcliffe efficiency.

Similar to the final recharge model for the Gila River, the final model selected to represent recharge from the Santa Cruz River was a piece-wise function based on a power law relationship with annual precipitation. When annual precipitation is less than 7.9 inches, annual recharge is minimal and set to zero. When annual precipitation is greater than 7.9 inches, recharge is estimated using a power law relationship with annual precipitation (Equation 5; Figure 42). The annual maximum precipitation event was not a significant predictor of recharge by streambed infiltration from the Santa Cruz River in any of the models evaluated here and therefore was not included in the final model. Figure 43 shows the observed (blue) and modeled (red) recharge results for the Santa Cruz River from 1950 to 2015. The final Santa Cruz model has an excellent NSE of 0.85 and the residuals were not autocorrelated (Appendix Figure A6). In addition, the total recharge observed from 1950-2015 was 1.38 million acre-feet while the total modeled recharge over this same period was 1.29 million acre-feet. This is a 7.0% difference in total natural recharge over the 65-year period and is a conservative estimate.

Santa Cruz River recharge regression model

$$\textbf{If Precip} < \textbf{7.9 inches}$$
$$Recharge(t) = 0 \text{ acre-feet}$$
$$\textbf{If Precip } \geq \textbf{7.9 inches}$$
$$Recharge(t) = 15{,}000 + 0.005 * Precip(t)^{6.2}$$

(Equation 5)

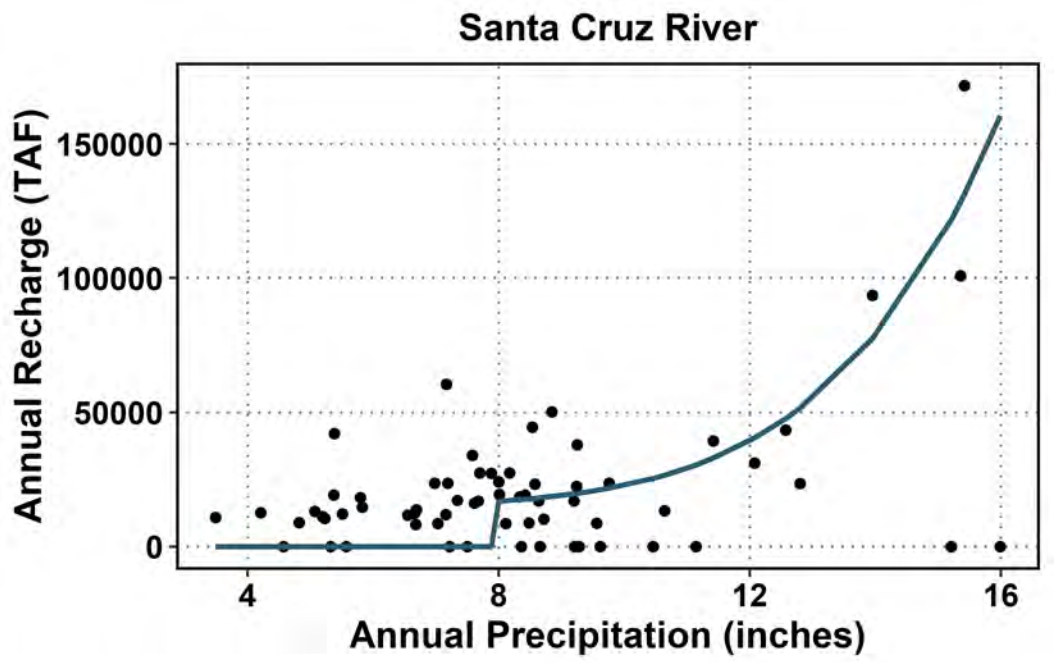

Figure 42. Scatter plot of annual precipitation compared to observed streamflow (in thousand acre-feet, TAF) for the Santa Cruz River. The line shows the power law relationship with annual precipitation.

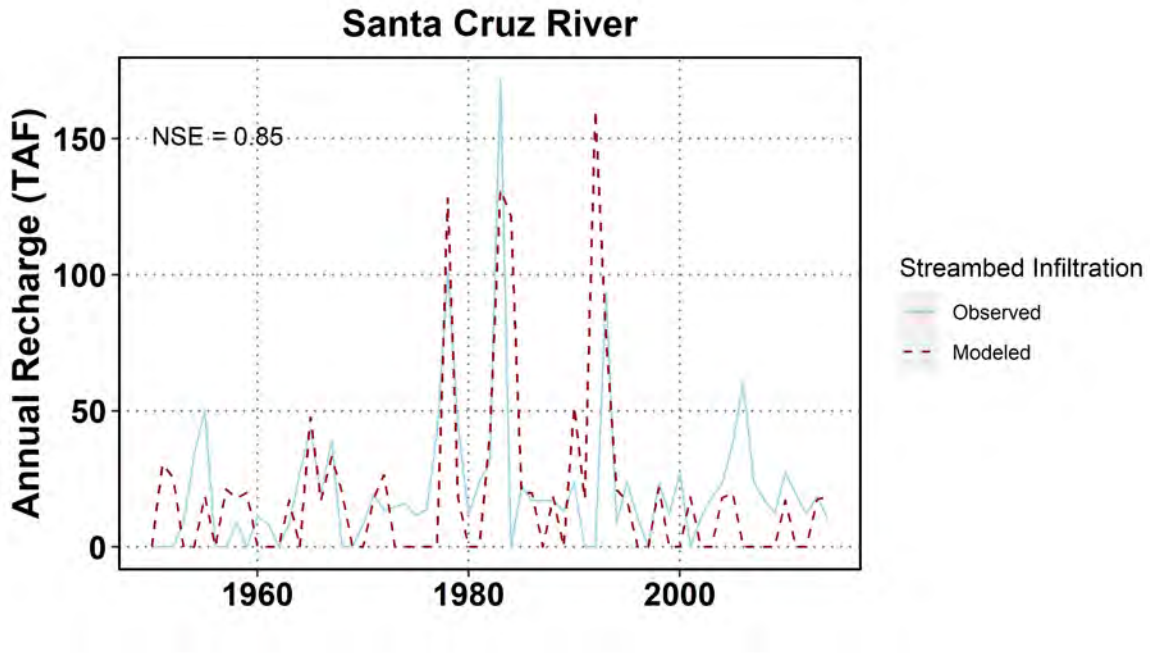

Figure 43. Observed (solid light blue line) and modeled (dashed red line) recharge (i.e., streambed infiltration) in thousand acre-feet (TAF) for the Santa Cruz River from 1950 to 2015. NSE= Nash-Shutcliffe efficiency.

5.1.3. Model Limitations

This modeling effort estimated annual recharge from streambed infiltration on the Gila and Santa Cruz Rivers under future climate scenarios, where the annual volume of streambed infiltration is assumed to equal the annual volume of streamflow entering the model domain. There are three general categories of rainfall-runoff models:

- *Physics-based (process-based) models* such as the Variable Infiltration Capacity (VIC) Macroscale Hydrologic Model (Liang et al., 1994) was outside of the scope of this project. Moreover, physics-based land surface hydrology models often do a poor job representing losing streams such as the Gila and Santa Cruz Rivers, as well as managed streams such as the Gila.

- *Conceptual models* use simplified parameterizations to represent physical processes. However, the parameters are not always directly measurable and usually represent lumped, spatially-averaged catchment characteristics.

- *Metric (empirical) models,* such as the regression models described above in Section 5.1.2, are based solely on the observed relationship between rainfall and streamflow and do not reflect an explicit conceptual or physical representation of the dominant hydrological processes.

Hybrid modeling approaches have also been developed that combine concepts from these general categories of models. For example, hybrid models have been developed that combine physical parameterizations (conceptual approach) with observed relationships (empirical approach) to develop models that are both physically plausible and statistically rigorous (Ye et al., 1997).

This study investigated the use of both conceptual and empirical models to determine the best and most robust model to estimate annual recharge under future climate scenarios. In addition to the empirical models described above, several different hybrid empirical-conceptual models were considered to estimate streamflow or streambed infiltration for the two rivers in the EMS Basin Study area. The main hybrid model considered was the Identification of Hydrographs and Components from Rainfall, Evaporation, and Streamflow (IHACRES) data transfer function model (Ye et al., 1997). IHACRES uses a soil moisture accounting model to determine the effective rainfall or the amount of rainfall that becomes streamflow followed by a unit hydrograph routing model to determine the timing of that streamflow. In the IHACRES model, two different soil moisture accounting models were considered:

- the catchment moisture deficit model (cmd) and

- the catchment wetness index model (cwi).

In addition, four different routing models were considered:

- the autoregressive moving average linear transfer function (armax),
- the exponential component transfer function (expuh),
- a transfer function with two exponential components and variable partitioning (lambda),
- and the power law transfer function model (powuh).

While IHACRES models have been shown to be effective at modeling rainfall-runoff response in a variety of catchments (Ye et al., 1997), they were not ideal for the data in this study. Most of model runs using the IHACRES model had autocorrelated residuals and/or very low NSE. The models that had a reasonable NSE either exhibited autocorrelated residuals or they captured peak responses well—but did not capture any of the baseline streamflow trends. The IHACRES models were not able to capture any of the streamflow trends (except for the two large flood events that occurred in 1983 and 1993). Most likely, this is because the Gila River is a managed system and effluent flows dominate in the Santa Cruz River therefore flows in both rivers do not entirely represent the physical processes that create a runoff response.

In addition to the general limitations of empirical models, it should be noted that the empirical models developed for the Gila and Santa Cruz Rivers are based on the relationship between annual streamflow into the model domain and basin-averaged climate conditions over the EMS study area-averaged, rather than climate conditions over each river's upstream drainage area. The Gila River drains an area of nearly 60,000 square miles, with about half of that area upstream of the EMS Basin Study area. The Santa Cruz River drains approximately 8,000 square miles in the United States and a small area of Mexico. Developing climate scenarios encompassing the upstream drainage areas of the Gila and Santa Cruz Rivers was beyond the scope of this study. In addition, Gila River streamflow entering the study area is regulated by operation of Coolidge and Ashurst-Hayden Dams, whereas Santa Cruz River streamflow entering the study area is strongly influenced by treated effluent discharged to the river in Nogales, Tucson, and other upstream communities. Streamflow entering the study area is, therefore, strongly influenced by upstream operations and management activities. Modeling the effects of upstream operations and management on streamflows entering the study area was also beyond the scope of this study.

A correlation analysis was performed between climate variability over the EMS Basin Study area and the upstream watersheds of the Santa Cruz and Gila Rivers. This analysis indicates that interannual variability and long-term trends in historical precipitation are consistent between the Basin Study area and the upstream watersheds. Appendix Figure A7 compares observed historical annual precipitation from the Livneh 2015 dataset averaged over each respective drainage area to observed historical annual precipitation

averaged over the EMS basin study area. Annual precipitation in both watersheds is significantly correlated with annual precipitation over the EMS Basin Study area (Pearson test, p-value < 0.001). The correlation coefficients for the Santa Cruz and the Gila Rivers are 0.84 and 0.81, respectively. Given the strongly correlated relationship between annual precipitation in the three watersheds, it is likely that the statistical relationship between spatially-averaged precipitation and streambed infiltration for each river is similar to the relationship developed with respect to basin-averaged precipitation over the EMS Basin Study area. In addition, a literature review of projected climate change over the Southwestern U.S. indicates that projected changes in temperature and precipitation are largely consistent between the basin study area and upstream watersheds (for example, Seager et al., 2013). It would be insightful for future studies to investigate these relationships with independent climate datasets.

5.2. Future Recharge Scenarios

Future recharge scenarios were developed from the climate scenarios described in Section 4. Daily and annual precipitation from each scenario was input into the model equations described above (Equations 4 and 5) to develop projected annual groundwater recharge for each river. One future recharge scenario was developed corresponding to each future climate scenarios; the same nomenclature is used for recharge scenarios as for the future climate scenarios: Hot-Wet (HW), Hot-Dry (HD), Warm-Wet (WW), Warm-Dry (WD) and Central-Tendency (CT).

Similar to the future precipitation scenarios, future recharge scenarios reflect large uncertainties in future climate conditions, with wetter scenarios indicating increased recharge and drier scenarios indicating decreased recharge from both rivers (Table 6; Figure 45; Figure 46). Figure 47 and Figure 48 show projected recharge over the next century for each future scenario for the near future time period (2045–2074) for the Gila River and Santa Cruz River respectively. Figures A8 and A9 in the appendix show the projected recharge for each river under each future scenario for the far future time period (2065–2094). In the near future, the wet scenarios project the average annual recharge to increase by 15% (HW) and 31% (WW) for the Gila River and by 4% (HW) and 8% (WW) for the Santa Cruz River. On the other hand, in the near future the dry scenarios project the average annual recharge to decrease by 37% (HD) and 35% (WD) for the Gila River and by 51% (HD) and 52% (WD) for the Santa Cruz River. The Central Tendency scenario suggests that by the far future, average annual recharge will decrease by 4% for the Gila River and 12% for the Santa Cruz River.

Table 6. The average annual change in natural recharge over the 101-year period from the Santa Cruz and Gila Rivers between baseline and two simulated future periods for each future climate scenario

Time Period	Scenario	Change in Recharge from Baseline to Future			
		Gila River		Santa Cruz River	
		(TAF)	(%)	(TAF)	(%)
1981-2010	Baseline	42	-	26	-
2045-2074	CT	-10	-23	-8	-32
	HD	-16	-37	-13	-51
	HW	6	15	4	15
	WD	-15	-35	-14	-52
	WW	13	31	8	30
2065-2094	CT	-2	-4	-3	-12
	HD	-21	-49	-16	-63
	HW	20	48	11	41
	WD	-18	-43	-16	-60
	WW	27	65	16	60

Note:

- Color indicates degree of change, with red indicating a decrease in recharge and blue indicating an increase in recharge from baseline conditions.
- Change is designated in thousand acre-feet (TAF) and percent change (%). The baseline average annual recharge is indicated in bold for each river

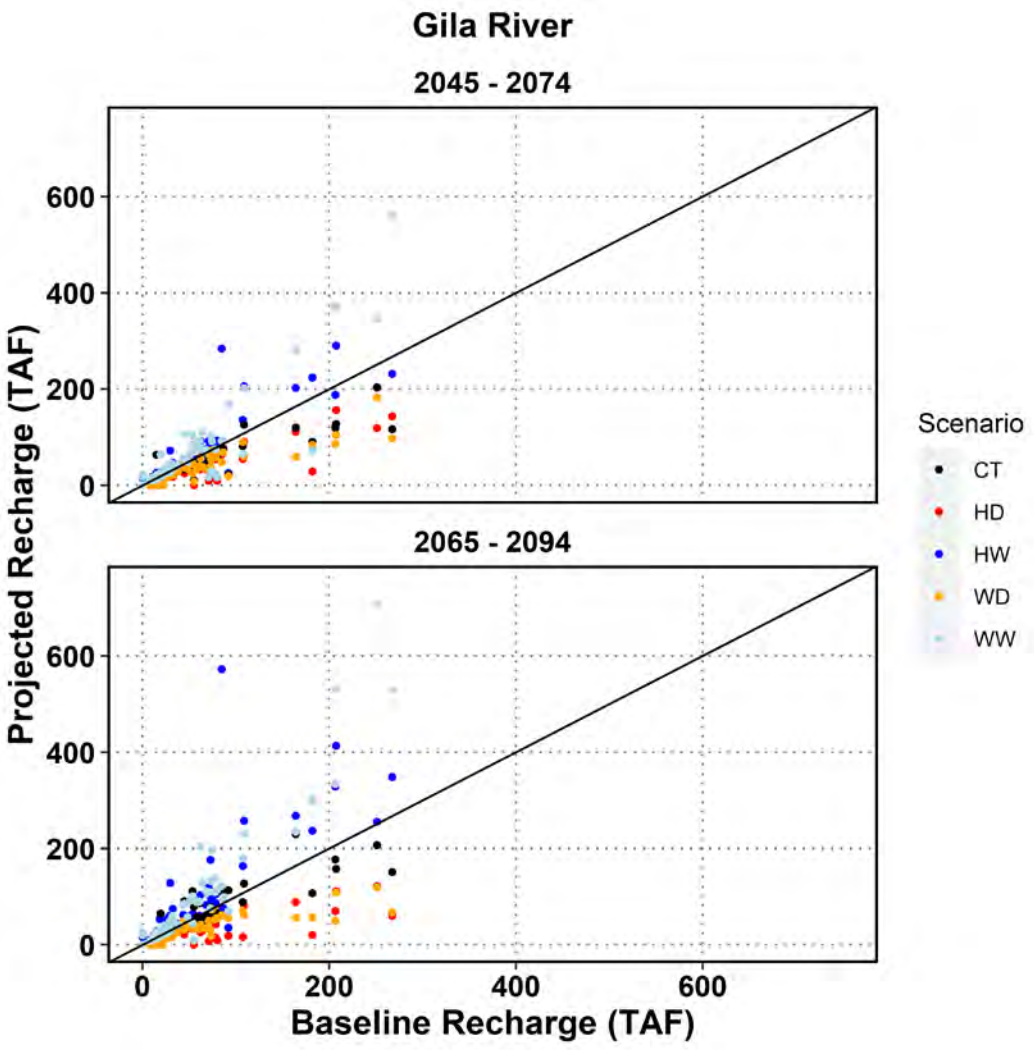

Figure 44. Scatterplot of baseline annual recharge compared to projected annual recharge for the Gila River for both future time periods and each future climate scenario. Points above the line represent projected increases in recharge while points below the line represent projected decreases in recharge from the baseline scenario.

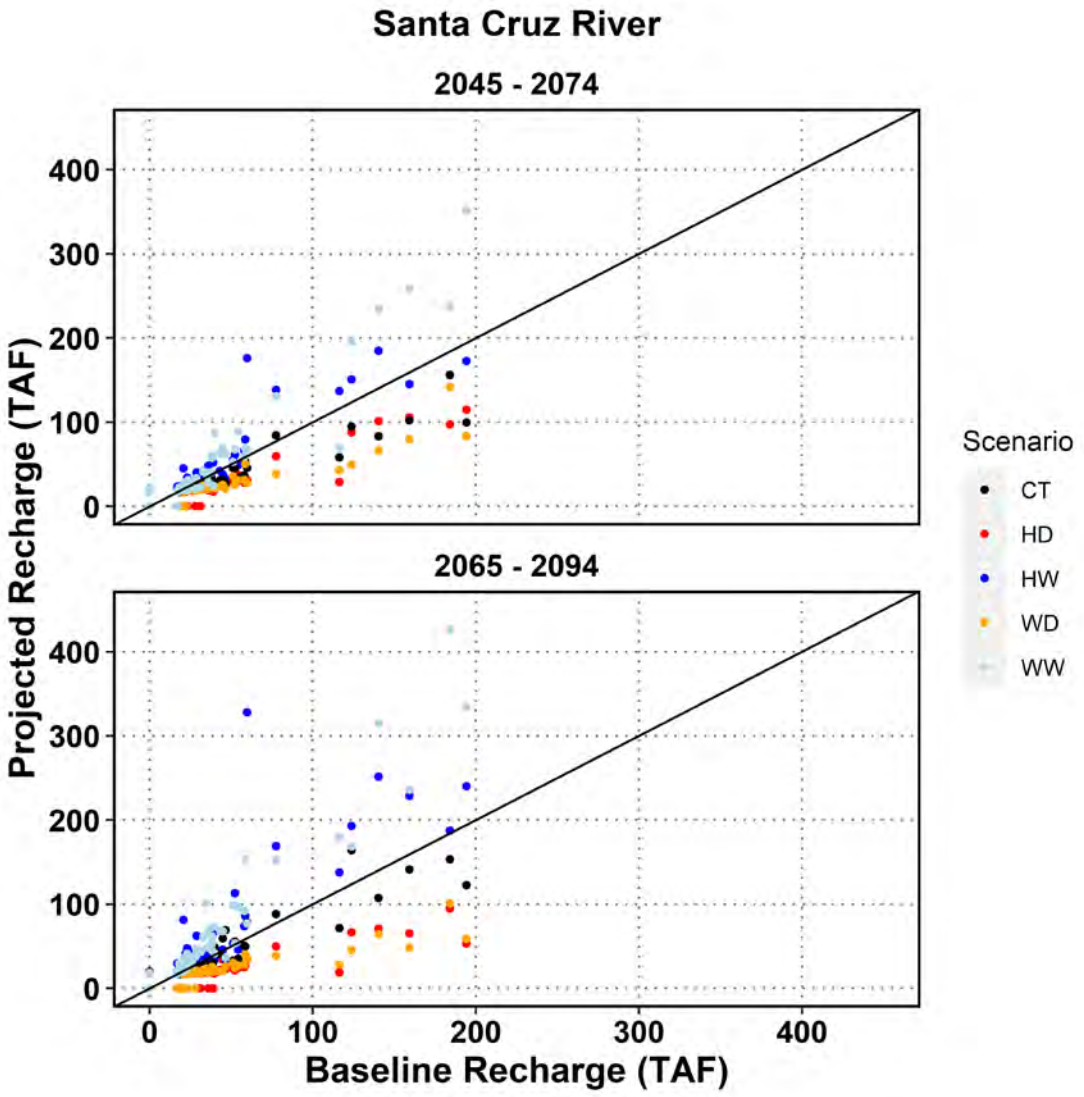

Figure 45. Timeseries of projected annual natural recharge from the Santa Cruz River for both future time periods and each future climate scenario.

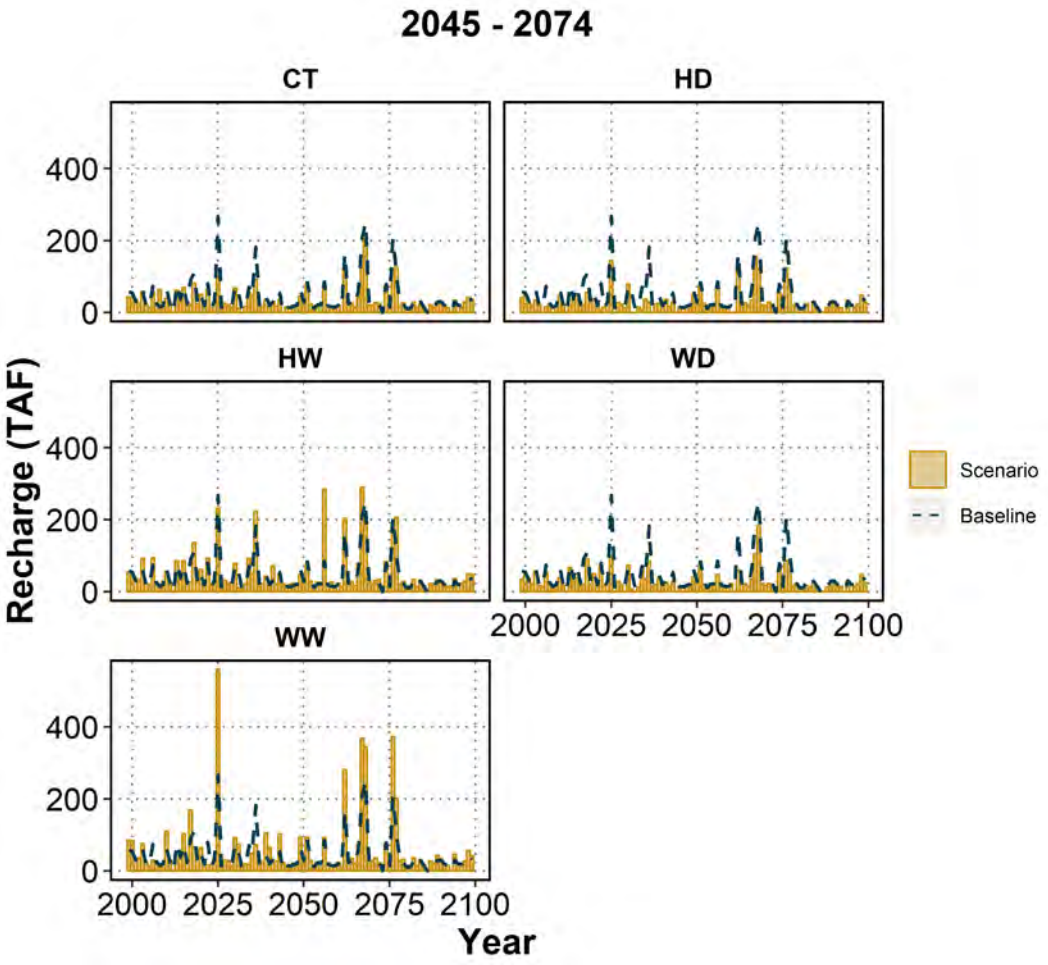

Figure 46. Gila River projected recharge for each future climate scenario (tan bars) compared to the historic baseline recharge (dashed blue line) for the 2045-2074 future time period. Note the different Y-axis scales for each scenario.

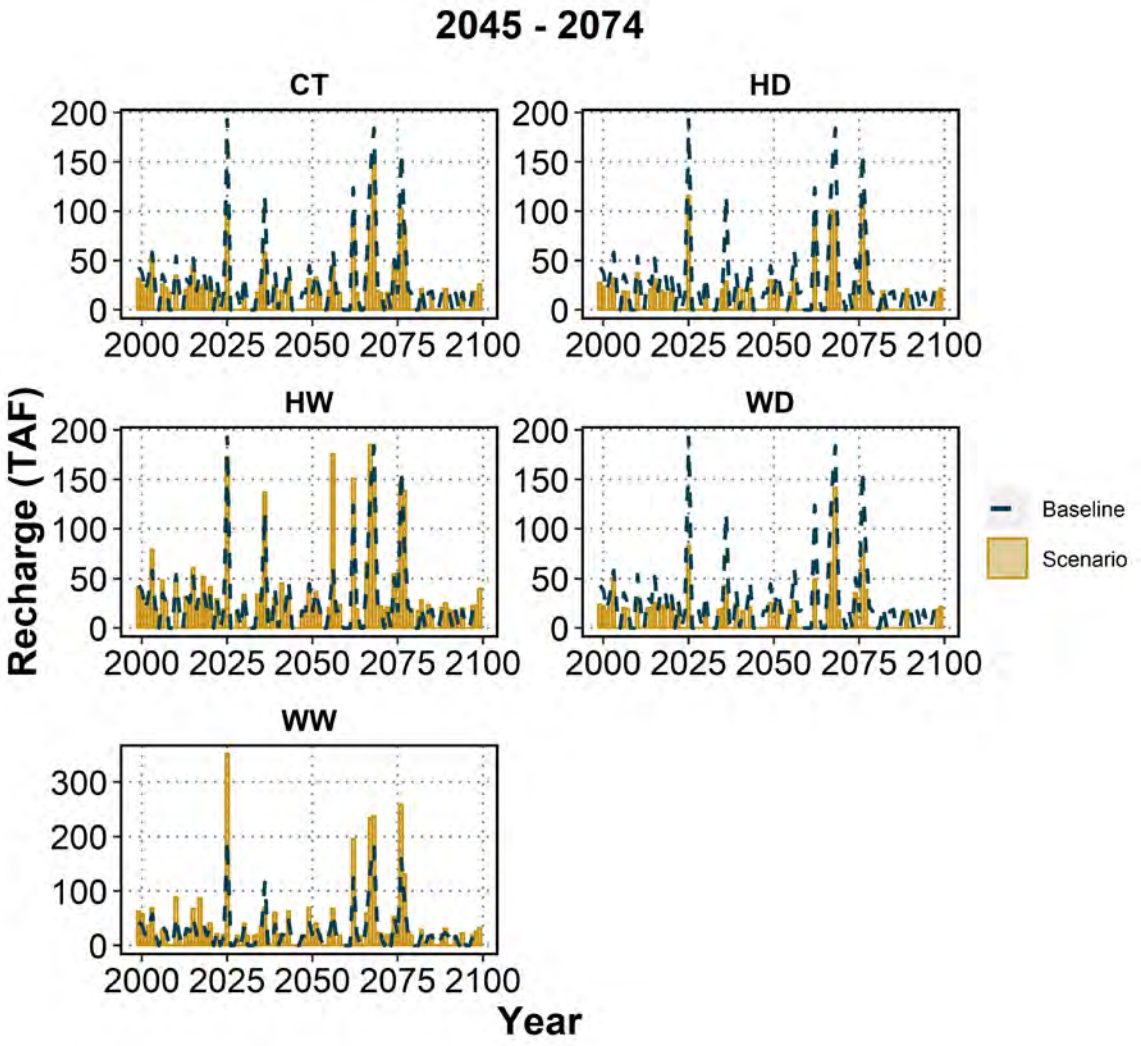

Figure 47. Santa Cruz River projected recharge for each future climate scenario (tan bars) compared to the historic baseline recharge (dashed blue line) for the 2045-2074 future time period. Note the different Y-axis scales for each scenario.

These projections suggest a slightly larger decrease in mean annual recharge than was estimated in a recent study that used the USGS Soil Water Balance model (SWB; Westenbroek et al., 2018) to estimate recharge over the entire lower Colorado River Basin (Tillman et al., 2020). This study found that the median change in annual groundwater recharge across the lower Colorado River Basin based on 97 CMIP5 projections decreased by about 1% compared to estimated recharge under historical climate conditions. Similar to the range of projections used in this study, in Tillman et al. (2020), the upper quartile (from the wetter projections) projected change in recharge suggests an increase of approximately 20-30% while the lower quartile (from the drier projections) projected change in recharge suggests a decrease of approximately 20-40% over the next century.

The cumulative total baseline scenario recharge from 1915 to 2015 for the Gila River is 4,333 TAF. In comparison, total recharge under the wet scenarios ranges from 5,640 TAF (WW) to 4,956 TAF (HW) for the near future time period (2045-2074), and from 7,110 TAF (WW) to 6,349 TAF (HW) for the far future time period (2065-2094). This translates into an increase in cumulative total recharge of approximately 30-60 percent the Warm-Wet (WW) scenarios and 10-50 percent for the Hot-Wet (HW) scenarios over a century.

The cumulative total baseline scenario recharge from 1915 to 2015 for the Santa Cruz River is about 60% that of the Gila River at approximately 2,606 TAF. Recharge from the Santa Cruz River is projected to change by roughly the same percentages as the Gila river. Cumulative total recharge is projected to increase by 10-50 percent under both the Warm-Wet (WW) and Hot-Wet (HW) future scenarios compared to the baseline. Specifically, under the Warm-Wet (WW) scenarios, cumulative total recharge over the 101-year simulation period is projected to increase to 3,410 TAF (+30%) for the near-future period (2045-2074) and to 4,204 TAF (+60%) for the far-future period (2065-2094). Under the hot-wet scenarios, cumulative total recharge is projected to increase to 2,988 TAF (+15%) for the near-future period and to 3,682 TAF (+41%) for the far-future time period.

Figure 48 and Figure 49 display the relationship between annual precipitation and recharge for the central-tendency scenario for the Gila River and the Santa Cruz River respectively. It is apparent in these figures that increases in annual precipitation above a certain amount lead to proportionally larger increases in recharge due to the power law relationship between annual precipitation and recharge. Individual figures showing projected recharge and precipitation for each scenario and each river can be found in the Appendix Figures A10-A17.

The power law relationship between annual precipitation and recharge (Section 5.1.1; Figure 40 and Figure 42) results in a larger projected change in recharge under wet future scenarios compared to projected changes under the dry scenarios. This larger increase is based primarily on the handful of years projected to experience extremely wet conditions. Extremely wet conditions are defined as those years in which annual precipitation exceeds the 95th percentile of historical observed annual precipitation (see Section 4.2.2 and Table 5). Both wet scenarios indicate more extremely wet years than the baseline scenario for both future time periods (see Section 4.2.2 and Table 5). This increase in the frequency of extreme annual precipitation drives a similar increase in the frequency of extremely wet recharge under all of the wet scenarios, where extremely wet recharge is defined as annual recharge greater than the 95th percentile of annual recharge under the baseline scenario. The frequency of years with extreme recharge increases from 2 years over a 30-year period under the baseline scenario to three years over a 30-year period under the near future WW scenario and 4 years out of a 30-year period under the far future wet scenarios (Table 7). In contrast, there are no extremely wet recharge years under the dry scenarios, which results in a significant decrease in projected recharge under these scenarios compared to the baseline scenario.

Table 8 shows the number of extremely dry recharge years for each future time period and scenario, where the extremely dry recharge is defined as annual recharge less than the 5th percentile of annual recharge under the baseline scenario. For Gila River recharge, the frequency of extremely dry recharge years is projected to decrease under the wetter scenarios for both future time periods while the frequency of extremely dry recharge is projected to increase by as much as 250% under the drier scenarios. Natural streamflow from precipitation in the Santa Cruz River in the EMS basin study area is much less than that of the Gila with many years experiencing zero streamflow. In fact, there were 10 years out of 30 during the baseline period (1981-2010) where none of the Santa Cruz River streamflow was attributed to precipitation (i.e., there was no natural streamflow and all the flow in the Santa Cruz was effluent dominated). When projecting how future precipitation trends will influence Santa Cruz natural streamflow or recharge, the wetter scenarios all suggest the number of years with no flow will remain the same or slightly decrease while the drier scenarios project an increase of up to 22 years with no flow out of the 30-year future time period.

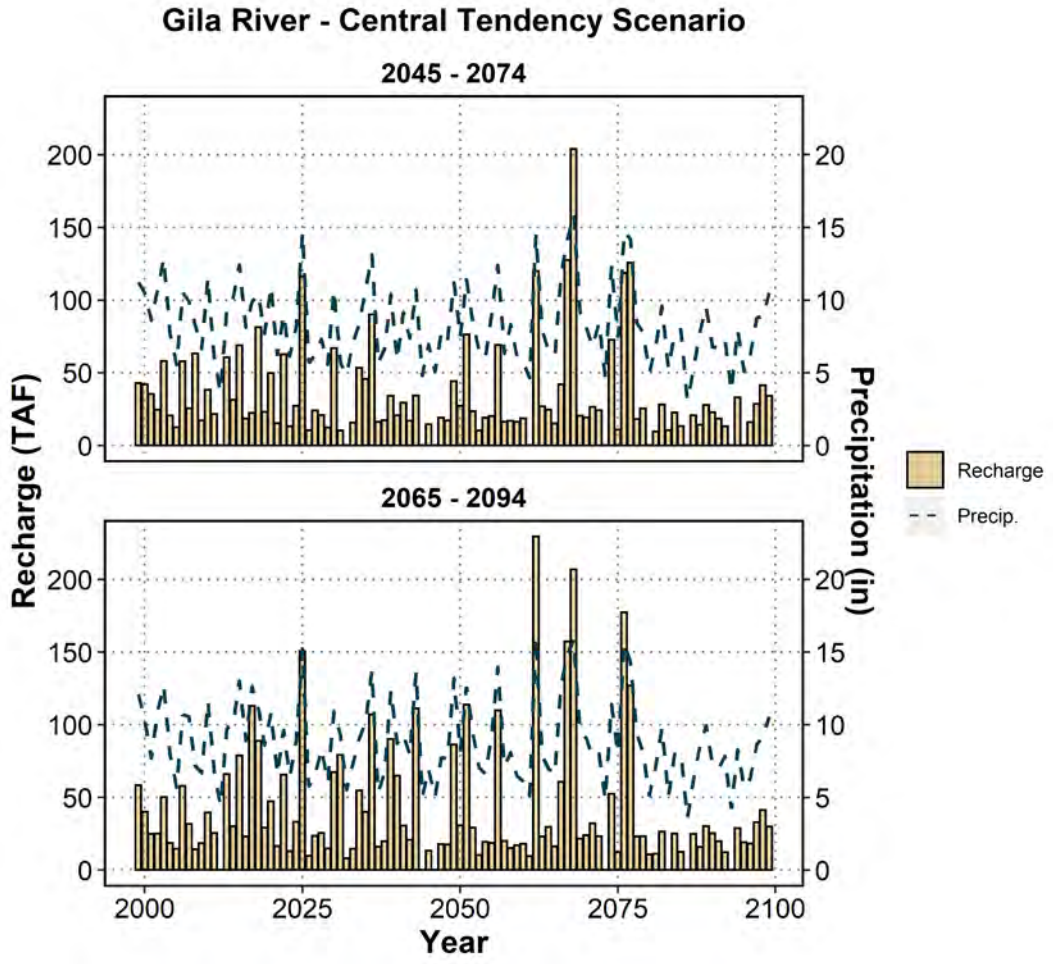

Figure 48. Projected annual recharge for the **Central Tendency (CT)** scenario and both future time periods for the Gila River (tan bars). The dashed blue line shows the projected annual precipitation for the same scenario and time period.

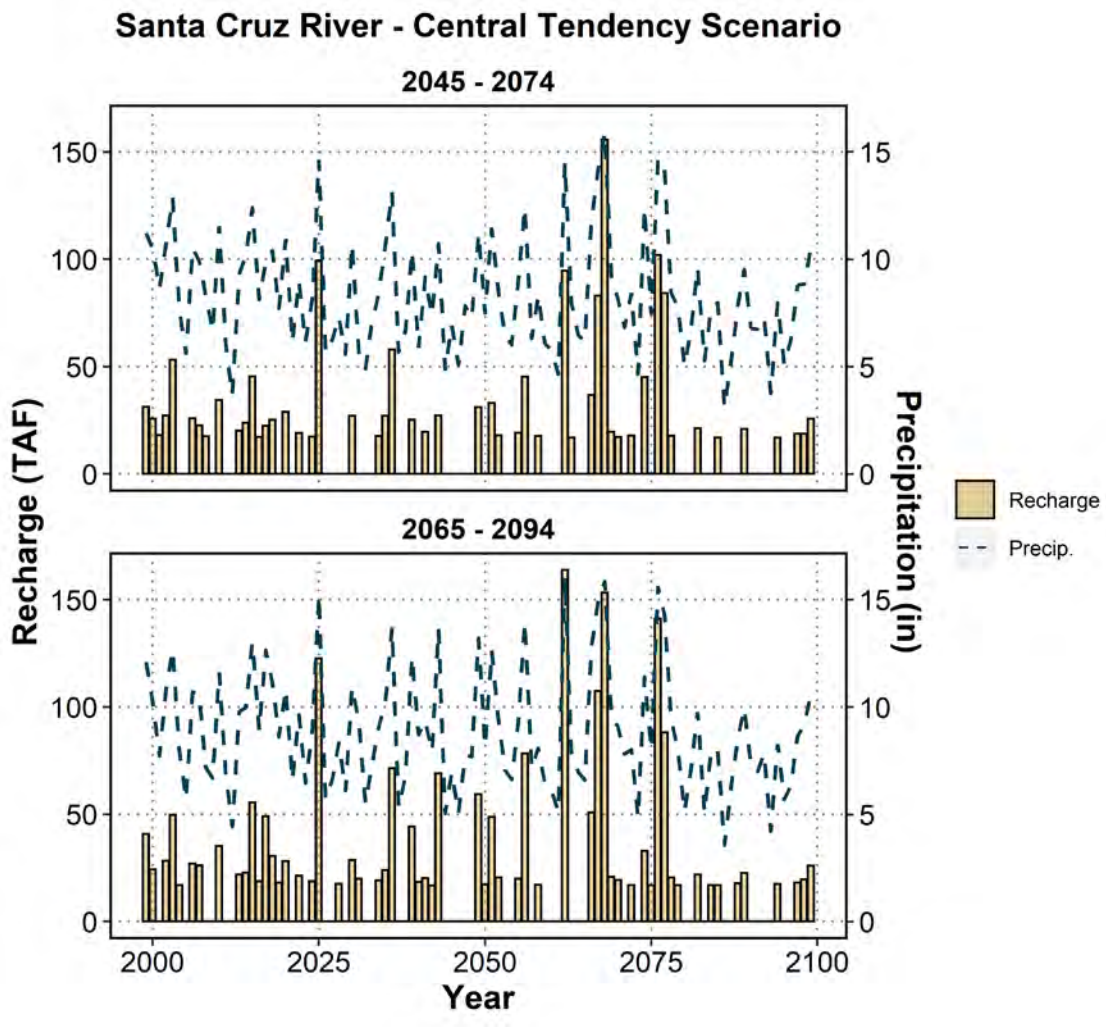

Figure 49. Projected annual recharge for the **Central Tendency (CT) scenario** and both future time periods for the Santa Cruz River (tan bars). The dashed blue line shows the projected annual precipitation for the same scenario and time period.

Table 7. The number of extremely wet recharge years for each future scenario and time period where the annual recharge is projected to surpass the 95th percentile of the baseline scenario annual recharge

Extremely Wet Recharge Years				
Time Period	**Scenario**	**Stat**	**# of Years in 30-year period**	
			Gila	**Santa Cruz**
1981 - 2010	Baseline	0.95	2	2
2045_2074	CT	0.95	0	1
	HD	0.95	0	0
	HW	0.95	1	2
	WD	0.95	0	0
	WW	0.95	3	3
2065_2094	CT	0.95	0	1
	HD	0.95	0	0
	HW	0.95	4	4
	WD	0.95	0	0
	WW	0.95	4	4

*The baseline scenario 95th percentile for the Gila River is 207 TAF and for the Santa Cruz River is 150 TAF.

Table 8. The number of extremely dry recharge years for each future scenario and time period where the annual recharge is projected to be less than the 5th percentile baseline scenario recharge

Extremely Dry Recharge Years				
Time Period	**Scenario**	**Stat**	**# of Years in 30-yr period**	
			Gila	**Santa Cruz**
1981 - 2010	Baseline	0.05	3	10
2045_2074	CT	0.05	4	16
	HD	0.05	6	20
	HW	0.05	1	7
	WD	0.05	5	22
	WW	0.05	2	10
2065_2094	CT	0.05	4	12
	HD	0.05	7	22
	HW	0.05	2	9
	WD	0.05	7	22
	WW	0.05	2	8

*The baseline scenario 5th percentile for the Gila River is 250 TAF and for the Santa Cruz River is 0 TAF.

6. References

Bates, B. (2020). Personal Communication.

Chen, X. and S.J. Jeong (2018). Irrigation enhances local warming with greater nocturnal warming effects than daytime cooling effects. Environmental Research Letters, 13(2). https://doi.org/10.1088/1748-9326/aa9dea.

Cheng, Q. (2008). A combined power-law and exponential model for streamflow recessions. Journal of Hydrology, 352, 157-167.

CPC. (2015). Climate Glossary. National Oceanic and Atmospheric Administration, National Weather Service, Climate Prediction Center, http://www.cpc.ncep.noaa.gov/ products/outreach/glossary.shtml.

Crosbie, R.S., B.R., Scanlon, F.S. Mpelasoka, R.C. Reedy, J.B. Gates, and L. Zhang (2013). Potential climate change effects on groundwater recharge in the High Plains Aquifer, USA. Water Resources Research, 49(7), 3936–3951. https://doi.org/10.1002/wrcr.20292.

Duan, Q., S. Sorooshian, and V. Gupta (1992). Effective and Efficient Global Optimization for Conceptual Rainfall-Runoff Models. Water Resources Research, 28(4), 1015-1031.

Duan, Q., S. Sorooshian, and V. Gupta (1994). Optimal use of the SCE-UA global optimization method for calibrating watershed models. Journal of Hydrology, 158, 265-284.

Hirsch, R.M., R.B. Alexander, and R.A. Smith (1991). Selection of methods for the detection and estimation of trends in water quality. Water Resources Research, 27(5), 803-813.

Intergovernmental Panel on Climate Change (IPCC) (2013). Climate Change 2013: The Physical Science Basis. Contribution of Working Group I to the Fifth Assessment Report of the Intergovernmental Panel on Climate Change. (T.F. Stocker, D. Qin, G-K. Plattner, M. Tignor, S.K. Allen, J. Boschung, A. Nauels, Y. Xia, V. Bex, and P.M. Midgley [Editors]). Cambridge University Press; Cambridge, United Kingdom and New York, New York, United States, 1535.

IPCC (2014a). Climate Change 2014: Impacts, Adaptation, and Vulnerability. Contribution of Working Group II to the Fifth Assessment Report of the Intergovernmental Panel on Climate Change. (C.B. Field, V.R. Barros, D.J. Dokken, K.J. Mach, M.D. Mastrandrea, T.E. Bilir, M. Chatterjee, K.L. Ebi, Y.O. Estrada, R.C. Genova, B. Girma, E.S. Kissel, A.N. Levy, S. MacCracken, P.R. Mastrandrea, and L.L. White [Editors]), Cambridge, 1132.

IPCC (2014b). Climate Change 2014: Synthesis Report. Contribution of Working Groups I, II and III to the Fifth Assessment Report of the Intergovernmental Panel on Climate Change. (Core Writing Team, R.K. Pachauri and L.A. Meyer [Editors]), IPCC, Gene, 151.

Lawrence Livermore National Laboratory (LLNL) (2019). Green Data Oasis. URL: https://hpc.llnl.gov/services/green-data-oasis. Accessed August, 2020.

Liang, X., D.P. Lettenmaier, E.F. Wood, and S. J. Burges (1994). A simple hydrologically based model of land surface water and energy fluxes for GSMs. Journal of Geophysical Research, 99(D7), 14415–14428.

Lin, F., X.,Chen, and H. Yao (2017). Evaluating the use of Nash-Sutcliffe efficiency coefficient in goodness-of-fit measures for daily runoff simulation with SWAT. Journal of Hydrologic Engineering, 22(11), 05017023.

Liu, S., K. Nelson, D. Yunker, W., Hipke, and F. Corkhill (2014). Regional Groundwater Flow Model of the Pinal Active Management Area, Arizona: Model Update and Calibration. Arizona Department of Water Resources, Model Report, 381.

Livneh, B. (2016). Livneh 2016 dataset. Personal Communication.

Livneh, B., E.A. Rosenberg, C. Lin, B. Nijssen, V. Mishra, K.M. Andreadis, et al. (2013). A long-term hydrologically based dataset of land surface fluxes and states for the conterminous United States: Update and extensions. Journal of Climate, 26(23), 9384–9392. https://doi.org/10.1175/JCLI-D-12-00508.

Livneh, B., T. Bohn, D. Pierce, F. Munoz-Ariola, B. Nijssen, R. Vose, R., et al. (2015). A Spatially Comprehensive, Hydrometeorological Dataset for Mexico, the U.S., and Southern Canada 1950-2013. Nature Scientific Data, 5(150042). doi:10.1038/sdata.2015.42.

Mason, D. and W. Hipke (2013). Regional Groundwater Model of the Tucson Active Management Area, Arizona, Model Update and Calibration. Arizona Department of Water Resources. Modeling Report No. 24.

Menne, M., I. Durre, B. Korzeniewski, S. McNeal, K. Thomas, X. Yin, et al. (2012). Global Historical Climatology Network—Daily (GHCN Daily), Version 3.22. NOAA National Climatic Data Center. Retrieved from https://docs.opendata.aws/noaa-ghcn-pds/readme.htmlh.

Moriasi, D.N., J.G. Arnold, M.W. Liew, R.L. Van, Bingner, R.D. Harmel, and T.L. Veith (2007). Model Evaluation Guidelines for Systematic Quantification of Accuracy in Watershed Simulations. American Society of Agricultural and Biological Engineers: Soil and Water Division, 50(3), 885-900.

National Weather Service (NWS) (2015). National Weather Service Glossary. https://w1.weather.gov/glossary/. Accessed August 2, 2019.

Pierce, D.W., D.R. Cayan, and B.L. Thrasher (2014). Statistical downscaling using localized constructed analogs (LOCA). Journal of Hydrometeorology, 15(6), 2558–2585.

Reclamation (2010). Draft Feasibility-Level Engineering Report Continued Phased Development of the Columbia Basin Project—Enlargement of the East Low Canal and Initial Development of the East High Area. (October 2010).

Reclamation (2016a). Klamath River Basin Study. Technical Memorandum 86-68210-2016-06. Denver, Colorado. https://www.usbr.gov/watersmart/bsp/docs/klamath/fullreport.pdf.

Reclamation (2016b). Sacramento and San Joaquin Basins Study,. https://www.usbr.gov/watersmart/bsp/docs/finalreport/sacramento-sj/Sacramento_SanJoaquin_TechnicalReport.pdf.

Reclamation (2020). American River Basin Study: Development of Future Climate and Hydrology Scenarios. Technical Memorandum No. ENV-2020-067, Denver, Colorado.

Seager, R., M. Ting, C. Li, N. Naik, B. Cook, J. Nakamura, J., and H. Liu (2013). Projections of declining surface-water availability for the Southwestern United States. Nature Climate Change, 3(5), 482-486. https://doi.org/10.1038/nclimate1787.

Shepard, D. (1984). Computer Mapping: The SYMAP Interpolation Algorithm. Spatial Statistics and Models. G.L. Gaile and C.J. Wilmott [Editors]. D. Reidel, 133-145.

Taylor, K.E., R.J. Stouffer, and G.A. Meehl (2012). An overview of CMIP5 and the experiment design. Bulletin of the American Meteorological Society, 93(4), 485-498.

Thyer, M., G. Kuczera, and B.C. Bates (1999). Probabilistic optimization for conceptual rainfall-runoff models: A comparison of the shuffled complex evolution and simulated annealing algorithms. Water Resources Research, 35(3), 767-773.

Tillman, F.D., S. Gangopadhyay, and T. Pruitt (2020). Trends in historical and projected climate data for the Colorado River Basin and potential effects on groundwater availability. U.S. Geological Survey Scientific Investigations Report, 2020-5107. https://pubs.er.usgs.gov/publication/sir20205107.

Westenbroek, S.M., J.A. Engott, V.A. Kelson, and R.J. Hunt (2018). SWB Version 2.0—A Soil-Water-Balance code for estimating net infiltration and other water-budget components: U.S. Geological Survey Techniques and Methods, Book 6, chap. A59, 118. https://doi.org/10.3133/tm6A59.

Ye, W., B.C. Bates, N.R. Viney, and M. Sivapalan (1997). Performance of conceptual rainfall-runoff models in low-yielding ephemeral catchments, 33(1), 153-166.

Appendix A

Historical Climate

The following figures show the comparison of gridded Livneh average maximum temperatures in the EMS Basin Study area to station data.

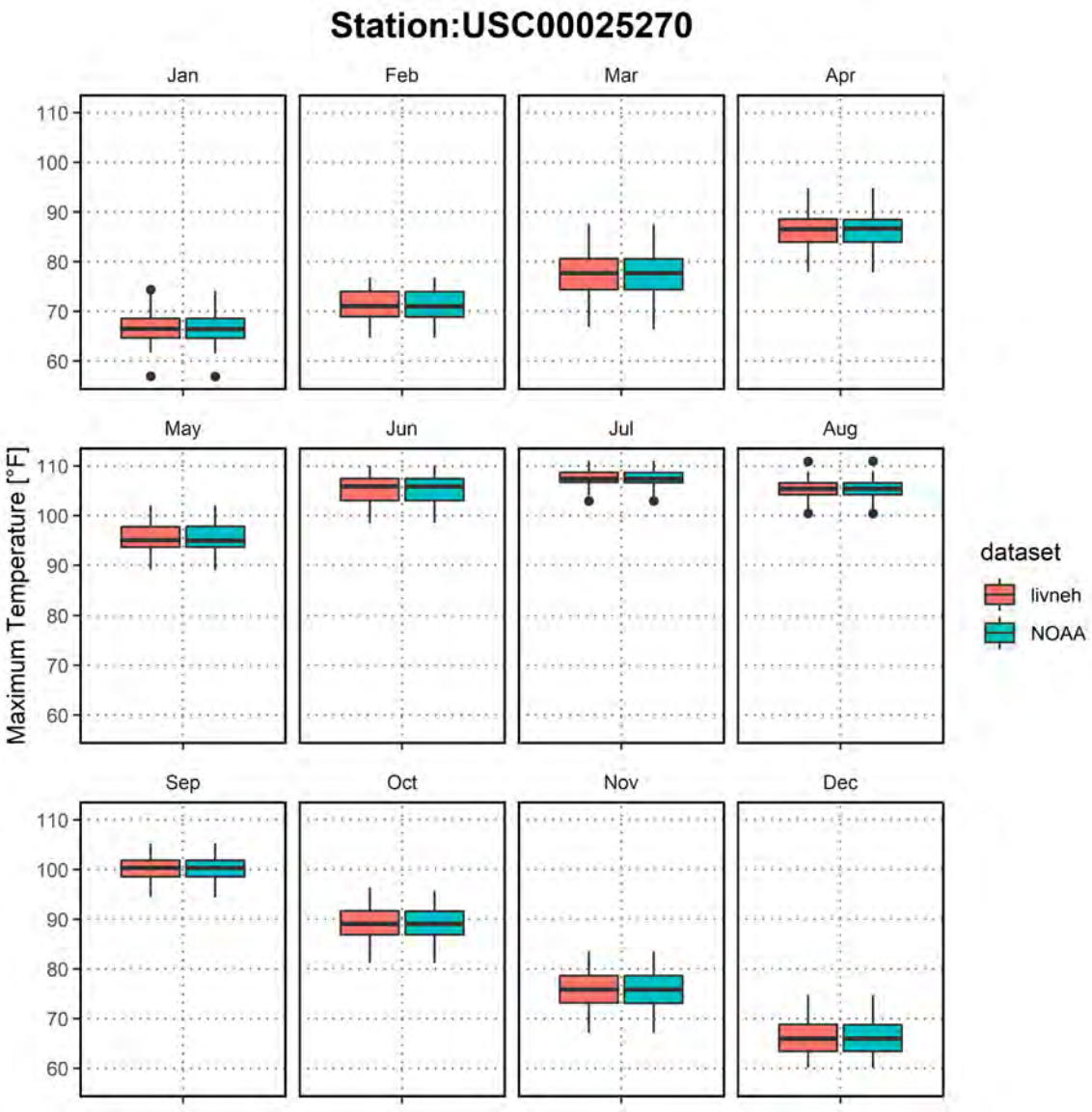

Figure A1. Boxplot of monthly average maximum temperatures from 1950-2015 at the USC00025270 Maricopa station, compared to the corresponding L2015 data from the respective grid cell.

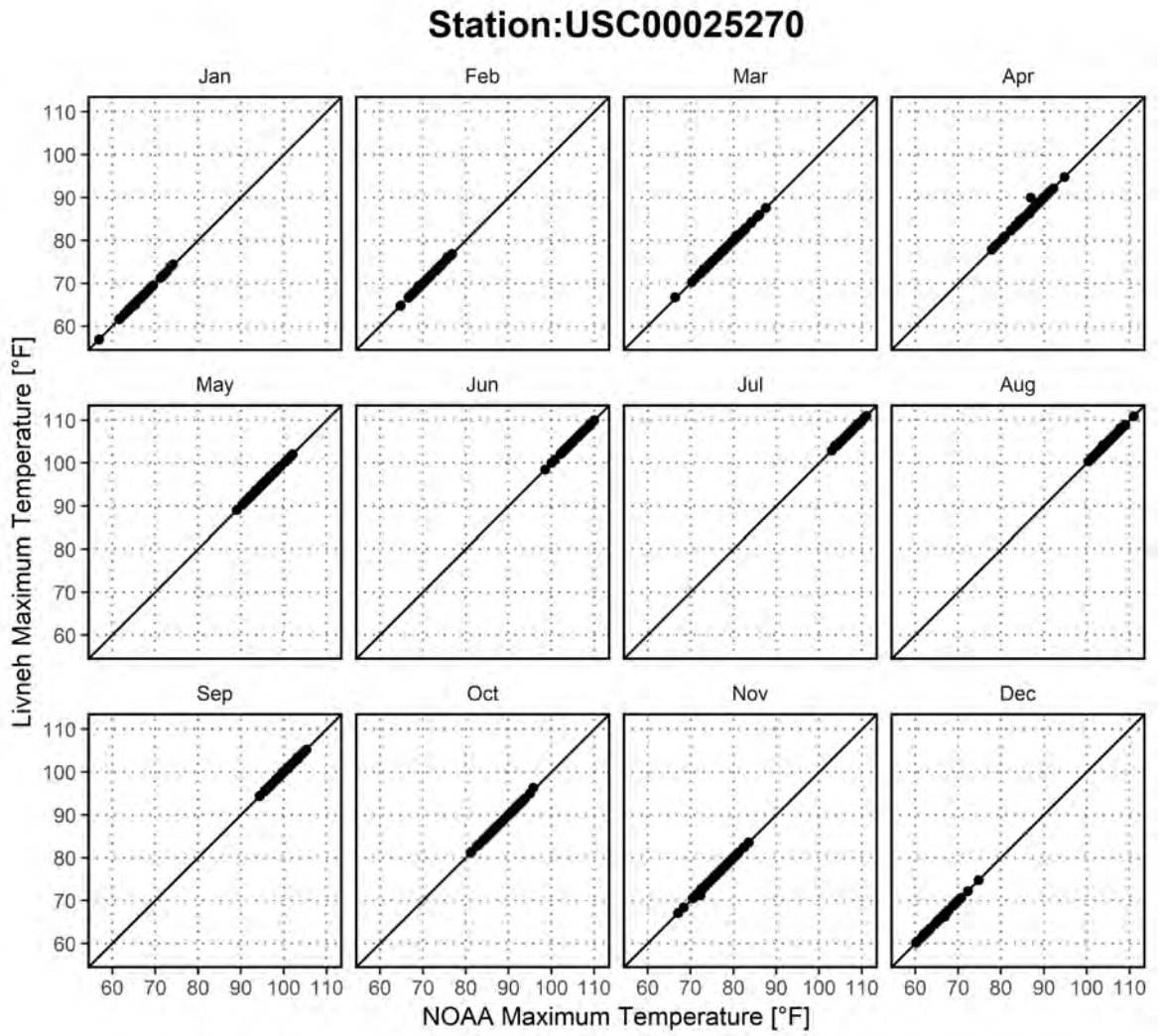

Figure A2. Scatterplot of monthly average maximum temperatures from 1950-2015 at the USC00025270 Maricopa station compared to the corresponding L2015 data from the respective grid cell.

Temporal Disaggregation of Annual Streamflow for the Gila and Santa Cruz Rivers

Disaggregation of the annual streamflows for the Gila River to daily and monthly timeseries was performed by using a nearby 'training' datasets. On the Gila River, there are three upstream gages with daily timeseries (Figure 37):

- a gage at the Coolidge Dam outflow (USGS 09469500; 'gila river below coolidge dam';1930-present),
- a gage at Kelvin (USGS 09474000 'gila river at kelvin'; 1930-present) that represents inflow into the Gila River, and
- a gage at the Florence Casa Grande Canal (USGS 09475500; 'florence-casa grande canal'; 1985-present) that also represents inflow into the Gila River.

There are two ways to use these gage datasets to estimate a daily flow regime for the water that flows on the Gila River and then to disaggregate the annual SCIP reports that represent the water inflow into the domain:

- Subtracting the Coolidge Dam outflow and the Kelvin inflow and
- Subtracting the Coolidge Dam outflow and the Florence Casa Grande Canal inflow into the Gila.

Both of those differences represent a daily timeseries of flow that can be used as a training dataset to disaggregate the SCIP annual reports into monthly and daily timeseries using the same daily and monthly proportions of flow as the training datasets. It is important to note that this disaggregation technique is based on the disaggregation of a regulated flow (from Coolidge Dam) and, therefore, assumes that the releases from Coolidge Dam and Ashurst Hayden Dam are correlated in time. Both timeseries generated from each training dataset were used in the daily and monthly models.

Daily and monthly streamflow timeseries for the Santa Cruz River were estimated by subtracting the measured effluent from the Roger and Ina gages (effluent gages) from the Trico gage while also accounting for infiltration loss along the stream reach before it entered the model domain (Figure 37). Average infiltration loss was calculated as a loss in cubic feet per second (cfs) per mile) using measured losses from the Cortaro gage to the Trico gage and then applying this average loss from the Trico gage to the model domain boundary.

For example, Figure A3 shows the generated monthly flows for the Gila River using the Florence Casa Grande Canal dataset and the Santa Cruz River.

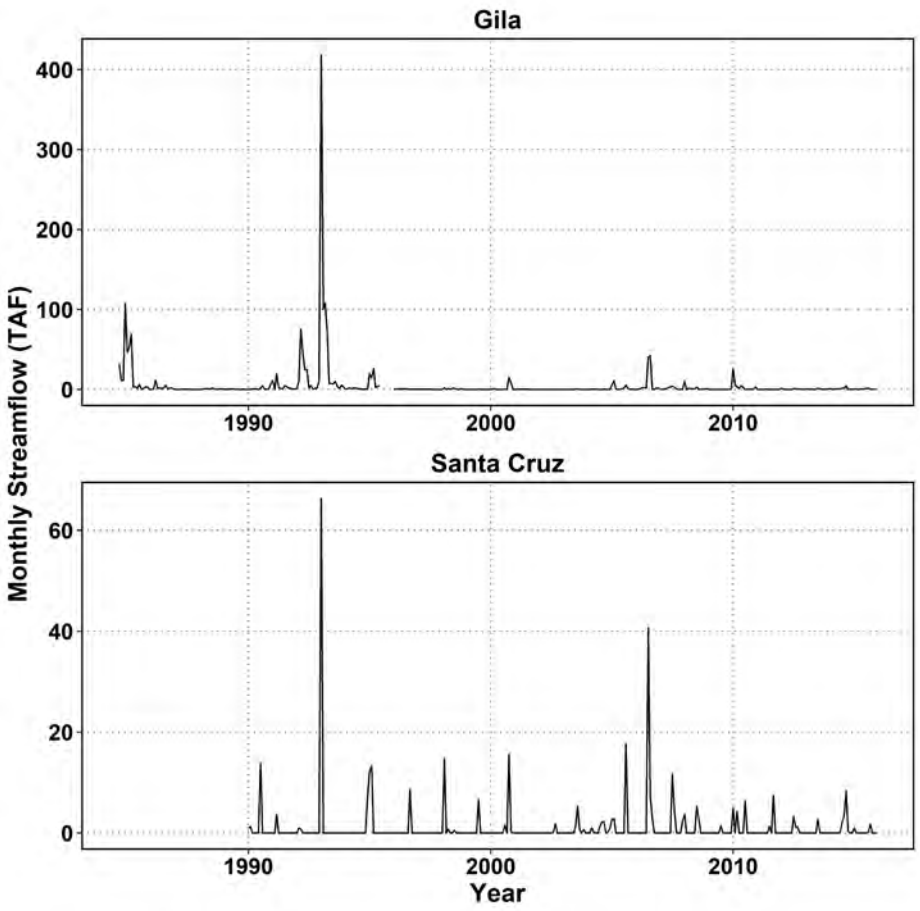

Figure A3. Monthly flows in thousand acre-feet (TAF) for the Gila and the Santa Cruz River generated through disaggregation techniques.

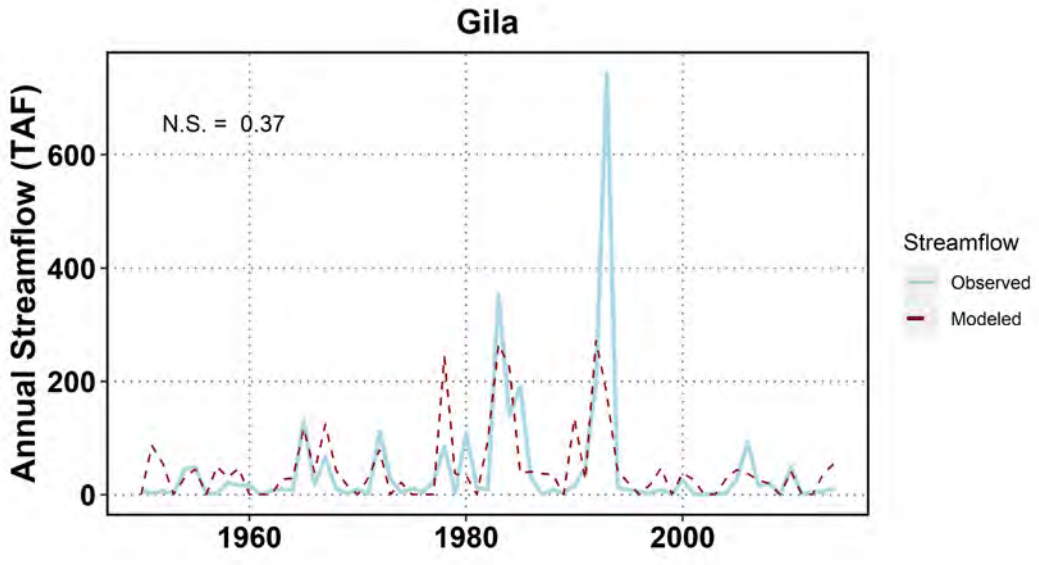

Figure A4. Observed (solid light blue line) and modeled (dashed red line) streamflow data for the Gila River using all available data from 1950-2015. N.S. = Nash-Shutcliffe efficiency.

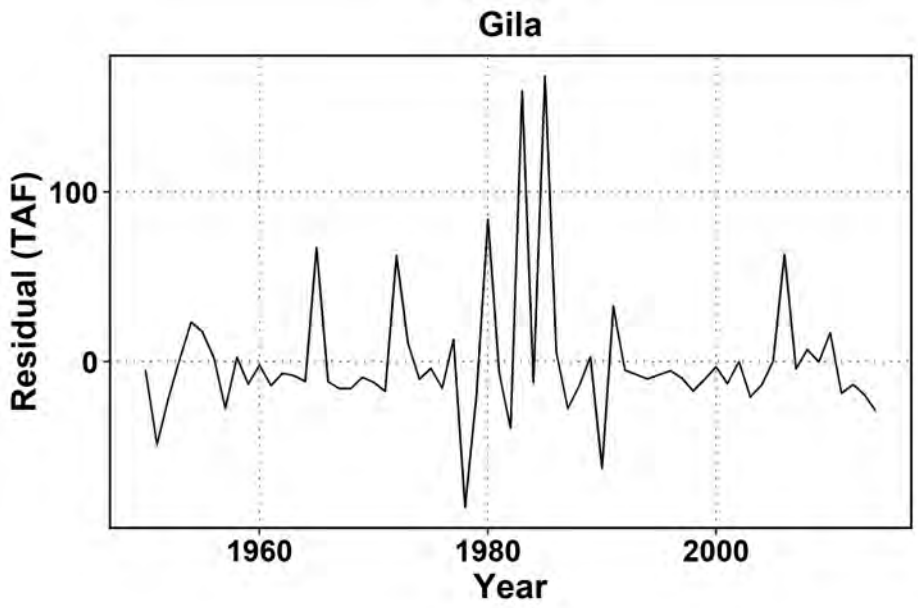

Figure A5. Residuals from the Gila rainfall-runoff model.

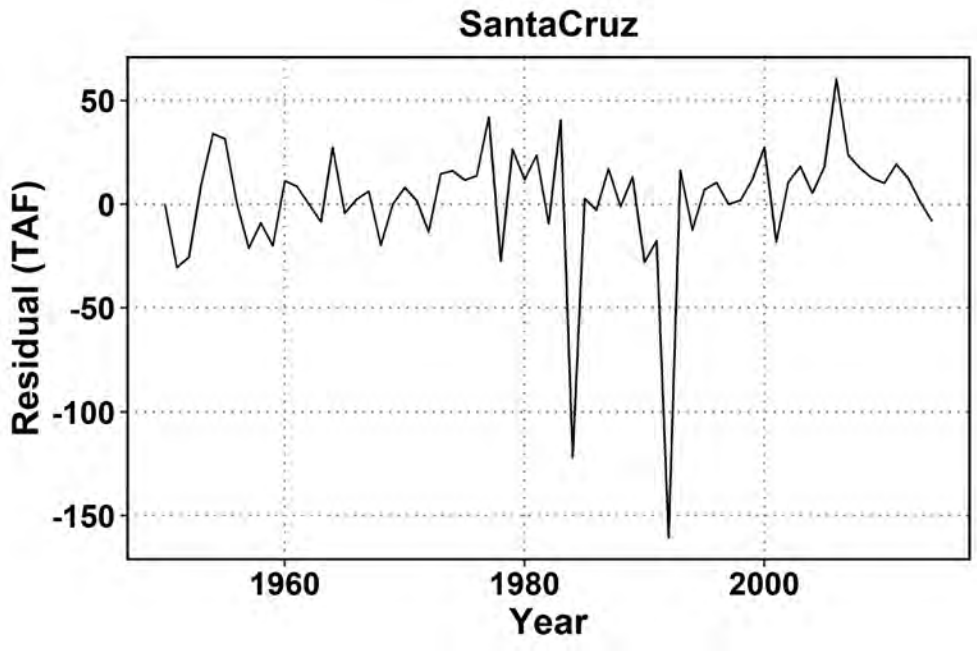

Figure A6. Residuals from the Santa Cruz rainfall-runoff model.

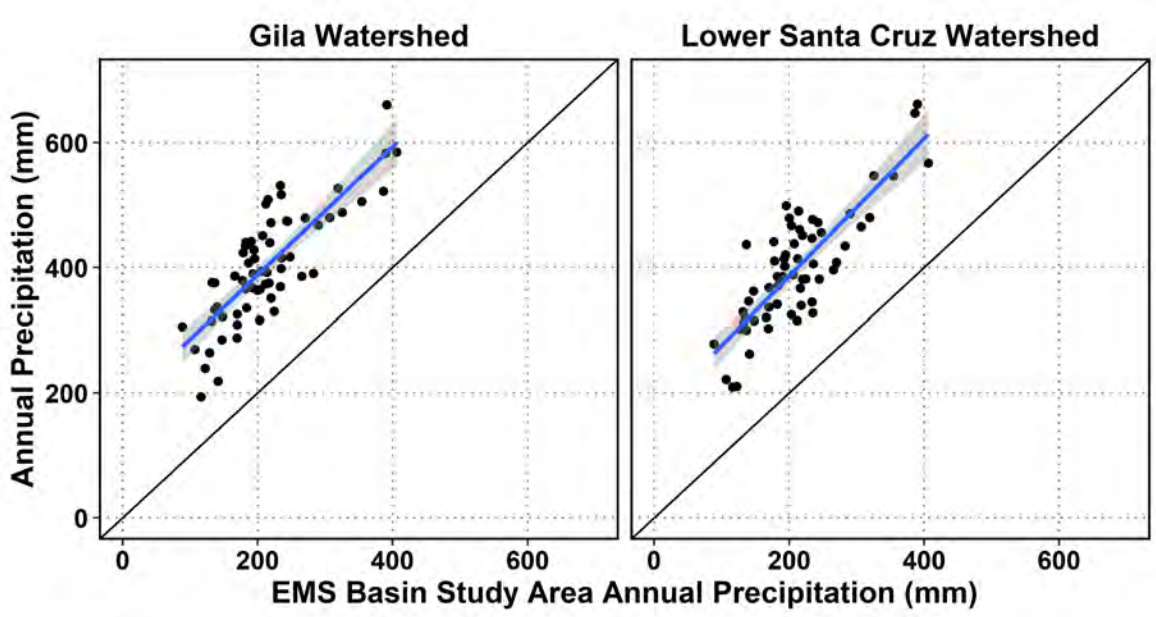

Figure A7. Scatterplot of annual precipitation for the entire drainage areas of the Gila (left) and Santa Cruz (right) Rivers compared to the annual precipitation across the EMS basin study area. Annual precipitations were calculated using the Livneh 2015 dataset and spatially-averaged across the respective domains. The linear trendline is depicted in blue with the 95% confidence interval shaded in grey.

Recharge Scenario Results

Figures A8 and A9 in the appendix show the projected recharge for each river under each future scenario for the far future time period (2065–2094).

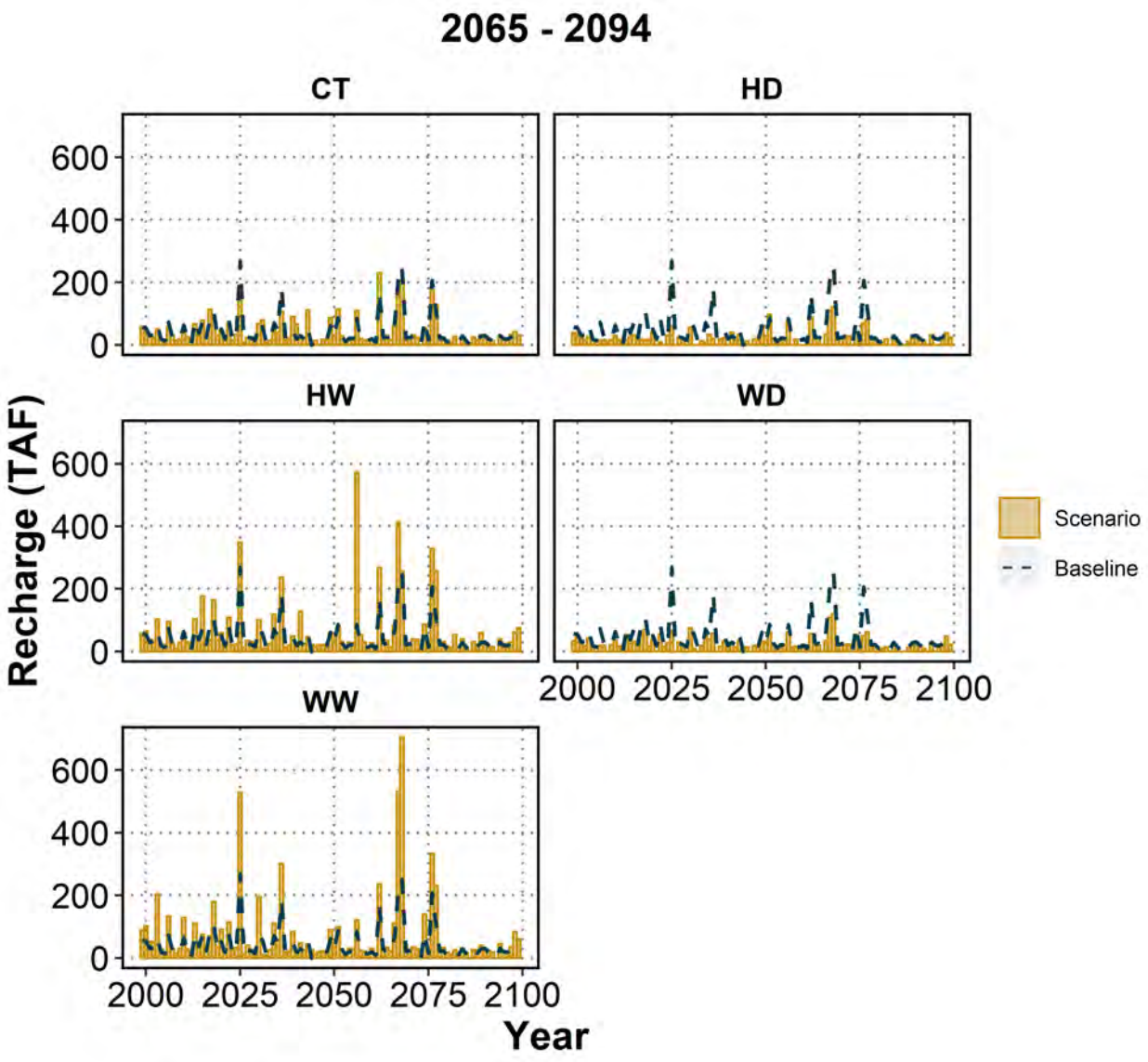

Figure A8. Gila River projected recharge for each future climate scenario (tan bars) compared to the historic baseline recharge (dashed blue line) for the 2065-2094 future time period. Note the different Y-axis scales for each scenario.

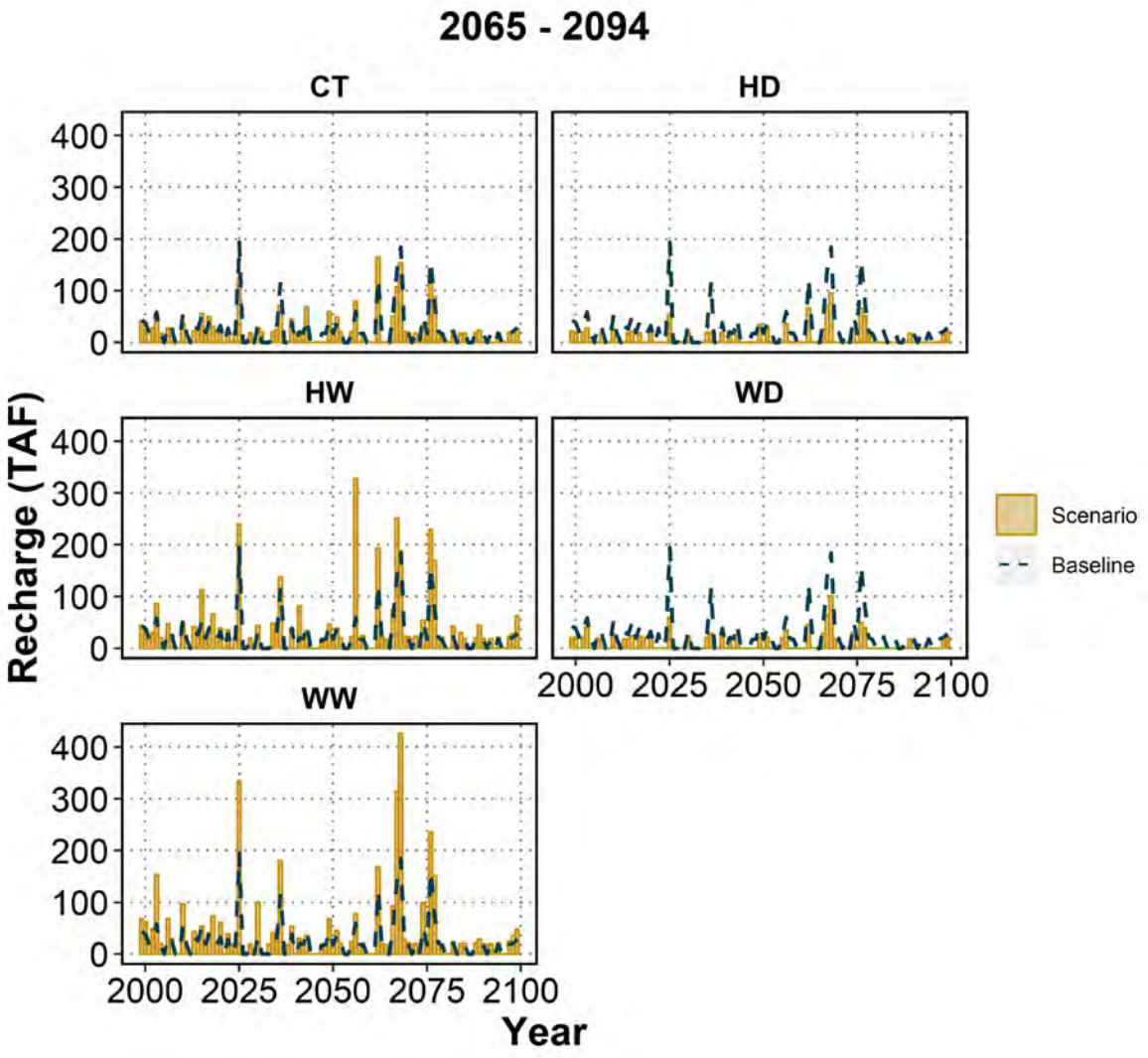

Figure A9. Santa Cruz River projected recharge for each future climate scenario (tan bars) compared to the historic baseline recharge (dashed blue line) for the 2065-2094 future time period. Note the different Y-axis scales for each scenario.

Individual figures showing projected recharge and precipitation for each scenario and each river are shown in the following appendix figures (A10 – A17).

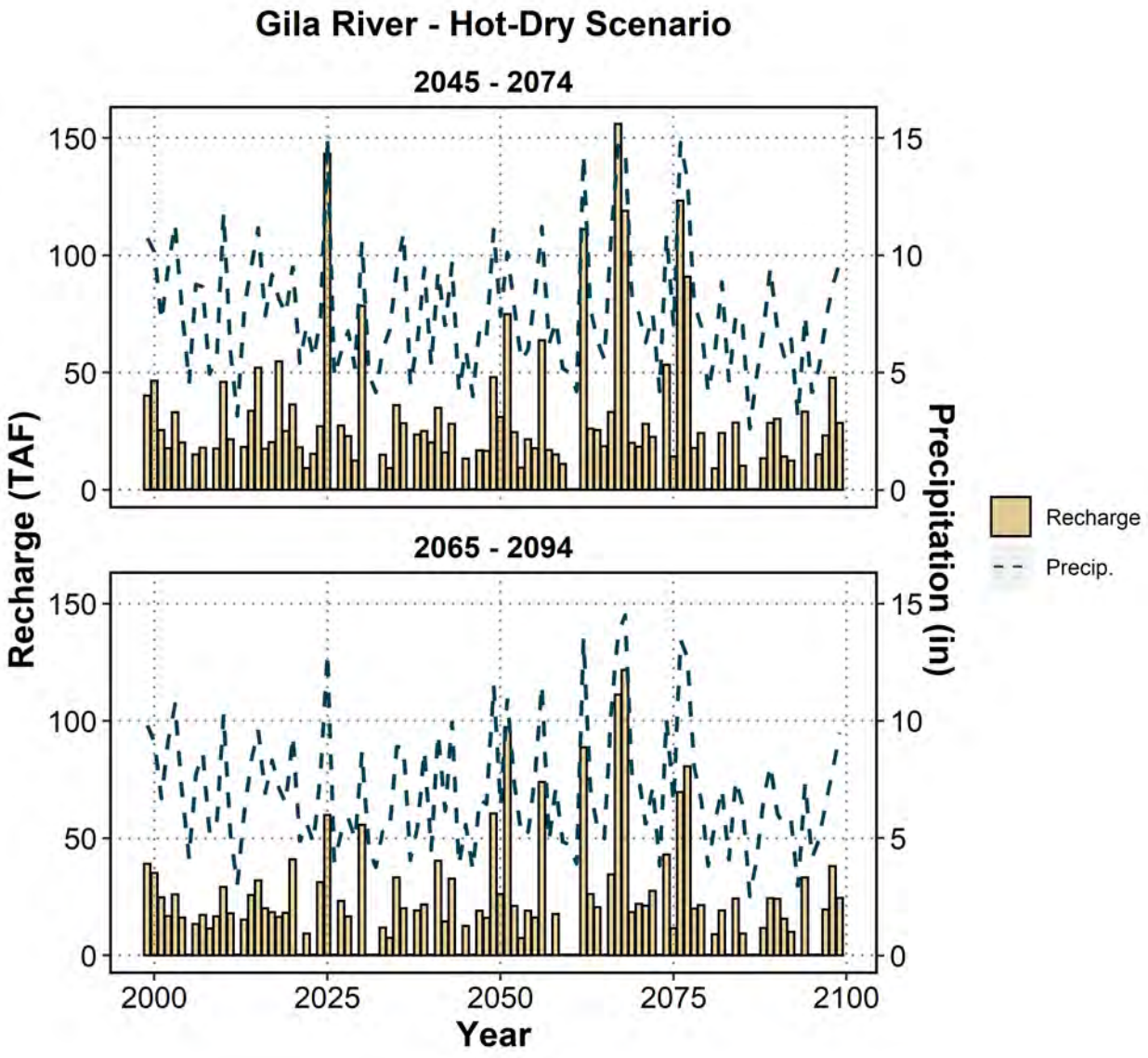

Figure A10. Projected annual recharge for the **Hot-Dry (HD) scenario** and both future time periods for the Gila River (tan bars). The dashed blue line shows the projected annual precipitation for the same scenario and time period.

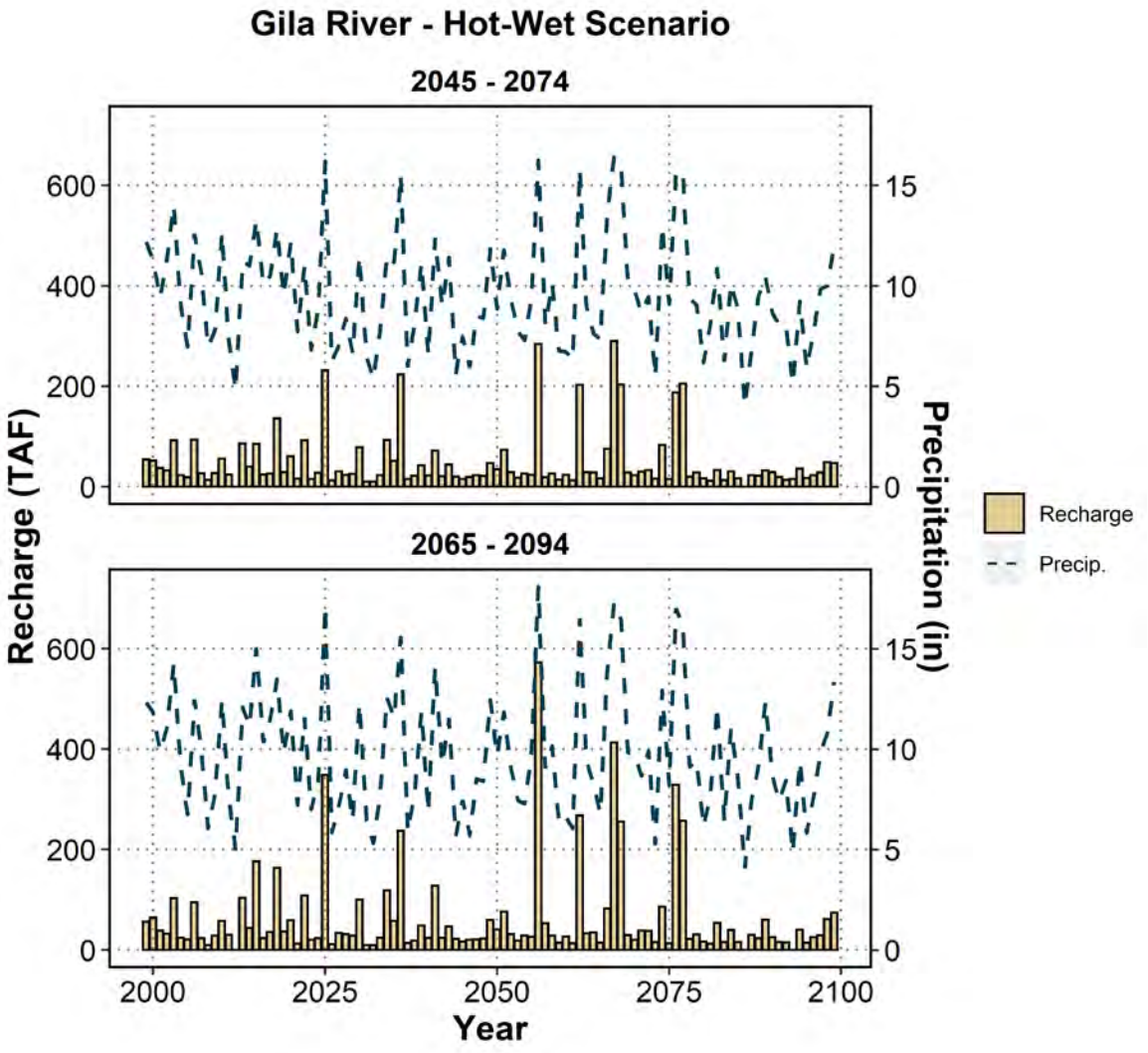

Figure A11. Projected annual recharge for the **Hot-Wet (HW) scenario** and both future time periods for the Gila River (tan bars). The dashed blue line shows the projected annual precipitation for the same scenario and time period.

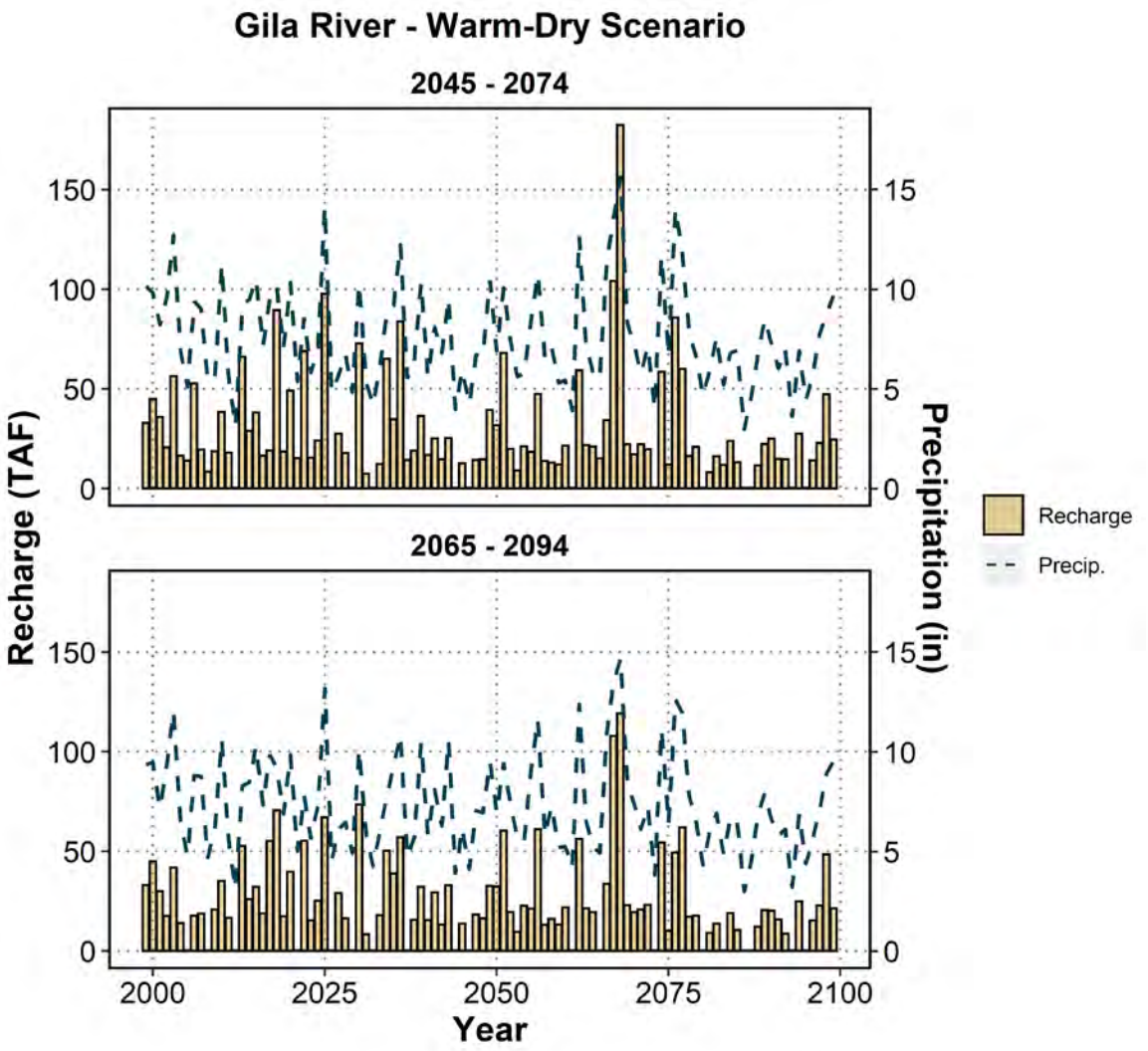

Figure A12. Projected annual recharge for the **Warm-Dry (WD) scenario** and both future time periods for the Gila River (tan bars). The dashed blue line shows the projected annual precipitation for the same scenario and time period.

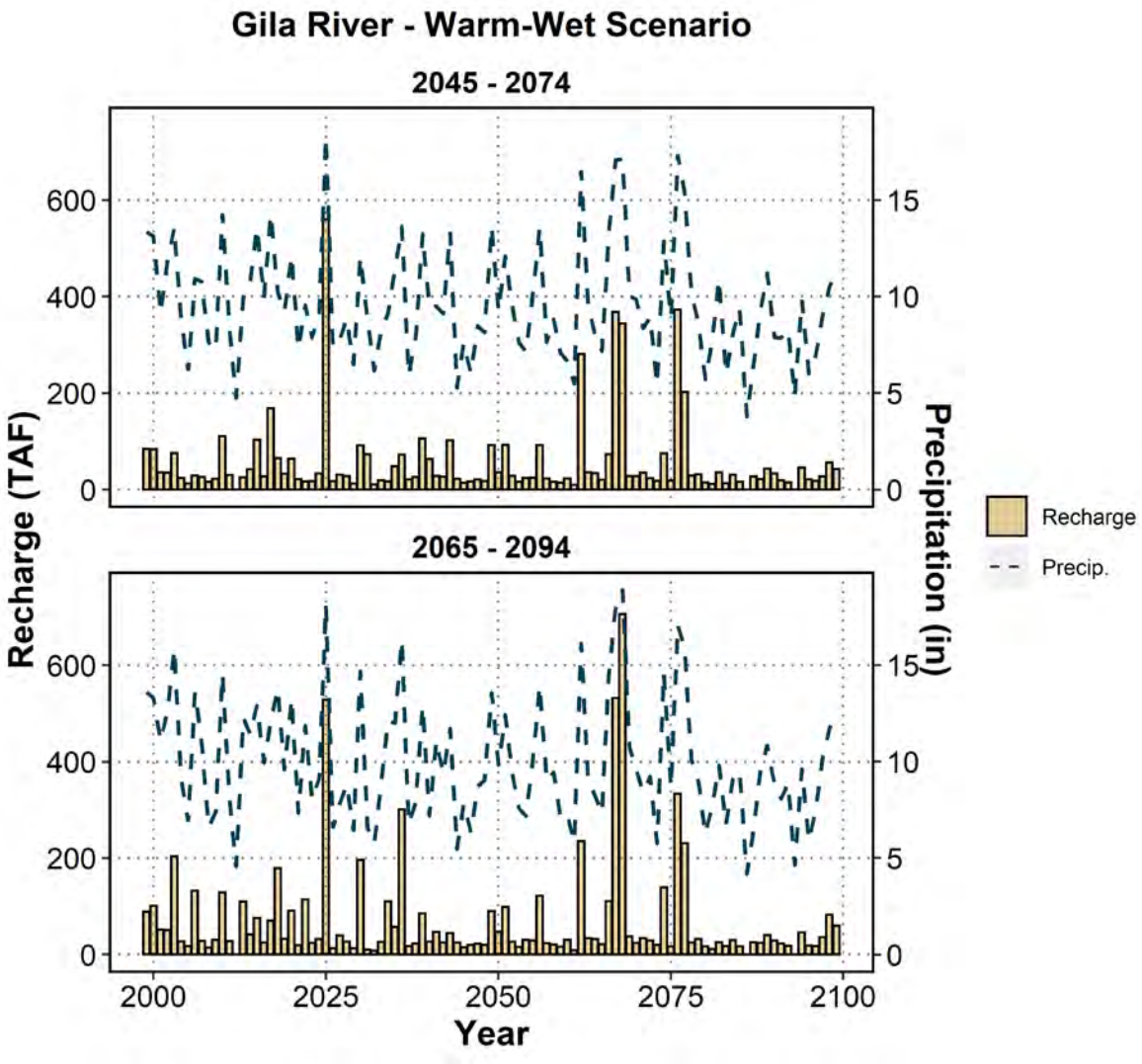

Figure A13. Projected annual recharge for the **Warm-Wet (WW) scenario** and both future time periods for the Gila River (tan bars). The dashed blue line shows the projected annual precipitation for the same scenario and time period.

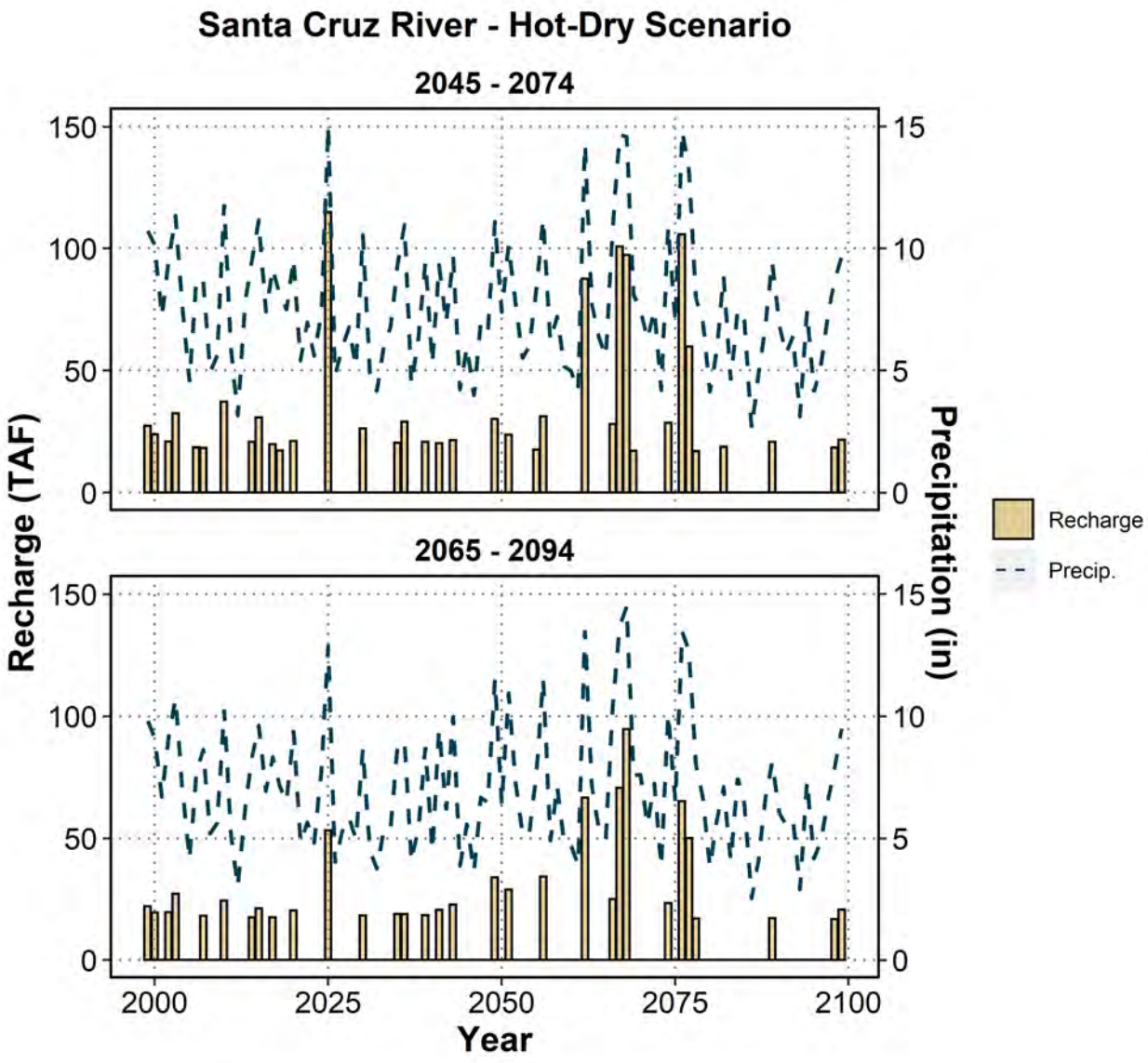

Figure A14. Projected annual recharge for the **Hot-Dry (HD) scenario** and both future time periods for the Santa Cruz River (tan bars). The dashed blue line shows the projected annual precipitation for the same scenario and time period.

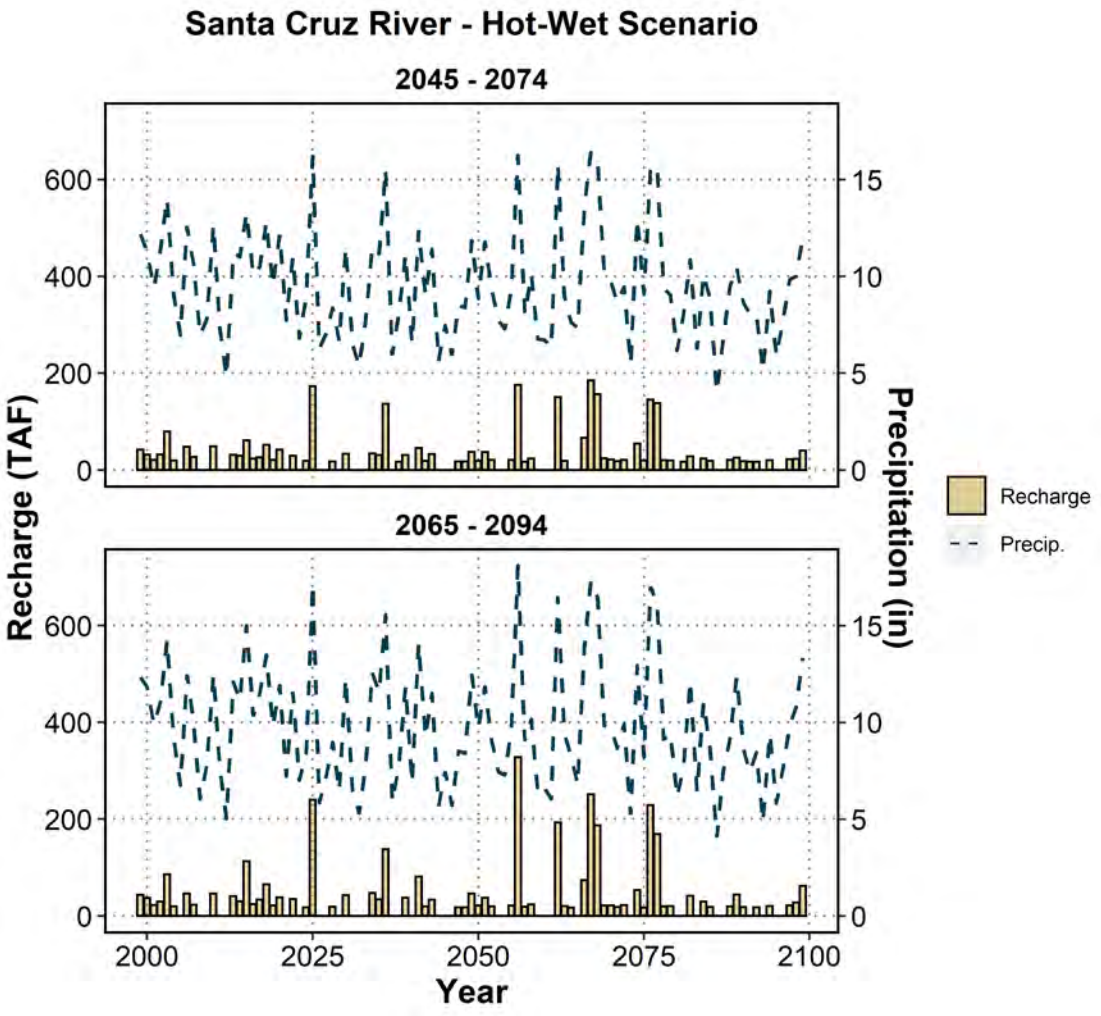

Figure A15. Projected annual recharge for the **Hot-Wet (HW) scenario** and both future time periods for the Santa Cruz River (tan bars). The dashed blue line shows the projected annual precipitation for the same scenario and time period.

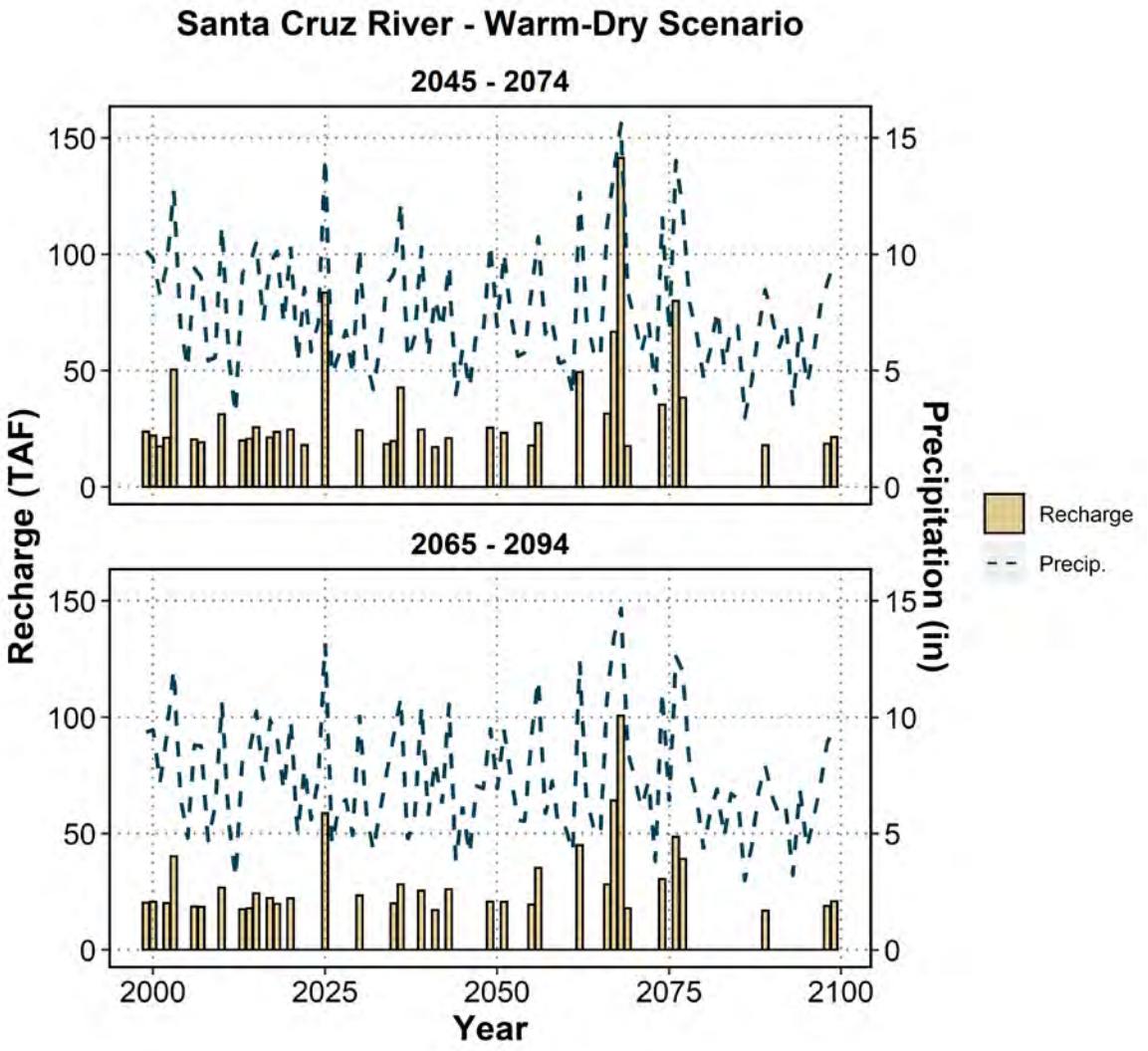

Figure A16. Projected annual recharge for the **Warm-Dry (WD) scenario** and both future time periods for the Santa Cruz River (tan bars). The dashed blue line shows the projected annual precipitation for the same scenario and time period.

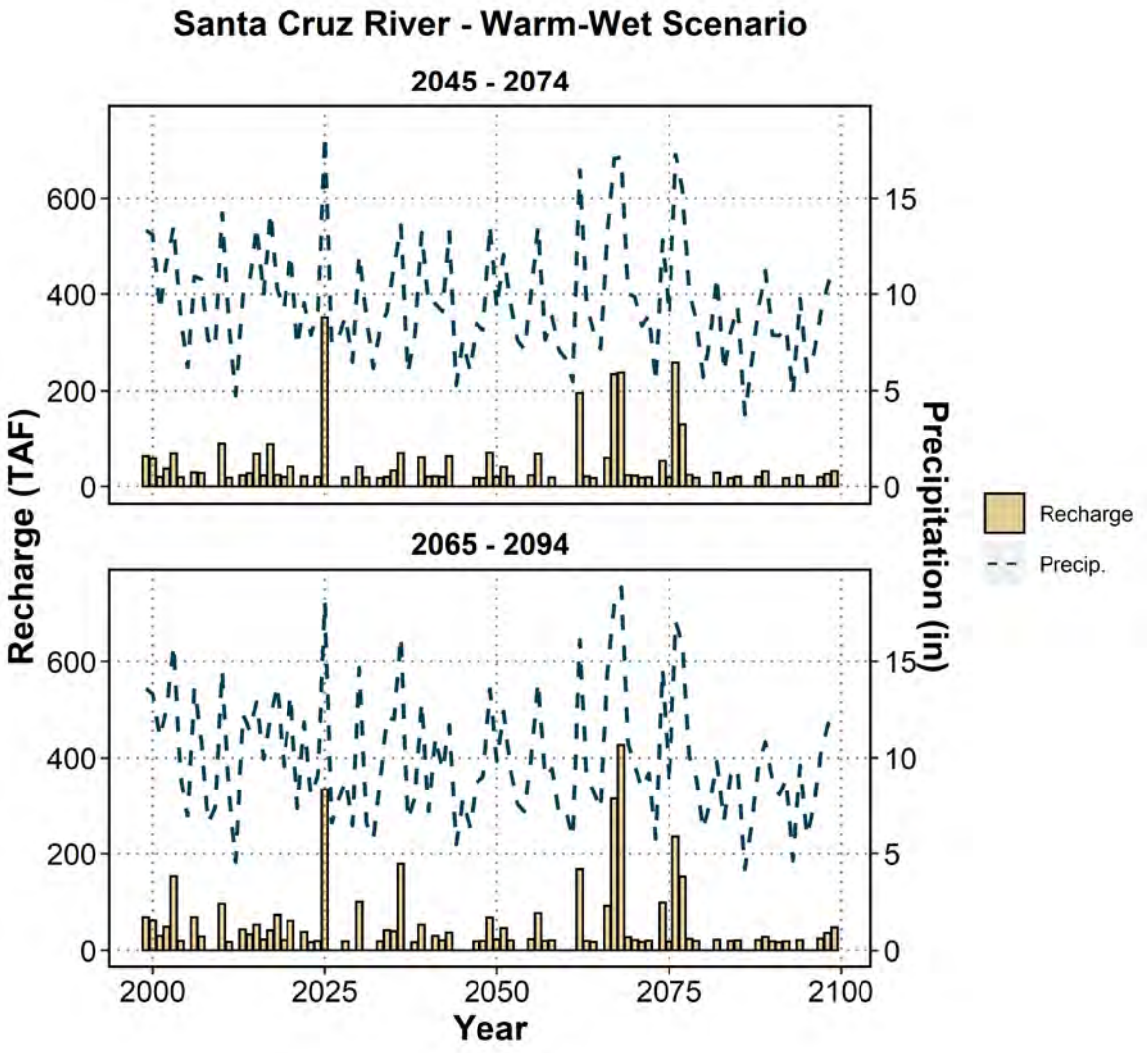

Figure A17. Projected annual recharge for the warm-wet (WW) scenario and both future time periods for the Santa Cruz River (tan bars). The dashed blue line shows the projected annual precipitation for the same scenario and time period.